PLASMA OSCILLATIONS AT MICROWAVE FREQUENCIES IN A STATIC MAGNETIC FIELD

by

DONALD JOHN NELSON

A THESIS

submitted to

OREGON STATE COLLEGE

in partial fulfillment of
the requirements for the
degree of

DOCTOR OF PHILOSOPHY

June 1954

APPROVED:

[redacted]

Professor of Physics

In Charge of Major

[redacted]

Head of Department of Physics

[redacted]

Chairman of School Graduate Committee

[redacted]

Dean of Graduate School

Date thesis is presented June 1954

Typed by Ruth Perry

ACKNOWLEDGEMENT

I wish to express my sincere appreciation to Dr. E. A. Yunker, under whose direction the work was done, for his encouragement during the work leading to this thesis and for his help and constructive criticism in its preparation. Credit is due the U. S. Air Force for sponsoring this research project and to the former members of the research group who built and assembled the experimental apparatus which I inherited. Thanks are also due to Ruth Perry for her infinite patience in a difficult typing job. Dick Whitely helped to take the data presented in Figure 5.1.

TABLE OF CONTENTS

TABLE OF ILLUSTRATIONS

PLASMA OSCILLATIONS AT MICROWAVE FREQUENCIES IN A STATIC MAGNETIC FIELD

INTRODUCTION

Some characteristics of a gas plasma

A plasma is a region in a gas in which there are high and approximately equal densities of free electrons and positive ions. The plasma tends to keep itself at a constant potential by forming space charge sheaths at the surfaces of electrodes and walls enclosing the plasma. These sheaths shield the plasma from the effects of the electrodes.

There are, within the plasma region, relatively large forces which tend to keep the electron and positive ion densities equal. Electron densities of the order of 10^{12} per cubic centimeter are typical. For example if, in a spherical region of radius 0.01 centimeter, the electron density is increased by one percent, the resulting electric field strength tending to make the electron and positive ion densities equal again is 60.4 volts per centimeter.

For an electron density of 10^{12} per cubic centimeter, the interelectronic distance is 10^{-4} centimeter. If all of the electrons throughout a certain region are displaced by this distance, the resulting electric field strength tending to force the displaced electrons back toward their equilibrium positions is 181 volts per centimeter. Thus at these high electron densities small displacements create large forces. Upon returning toward their equilibrium

positions these electrons acquire momentum which causes them to travel past their equilibrium positions. They come to rest again on the opposite side with the same magnitude of displacement. Large forces again accelerate the electrons toward their equilibrium positions and the process is repeated. Thus oscillations of the plasma electrons are possible if there is an exciting mechanism present which overcomes the mechanisms tending to damp the oscillations.

Plasma oscillations with no magnetic field and no thermal motions

Let us first consider the simplest case of oscillations of electrons in a plasma which is not in a magnetic field and which is at a temperature of absolute zero. The electrons and positive ions thus have no thermal motions and their equilibrium positions are not functions of time. This case was first treated by Tonks and Langmuir (125, pp. 195-203) and is given here as an introduction to the more complicated case of plasma oscillations, with thermal motions, in a static magnetic field.

With a given electric field strength in a region, the forces on the electrons and positive ions are equal and opposite. Since the mass of an atomic positive ion formed from an air molecule is on the order of 25,000 times the mass of an electron, the acceleration of the electron is on the order of 25,000 times that of the positive ion. The motions of the positive ions are therefore so negligible in comparison with the electronic motions that the

positive ions may be considered as remaining at rest.

The electron density and electron displacement are related by the continuity of charge equation which is obtained from two of Maxwell's equations.

$$\nabla \times \vec{H} = \vec{J} + \frac{\partial \vec{D}}{\partial t} \tag{1.01}$$

$$\nabla \cdot \vec{D} = \rho \tag{1.02}$$

where $\vec{H}$ is the magnetic field strength, $\vec{J}$ the conduction current density, $\vec{D}$ the electric flux density, and ρ the net charge density. Rationalized MKS units are used in all the derivations following but the answers will sometimes be given in other units. Since the divergence of the curl of a vector is identically zero, taking the divergence of equation (1.01) and using equation (1.02) yields the continuity of charge equation.

$$\nabla \cdot \nabla \times \vec{H} = 0 = \nabla \cdot \vec{J} + \nabla \cdot \frac{\partial \vec{D}}{\partial t} = \nabla \cdot \vec{J} + \frac{\partial}{\partial t} \nabla \cdot \vec{D}$$

$$0 = \nabla \cdot \vec{J} + \frac{\partial \rho}{\partial t} \tag{1.03}$$

Only the electron motions contribute to the current density.

$$\vec{J} = \vec{J}_- = -en_- \frac{\partial \vec{S}_-}{\partial t} \tag{1.04}$$

where n_- is the electron density, $\vec{S}_-$ the electron displacement, and $-e$ the electronic charge. The divergence of the current density is then

$$\nabla \cdot \vec{J} = -e \frac{\partial \vec{S}_-}{\partial t} \cdot \nabla n_- - e n_- \nabla \cdot \frac{\partial \vec{S}_-}{\partial t} \tag{1.05}$$

Let us consider a plane plasma wave of a single frequency propagated in the x direction. Then the electron density, the electron displacement, and the electric field strength are periodic functions of both time and the x direction of space. They all have the same time period T and the same space period (wavelength) λ. Let the electron density consist of a steady state component equal to the positive ion density plus a component periodic in space and time.

$$n_- = n + n_1 (x,t) \tag{1.06}$$

The electron displacement is

$$\vec{S}_- = \vec{S}(x,t) = \vec{\epsilon}_x S_x (x,t) + \vec{\epsilon}_y S_y (x,t)$$

$$+ \vec{\epsilon}_z S_z (x,t) \tag{1.07}$$

where $\vec{\epsilon}_x$, $\vec{\epsilon}_y$, $\vec{\epsilon}_z$ are the unit vectors and S_x, S_y, S_z are the components of $\vec{S}$ in the x, y, z directions respectively. Using equation (1.06) the net charge density is

$$\rho = +e (n_+ - n_-) = -e n_1 (x,t) \tag{1.08}$$

Substituting equations (1.05), (1.06), (1.07) and (1.08) into the continuity of charge equation (1.03) we have

$$0 = -e \frac{\partial}{\partial t} \vec{S}(x,t) \cdot \nabla n_1 (x,t)$$

$$-e\left[n + n_1(x,t)\right] \nabla \cdot \frac{\partial}{\partial t}\vec{S}(x,t) - e\frac{\partial}{\partial t} n_1(x,t) \qquad (1.09)$$

Since both $\vec{S}_-$ and n_- are simply periodic functions with the same periods in space and time.

$$\left|\frac{\partial \vec{S}}{\partial t} \cdot \nabla n_1\right|_{max} = \left|\frac{\partial n_1}{\partial t} \nabla \cdot \vec{S}\right|_{max} \qquad (1.10)$$

Two simplifying assumptions are introduced:

(A) The change of the electron density is small compared with the average electron density.

$$\left|\frac{n_1}{n}\right|_{max} << 1 \qquad (1.11)$$

(B) The electron displacement is small compared with the wavelength.

$$\left|\frac{2\pi S_x}{\lambda}\right|_{max} << 1 \qquad (1.12)$$

An equivalent statement is that the divergence of the electron displacement is small compared with unity.

$$\left|\nabla \cdot \vec{S}\right|_{max} = \left|\frac{\partial S_x}{\partial x}\right|_{max} << 1 \qquad (1.13)$$

It is shown experimentally that these approximations are justified.

Thus the terms in equation (1.09) containing the product $\frac{n_1}{n} \nabla \cdot \vec{S}$ are negligible compared with terms containing either

factor alone. The simplified equation then becomes

$$n \frac{\partial}{\partial t} \nabla \cdot \vec{S} + \frac{\partial n_1}{\partial t} = 0 \tag{1.14}$$

The time integral of this equation is

$$n \nabla \cdot \vec{S} + n_1 = \text{function of } (x, y, z) \tag{1.15}$$

The change of electron density is zero ($n_1 = 0$) when $\nabla \cdot \vec{S} = 0$ so that the function of (x, y, z) equals zero and equation (1.15) becomes

$$n_1 = -n \nabla \cdot \vec{S} \tag{1.16}$$

Using equations (1.02) and (1.08) and the relation

$$\vec{D} = \epsilon \vec{E} \tag{1.17}$$

where ϵ is the permittivity or inductive capacity of the plasma and $\vec{E}$ is the electric field strength, we obtain

$$\nabla \cdot \vec{D} = \rho = \epsilon \nabla \cdot \vec{E} = -en_1 \tag{1.18}$$

The polarizable material of the plasma which determines the permittivity is the neutral gas so ϵ is essentially the permittivity of free space.

Combining equations (1.16) and (1.18), we obtain

$$\nabla \cdot \vec{E} = + \frac{e}{\epsilon} n \nabla \cdot \vec{S} \tag{1.19}$$

or since $\vec{E}$ and $\vec{S}$ are functions of x and t only,

$$\frac{\partial E_x}{\partial x} = \frac{en}{\epsilon} \frac{\partial S_x}{\partial x} \tag{1.20}$$

Performing a space integration, we get

$$E_x = \frac{en}{\epsilon} S_x + \text{function of } (y,z,t) \tag{1.21}$$

where the function of (y,z,t) is the result of a source distribution other than the plasma electrons and positive ions. It gives rise to electric fields which excite the plasma electrons into oscillation and which damp the oscillation by the radiation of electromagnetic energy from the oscillating plasma electrons. A steady state oscillation is reached when the damping equals the excitation and the f(y,z,t) term becomes zero. Thus for a steady state oscillation the relation between the displacement of the plasma electrons from their equilibrium positions and the electric field strength produced by this displacement is

$$E_x = \frac{en}{\epsilon} S_x \tag{1.22}$$

The force on an electron due to an electric field only is

$$\vec{f} = -e\vec{E} \tag{1.23}$$

Using Newton's second law and equations (1.22) and (1.23) we get

$$f = -eE_x = m \frac{d^2 S_x}{dt^2} = \frac{-e^2 n}{\epsilon} S_x \tag{1.24}$$

where m is the electronic mass.

Writing ω^2 for $\frac{e^2 n}{\epsilon m}$ the differential equation for the motion of the plasma electrons is

$$\frac{d^2 S_x}{dt^2} + \omega^2 S_x = 0 \tag{1.25}$$

and its solution is

$$S_x = S_1 \cos(\omega t + \alpha) \tag{1.26}$$

where S_1 and α are two arbitrary constants with respect to time and $\omega = \frac{2\pi}{T}$ is the angular frequency of oscillation.

The plasma electrons thus may be excited into performing simple harmonic oscillations with a frequency proportional to the square root of the electron density and not a function of the wavelength. The wavelength of the disturbance is determined by the boundary conditions.

Since the frequency is not a function of the wavelength, the group velocity, which is the velocity at which energy is propagated, is zero.

$$v_{group} = \frac{\partial \omega}{\partial k} = \frac{\partial}{\partial k}\left[\frac{e^2 n}{\epsilon m}\right]^{1/2} = 0 \tag{1.27}$$

A solution periodic in the x coordinate and time is

$$S_x = S_1 \cos kx \cos \omega t \tag{1.28}$$

where $k = \frac{2\pi}{\lambda}$ is the propagation constant and S_1 is the maximum value of the displacement. The standing wave solution may be written in

the form of a traveling wave solution with two waves of equal amplitude, frequency, and wavelength traveling in opposite directions, by using a trigonometric identity.

$$S_x = \frac{S_1}{2} \cos(\omega t - kx) + \frac{S_1}{2} \cos(\omega t + kx) \tag{1.29}$$

Corresponding to the solution for the plasma electron displacement

$$S_x = S_1 \cos kx \cos \omega t \tag{1.28}$$

we have, using equations (1.16) and (1.22),

$$E_x = \frac{en}{\epsilon} S_1 \cos kx \cos \omega t \tag{1.30}$$

and

$$n_1 = + n k S_1 \sin kx \cos \omega t \tag{1.31}$$

All three quantities are in phase in time and n_1 is 90° out of phase in space with S_x and E_x as shown in Figure (1.1).

At time $t = 0$ all the electrons in the interval $-\frac{\pi}{2k} < x < \frac{\pi}{2k}$ are displaced in the plus x direction and all the electrons in the interval $\frac{\pi}{2k} < x < \frac{3\pi}{2k}$ are displaced in the minus x direction causing an accumulation of negative charge in the vicinity of $x = \frac{\pi}{2k}$ and a deficiency of negative charge in the vicinity of $x = -\frac{\pi}{2k}$ and $x = \frac{3\pi}{2k}$. The electric field is directed from positive to negative charges as shown.

The plasma waves are longitudinal waves since the electric field and the electron displacement are in the direction in which the waves

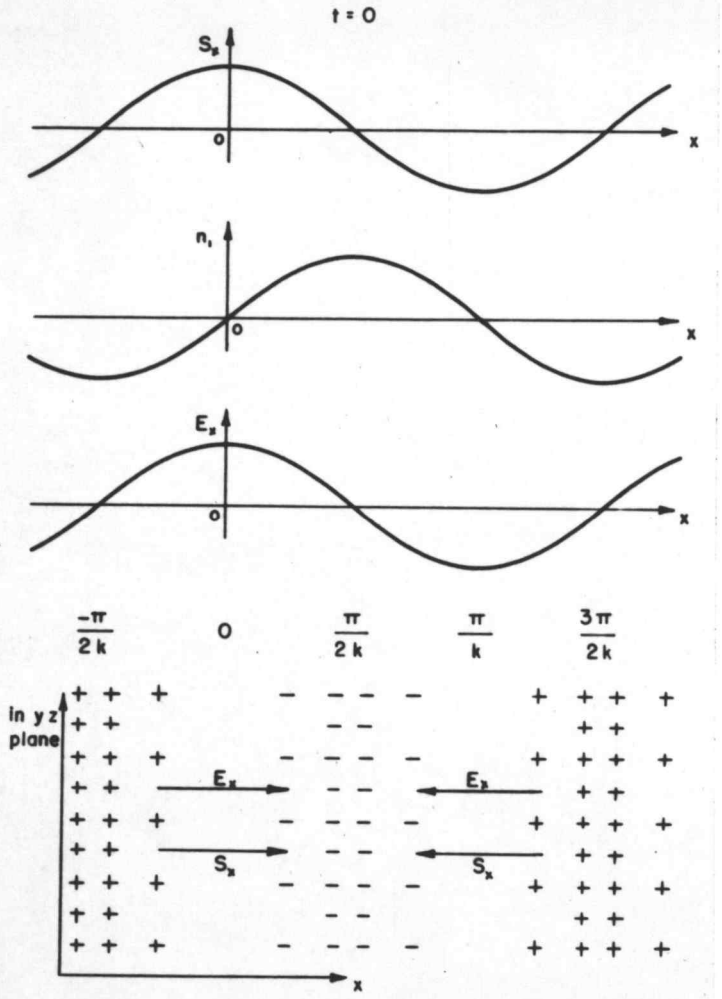

Figure (1.1)

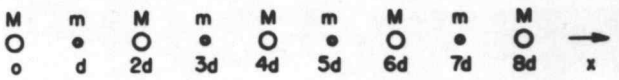

Figure (1.2)

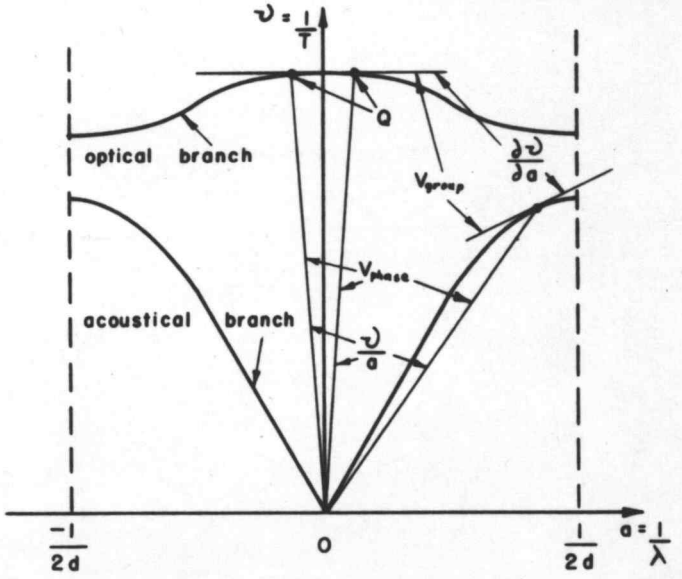

Figure (1.3)

are propagated.

Referring to equations (1.28) and (1.31),

$$\frac{\partial S_x}{\partial x} = - k S_1 \sin kx \cos \omega t$$

$$\frac{n_1}{n} = k S_1 \sin kx \cos \omega t$$

$$\text{so} \quad \frac{\partial S_x}{\partial x} = \frac{-n_1}{n} \tag{1.32}$$

The two approximations, equations (1.11) and (1.13) are thus equally valid. When the electron displacement is small compared with the wavelength of the plasma waves, the change of the electron density is small compared with the average electron density.

The frequency of the plasma oscillation is

$$\nu = \frac{\omega}{2\pi} = \frac{1}{2\pi} \left[\frac{e^2 n}{\epsilon m}\right]^{1/2} \tag{1.33}$$

where n is the electron density, e and m the electronic charge and mass, and ϵ the permittivity of the gas. This is also the frequency of the electromagnetic energy radiated by the oscillating plasma electrons. The frequency corresponding to an electron density of 10^{12} electrons per cubic centimeter is 8.98 kilomegacycles; the free-space wavelength of electromagnetic radiation of this frequency is 3.34 centimeters. Thus the plasma frequency, with easily attainable electron densities, is in the microwave region of the electromagnetic spectrum.

This suggests the possibility of generating electromagnetic waves with wavelengths of the order of a millimeter by increasing the plasma electron density, if a mechanism can be found to excite the plasma oscillations. Since the plasma frequency is proportional to the square root of the electron density, the electron density must be increased one hundred fold to obtain a frequency increase of ten fold. Thus an electron density of about 10^{15} electrons per cubic centimeter is required to produce electromagnetic radiation with wavelengths of the order of a millimeter.

Wave propagation in periodic structures

The phase velocity of any wave is equal to the product of the frequency and the wavelength of the wave.

$$v_{phase} = \nu\lambda \tag{1.34}$$

For any wave such as an electromagnetic wave traveling either in free space or through matter, a sound wave traveling through matter, a wave on a stretched elastic string, or a wave on a stretched elastic membrane, the properties of the medium in which the wave is propagated determine its phase velocity. For a medium of finite extent the boundary conditions determine the allowed wavelengths. The natural frequencies of oscillation of the medium of finite size are then fixed by equation (1.34).

For a plasma wave the properties of the plasma, such as the electron density and the magnetic flux density, determine the

frequency of the wave. For a plasma region of finite size the boundary conditions determine the allowed wavelengths. The natural phase velocities of propagation of the plasma waves are then fixed by equation (1.34).

Let us consider further these two types of wave propagation by investigating the propagation of waves in a periodic structure as shown by Brillouin (23, pp. 14-16). Figure (1.2) shows a one dimensional lattice consisting of large masses M and small masses m alternating at the points at equal intervals along the x axis defined by Nd, where d is the distance between nearest neighbors and N is an integer. Forces exist between the particles so that the structure can propagate a disturbance.

Figure (1.3) shows the relation between the frequency $\nu = 1/T$ and the wave number $a = 1/\lambda$, for waves propagating through such a lattice. There are two branches to the curve because there are two different masses in the lattice. The lower branch is called the acoustical branch. It corresponds to motion of the particles such that in each short section of the line all particles move in the same direction at a given instant. The upper branch is called the optical branch and corresponds to the motion of the large masses in one direction while the small masses move in the other.

The phase velocity, $v_{phase} = \nu\lambda = \lambda/T = \omega/k = \nu/a$, is given by the slope of a line drawn from the origin to the point on a curve in Figure (1.3) corresponding to a given wavelength. The group velocity $v_{group} = \partial\omega/\partial k = \partial\nu/\partial a$, is given by the slope of the frequency versus

wave number curve at the point. For wavelengths long compared with the length of the lattice cell 2d, the acoustical branch represents a constant phase velocity type of propagation, the optical branch a constant frequency type of propagation. The plasma oscillations thus are represented by the points Q in Figure (1.3) corresponding to two waves traveling in opposite directions with their frequency independent of wavelength.

Plasma oscillations with thermal motions in a uniform static magnetic field with very long wavelengths

Let us investigate the effect that a magnetic field has on the frequency of oscillation of the plasma electrons for wavelengths large compared with the radii of the helical paths of the plasma electrons due to their thermal motions. The problem is considered as a consistent field problem. First the motions of the plasma electrons in an alternating electric field are calculated and then the resultant electric field due to the motions of the plasma electrons is found and equated to the assumed field.

Let the assumed electric field be

$$\vec{E} = \vec{\epsilon}_x E_p \cos kx \cos \omega t \tag{1.35}$$

The force on an electron in an electric and a magnetic field is

$$\vec{f} = -e\vec{E} - e\vec{v} \times \vec{B} \tag{1.36}$$

so that Newton's law becomes

$$m \frac{d^2\vec{w}}{dt^2} = -e\, B \frac{d\vec{w}}{dt} \times \vec{\varepsilon}_z - e\, \vec{\varepsilon}_x E_p \cos \omega t \cos k x_o \qquad (1.37)$$

for the magnetic field in the z direction and the electron at $x = x_o$. The solution of this equation for $\vec{w}$, which is the motion of an electron between collisions, is the sum of a complementary function $\vec{u}$ and a particular integral $\vec{S}$. The complementary function, which is the solution of the equation with zero electric field, is a circular helical motion and represents the thermal motions. The particular integral is a plane elliptical motion and represents the plasma oscillations (73, p. 1297).

The x component of equation (1.37) is

$$\frac{d^2 w_x}{dt^2} + \omega_c \frac{dw_y}{dt} = - e/m\, E_p \cos k x_o \cos \omega t \qquad (1.38)$$

using the relation $\omega_c = \frac{eB}{m}$.

The y component is

$$\frac{d^2 w_y}{dt^2} - \omega_c \frac{dw_x}{dt} = 0 \qquad (1.39)$$

and the z component is

$$\frac{d^2 w_z}{dt^2} = 0 \qquad (1.40)$$

The motions in the x and y directions are coupled because of the magnetic field. The first integral of equation (1.39) is

$$\frac{dw_y}{dt} = \omega_c w_x + \text{constant}. \tag{1.41}$$

The constant term is a steady drift velocity in the y direction which we set equal to zero.

Substituting equation (1.41) into equation (1.38) yields

$$\frac{d^2 w_x}{dt^2} + \omega_c^2 w_x = -\frac{e}{m} E_p \cos kx_o \cos \omega t \tag{1.42}$$

The complementary function of this equation is

$$u_x = A \cos (\omega_c t + \alpha) \tag{1.43}$$

and the particular integral is

$$S_x = \frac{\frac{e}{m} E_p}{\omega^2 - \omega_c^2} \cos kx_o \cos \omega t \tag{1.44}$$

The y components of the solution are obtained by using equation (1.41). The complete solution then is

$$\vec{w} = \vec{u} + \vec{S} \tag{1.45}$$

$$\vec{u} = \vec{\epsilon}_x A \cos (\omega_c t + \alpha) + \vec{\epsilon}_y A \sin (\omega_c t + \alpha)$$

$$+ \vec{\epsilon}_z v_{\parallel} t \tag{1.46}$$

$$\vec{S} = \frac{\frac{e}{m} E_p}{\omega^2 - \omega_c^2} \cos kx_o \left[\vec{\epsilon}_x \cos \omega t + \frac{\omega_c}{\omega} \vec{\epsilon}_y \sin \omega t \right] \qquad (1.47)$$

where $A = \frac{v_\perp}{\omega_c}$ is the radius of the thermal helix.

The equilibrium position of a plasma electron changes with time because of its thermal motion. The x component of its thermal motion is

$$x = x_o + u_x = x_o + A \cos (\omega_c t + \alpha) \qquad (1.48)$$

where x_o is the x coordinate of the center of its thermal circle. Putting this value into the equation of the electric field we get

$$\vec{E} = \vec{\epsilon}_x E_p \cos k \left[x_o + A \cos (\omega_c t + \alpha) \right] \cos \omega t \qquad (1.49)$$

which is the electric field that the electron sees. The expansion of equation (1.49) is

$$\vec{E} = \vec{\epsilon}_x E_p \cos \omega t \left\{ \cos kx_o \cos \left[kA \cos (\omega_c t + \alpha) \right] \right.$$

$$\left. - \sin kx_o \sin \left[kA \cos (\omega_c t + \alpha) \right] \right\} \qquad (1.50)$$

When the radius of the thermal helix A is very small compared with a wavelength, kA approaches zero and the electron sees an oscillating electric field $E_p \cos kx_o$, of essentially constant amplitude, and equation (1.42) is the correct equation of motion. When kA is finite, the electron sees an oscillating electric field which is amplitude modulated at the cyclotron frequency rate. This situation will be discussed later.

Equation (1.20) gives the relation between the electron displacements and the electric field produced by these displacements for electron displacements and electric fields which are functions of x and t only.

$$\frac{\partial E_x}{\partial x} = \frac{en}{\epsilon} \frac{\partial w_x}{\partial x} \tag{1.51}$$

The electric field E_x is the resultant of the fields from all the particles. The individual particles have random phase angles α between their oscillations of frequency ω and ω_c so the displacements are summed over all the phase angles to find the total field. As $\int_o^{2\pi} \cos(\omega_c t + \alpha)\, d\alpha = 0$ the contributions of the thermal motions to the resultant electric field average to zero and

$$E_x = \frac{en}{\epsilon} S_x = E_p \cos kx_o \cos \omega t \tag{1.52}$$

for steady state oscillations.

Substituting this expression into equation (1.44) gives

$$\omega^2 = \omega_c^2 + \omega_p^2 \tag{1.53}$$

$\omega_p = \left[\frac{e^2 n}{\epsilon m}\right]^{1/2}$ was found to be the angular frequency of oscillation of plasma electrons with a density n not in a magnetic field and will hereafter be called the plasma angular frequency. The natural frequency of plasma electrons in a magnetic field is thus a function of the electron density and the magnetic flux density. The

oscillation frequency is always greater than the cyclotron frequency. The ratio of major to minor axes of the elliptical motion is

$$\frac{|S_x|_{max}}{|S_y|_{max}} = \frac{\omega}{\omega_c} \tag{1.54}$$

so, as ω increases, the ellipse becomes narrower and approaches the straight line motion obtained without a magnetic field. Also ω approaches ω_p, the oscillation angular frequency obtained without a magnetic field.

Wave propagation through a plasma with no thermal motions across a uniform static magnetic field

Let us consider a more general derivation which also gives the dispersion relation for the electromagnetic waves traveling through the plasma. Starting with Maxwell's two curl equations

$$\nabla \times \vec{H} = \vec{J} + \frac{\partial \vec{D}}{\partial t} \tag{1.55}$$

$$\nabla \times \vec{E} = -\frac{\partial \vec{B}}{\partial t} \tag{1.56}$$

the curl of each is taken and combined with the other.

$$\nabla \times \nabla \times \vec{E} = -\frac{\partial}{\partial t} \nabla \times \vec{B} = -\mu \frac{\partial}{\partial t} \nabla \times \vec{H}$$

$$= -\mu \frac{\partial \vec{J}}{\partial t} - \mu\varepsilon \frac{\partial^2 \vec{E}}{\partial t^2} \tag{1.57}$$

$$\nabla \times \nabla \times \vec{H} = \nabla \times \vec{J} + \varepsilon \frac{\partial}{\partial t} \nabla \times \vec{E} = \nabla \times \vec{J} - \mu\varepsilon \frac{\partial^2 \vec{H}}{\partial t^2} \tag{1.58}$$

The current density $\vec{J}$ is given in equation (1.04)

$$\vec{J} = -en \frac{\partial \vec{S}}{\partial t} \tag{1.59}$$

Putting this expression into equation (1.57) and using Newton's force equation gives two equations in two unknowns, $\vec{E}$ and $\vec{S}$.

$$\nabla \times \nabla \times \vec{E} = \mu e n \frac{\partial^2 \vec{S}}{\partial t^2} - \mu\varepsilon \frac{\partial^2 \vec{E}}{\partial t^2} \tag{1.60}$$

$$m \frac{d^2 \vec{S}}{dt^2} + e \frac{d\vec{S}}{dt} \times \vec{B} + e \vec{E} = 0 \tag{1.61}$$

Let the waves travel in the x direction and let the magnetic flux density be in the z direction. The general expressions for $\vec{E}$, $\vec{H}$, and $\vec{S}$ contain components in all directions.

$$\vec{E} = \vec{\varepsilon}_x E_x \cos(\omega t \pm kx) + \vec{\varepsilon}_y E_y \sin(\omega t \pm kx)$$

$$+ \vec{\varepsilon}_z E_z \cos(\omega t \pm kx) \tag{1.62}$$

$$\vec{H} = \vec{\epsilon}_x H_x \sin(\omega t \pm kx) + \vec{\epsilon}_y H_y \cos(\omega t \pm kx)$$

$$+ \vec{\epsilon}_z H_z \sin(\omega t \pm kx) \tag{1.63}$$

$$\vec{S} = \vec{\epsilon}_x S_x \cos(\omega t \pm kx) + \vec{\epsilon}_y S_y \sin(\omega t \pm kx)$$

$$+ \vec{\epsilon}_z S_z \cos(\omega t \pm kx) \tag{1.64}$$

The curl curl vector identity is

$$\nabla \times \nabla \times \vec{E} = \nabla \nabla \cdot \vec{E} - \nabla \cdot \nabla \vec{E} \tag{1.65}$$

Written out in component form

$$\nabla \nabla \cdot \vec{E} = \vec{\epsilon}_x (-k^2) E_x \cos(\omega t \pm kx) \tag{1.66}$$

and

$$-\nabla \cdot \nabla \vec{E} = +k^2 \left[\vec{\epsilon}_x E_x \cos(\omega t \pm kx) + \vec{\epsilon}_y E_y \right.$$

$$\left. \sin(\omega t \pm kx) + \vec{\epsilon}_z E_z \cos(\omega t \pm kx) \right] \tag{1.67}$$

also

$$\nabla \times \vec{J} = en\omega k \left[\mp \vec{\epsilon}_y S_z \cos(\omega t \pm kx) \pm \vec{\epsilon}_z S_y \right.$$

$$\left. \sin(\omega t \pm kx) \right] \tag{1.68}$$

The x, y, and z components of equation (1.60) become

$$\vec{\varepsilon}_x \left[0 = -\mu e n \omega^2 S_x + \mu\varepsilon\omega^2 E_x \right] \cos(\omega t \pm kx) \tag{1.69}$$

$$\vec{\varepsilon}_y \left[k^2 E_y = -\mu e n \omega^2 S_y + \mu\varepsilon\omega^2 E_y \right] \sin(\omega t \pm kx) \tag{1.70}$$

$$\vec{\varepsilon}_z \left[k^2 E_z = -\mu e n \omega^2 S_z + \mu\varepsilon\omega^2 E_z \right] \cos(\omega t \pm kx) \tag{1.71}$$

and from equation (1.69) we get, as before,

$$E_x = \frac{en}{\varepsilon} S_x \tag{1.72}$$

From equations (1.70) and (1.71) we obtain

$$E_y = \frac{\frac{en}{\varepsilon}\omega^2 S_y}{\omega^2 - c^2 k^2} \tag{1.73}$$

$$E_z = \frac{\frac{en}{\varepsilon}\omega^2 S_z}{\omega^2 - c^2 k^2} \tag{1.74}$$

where $1/\mu\varepsilon$ equals the velocity of light squared.

$$1/\mu\varepsilon = c^2 \tag{1.75}$$

The solution of equation (1.61), neglecting the random thermal motions, is

$$\vec{S} = \vec{\varepsilon}_x \frac{\frac{e}{m}}{\omega^2 - \omega_c^2} \left[E_x + \frac{\omega_c}{\omega} E_y \right] \cos(\omega t \pm kx)$$

$$+ \vec{\varepsilon}_y \frac{\frac{e}{m}}{\omega^2 - \omega_c^2} \left[\frac{\omega_c}{\omega} E_x + E_y \right] \sin(\omega t \pm kx)$$

$$+ \vec{\varepsilon}_z \frac{\frac{e}{m}}{\omega^2 - \omega_c^2} E_z \cos(\omega t \pm kx) \qquad (1.76)$$

Using equations (1.72), (1.73), and (1.74) the components of equation (1.76) may be written as

$$\vec{\varepsilon}_x \left[\frac{E_x}{\omega_p^2} = \frac{E_x + \frac{\omega_c}{\omega} E_y}{\omega^2 - \omega_c^2} \right] \cos(\omega t \pm kx) \qquad (1.77)$$

$$\vec{\varepsilon}_y \left[\frac{\omega^2 - c^2k^2}{\omega^2} \frac{E_y}{\omega_p^2} = \frac{\frac{\omega_c}{\omega} E_x + E_y}{\omega^2 - \omega_c^2} \right] \sin(\omega t \pm kx) \qquad (1.78)$$

$$\vec{\varepsilon}_z \left[\frac{\omega^2 - c^2k^2}{\omega^2} \frac{E_z}{\omega_p^2} = \frac{E_z}{\omega^2} \right] \cos(\omega t \pm kx) \qquad (1.79)$$

The dispersion relations are obtained from this set of equations. The uniform magnetic field couples a transverse E_y and the longitudinal E_x components of the wave so a wave is never purely longitudinal, and is purely transverse only when $E_z \neq 0$ and $E_y = 0$. When the magnetic field is zero, $\omega_c = 0$, the wave types are uncoupled and

we obtain the dispersion relation for the longitudinal plasma waves from equation (1.77)

$$\omega^2 = \omega_p^2 \tag{1.80}$$

as before. The dispersion relation for the E_y component of the transverse electromagnetic waves is obtained from equation (1.78)

$$\omega^2 = c^2k^2 + \omega_p^2 \, . \tag{1.81}$$

When ω_p also equals zero it becomes the dispersion relation for an electromagnetic wave in free space

$$\omega^2 = c^2k^2 \tag{1.82}$$

which is also the dispersion relation for the wave with its electric field in the direction of the uniform magnetic field as obtained from equation (1.79).

When ω_c is not zero, the longitudinal and transverse waves tend to become uncoupled in the limit that ck becomes much larger than ω_p and ω_c. For the plasma waves in this experiment with a plate voltage of 600 volts, ck/ω equals 20.65. The ratio of the plasma electric field E_x to the small transverse electric field E_y accompanying the plasma wave is

$$\frac{E_x}{E_y} \approx \frac{\omega^2 - c^2k^2}{\omega^2} \frac{\omega}{\omega_c} = -425.5 \frac{\omega}{\omega_c} \tag{1.83}$$

The ratio $\frac{\omega}{\omega_c}$ ranges from 2 to about 14 so E_y is practically zero and the plasma wave is almost purely longitudinal. The dispersion relation for the plasma wave, from equation (1.77) is, as before,

$$\omega^2 = \omega_c^2 + \omega_p^2 \tag{1.84}$$

The oscillating plasma electrons radiate electromagnetic waves with an electric field component in the same direction as the plasma-wave electric field and which travel away from the plasma oscillations in the y and z directions. These electromagnetic waves have the same angular frequency, ω, as the plasma waves but have a different propagation constant k. For these electromagnetic waves ck is of the same order of magnitude as ω_p and ω_c. Thus the radiated electromagnetic wave traveling in the y direction is not a purely transverse wave while it is still in the plasma. Its wavelength while still in the plasma is found by choosing the correct root from the complete dispersion relation which is obtained by eliminating E_x and E_y from equations (1.77) and (1.78). Its wavelength after leaving the plasma region is the free space wavelength corresponding to its frequency $\frac{\omega}{2\pi}$, which is still the same as that of the plasma waves.

The radiated electromagnetic wave traveling in the z direction is purely transverse although very slightly elliptically polarized. The direction of polarization rotates about the z axis as the wave progresses.

The x, y, and z components of equation (1.58) are

$$\vec{\varepsilon}_x \left[0 = \frac{\omega^2}{c^2} H_x \right] \sin(\omega t \pm kx) \tag{1.85}$$

$$\vec{\varepsilon}_y \left[k^2 H_y = \mp en\omega k S_z + \frac{\omega^2}{c^2} H_y \right] \cos(\omega t \pm kx) \tag{1.86}$$

$$\vec{\varepsilon}_z \left[k^2 H_z = \pm en\omega k S_y + \frac{\omega^2}{c^2} H_z \right] \sin(\omega t \pm kx) \tag{1.87}$$

We see that $H_x = 0$ from equation (1.85) so there is no longitudinal component of magnetic field. Equations (1.86) and (1.87) give

$$H_y = \frac{\pm c^2 en\omega k}{\omega^2 - c^2k^2} S_z \tag{1.88}$$

$$H_z = \frac{\mp c^2 en\omega k}{\omega^2 - c^2k^2} S_y \tag{1.89}$$

The impedance presented to the transverse components of the wave by the plasma is

$$Z = \frac{E_y}{H_z} = \frac{-E_z}{H_y} = \mp \mu \frac{\omega}{k} = \mu v_{phase} \tag{1.90}$$

The energy flow associated with the transverse components of the wave is

$$\vec{W}_x = \vec{E}_y \times \vec{H}_z - \vec{E}_z \times \vec{H}_y = \mp \frac{k}{\mu\omega} \left[E_y^2 \sin^2 (\omega t \pm kx) \right.$$

$$\left. + E_z^2 \cos^2 (\omega t \pm kx) \right] = \frac{c^2 \epsilon}{v_{phase}} \left[E_y^2 \sin^2 (\omega t \pm kx) \right.$$

$$\left. + E_z^2 \cos^2 (\omega t \pm kx) \right] \qquad (1.91)$$

APPARATUS

The gas discharge tube

The gas discharge diode tube consists of an axial filament within a cylindrical anode whose axis coincides with the direction of the uniform magnetic field. The glass envelope has a ground tapered joint, sealed with silicone high-vacuum grease, so that the electrode structure may be changed easily.

The plates at the ends of the filament, shown in Figure (2.1), at filament potential, prevent the plasma electrons from leaving the plasma region along the magnetic field direction. The magnetic field restricts the plasma electron flow across the magnetic flux lines. Thus the combination of the end tabs, at a very negative potential with respect to the plasma potential, and the magnetic field, acts as an electron trap and keeps the plasma electrons in the region for a long time. If the end tabs were at plate potential the plasma would assume a potential a few tens of volts more positive than the end tabs and the electrons would be trapped just as effectively because they cannot leave the plasma at a greater rate than the positive ions.

The end tabs also prevent puncture of the glass envelope by the charged particles. With no end tabs the inner surfaces of the glass walls tend to become charged a few tens of volts negative with respect to the plasma potential which is approximately the same as the plate

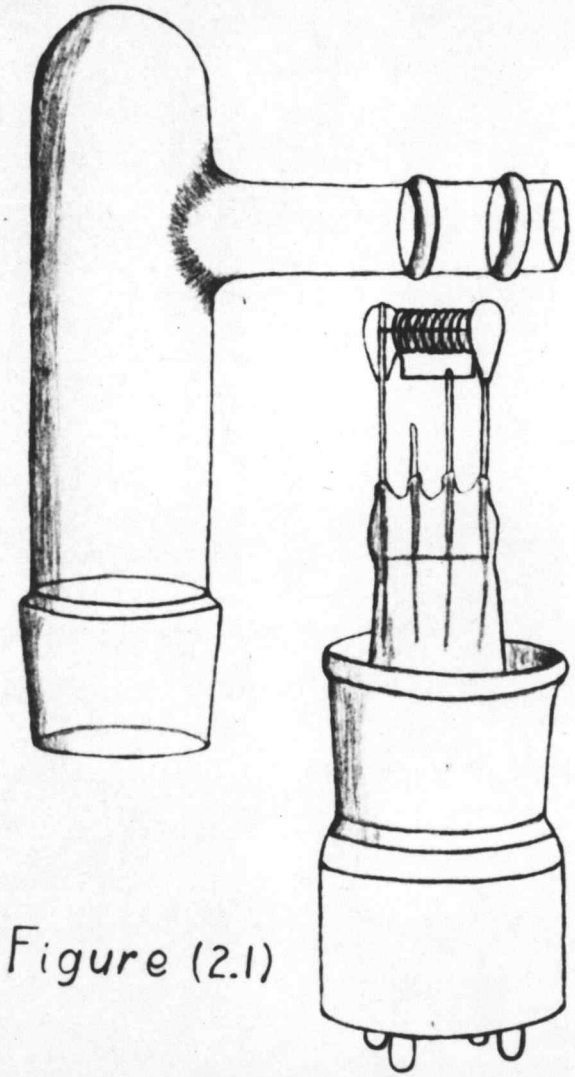

Figure (2.1)

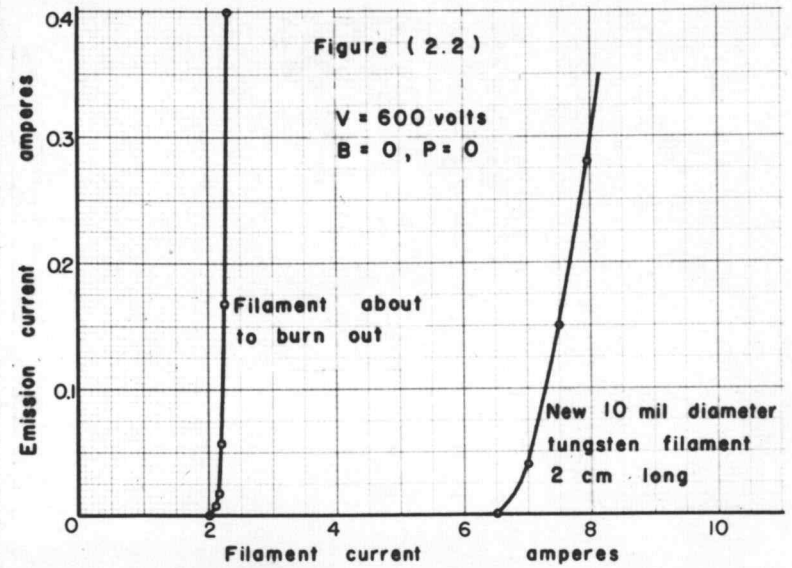
Figure (2.2)
V = 600 volts
B = 0 , P = 0
Emission current amperes
0.4
0.3
0.2
0.1
0
Filament about to burn out
New 10 mil diameter tungsten filament 2 cm long
2
4
6
8
10
Filament current amperes

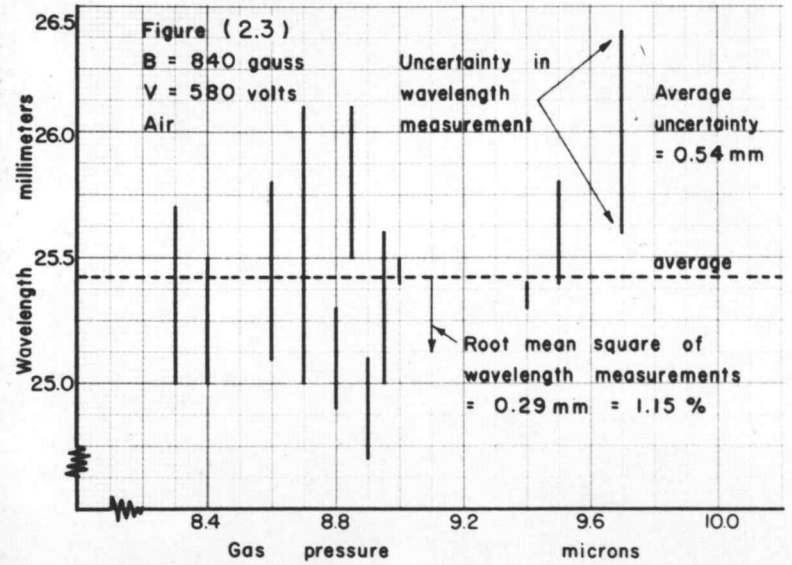
Figure (2.3)
B = 840 gauss
V = 580 volts
Air
Uncertainty in wavelength measurement
Average uncertainty = 0.54 mm
Wavelength millimeters
26.5
26.0
25.5
25.0
average
Root mean square of wavelength measurements = 0.29 mm = 1.15 %
8.4
8.8
9.2
9.6
10.0
Gas pressure microns

potential and several hundreds of volts more positive than the filament potential.

At the projections of the cathode space charge sheath on the glass envelope in the magnetic field directions, positive ions can arrive but plasma electrons cannot because the plasma electron motions are restricted to tight helices around magnetic flux lines. The inner surfaces of the glass walls there assume a potential a few tens of volts positive with respect to the plasma potential.

The potential distribution seems to act like an electron lens and focus some of the scattered, but still very energetic, emission electrons on the spots on the wall at the projections of the filament. The wall becomes heated in one spot, the glass softens and a puncture occurs.

Various anode structures were tried, such as helical coils of wire or cylindrical metal sheets of various sizes. A typical tube consists of a helical-coil anode 0.75 centimeters in diameter and 1.6 centimeters long, a 10 mil diameter tungsten filament 2 centimeters long, and end tabs 1 centimeter in diameter and 2 centimeters apart. The electrodes were spot welded to their supports. No magnetic materials were used for the electrodes and supports so there would be no distortion of the magnetic field.

The magnetic field

The magnetic field was produced by a Cenco No. 79,650 electromagnet operated from storage batteries. The magnetic flux density

could be varied from zero to 2500 gauss in either direction of field and was calibrated as a function of the magnet current by snatching a coil of known number of turns and effective area out of the magnetic field and reading the deflection of a Grassot fluxmeter. During the experiments the magnetic flux density was determined from the magnet current reading and the calibration curve. Two calibrations six months apart gave the same calibration curve. It was necessary to reverse the magnetic field several times at a constant current value to stabilize the hysteresis loop in order to get reproducible magnetic flux densities.

The gas system

A Distillation Products No. GF25W three stage fractionating oil diffusion pump with a Megavac forepump was used to obtain a vacuum of about one hundredth of a micron. This pressure was measured with an ionization gauge and a Pirani gauge zeroed at this value. Gas was then allowed to enter the vacuum system through a manually controlled leak which consisted of a pinch clamp on a piece of rubber hose with an 8 mil diameter wire inside. The wire inside made finer adjustment of the gas flow possible.

Since the gas pressure in the system is negligible compared to atmospheric pressure, the flow through the controlled leak is not a function of the pressure in the system and is only a function of the

effective area of the orifice. The gas pressure in the system is thus the pressure at which the pumping speed of the oil diffusion pump equals the gas flow through the leak.

The controlled leak gave good pressure control up to about 15 microns and satisfactory control to several hundred microns although slow pressure variations did exist. Above about 30 microns the forepump alone could maintain the vacuum. During the experiments the pressure was measured with a Pirani gauge which had been calibrated against a McLeod gauge and a calibration curve made.

The filament emission

A storage battery supplied the filament current. For a new 10 mil diameter tungsten filament the emission current could be varied from zero to about 0.3 amperes with a filament current variation from about six to eight amperes, as shown in Figure (2.2). Since the emission current is a steep function of the filament current, control of the latter is critical. Low frequency noise from the storage battery caused the filament current to be slightly unsteady.

The filament is heated by positive ion bombardment as well as by the filament current. Besides producing thermionic emission of electrons, this heat also evaporates the tungsten from the filament reducing the filament diameter and increasing its resistance during an experiment. This slow time variation of the emission characteristics of the filament makes the data unreproducible with respect to

the filament current. As the resistance increases, less filament current is required for the same heating of the filament and therefore the same emission current. Heat conduction to the filament supports cools the ends of the filament so that the tungsten evaporates from the center of the filament at a faster rate than at the ends. This increases the resistance of the center which increases the heating of the center relative to the ends. Thus the wasting away of the filament is a regenerative process causing burn-out at the center after one or two days of use. A typical emission characteristic just before the filament burns out is shown in Figure (2.2). Since the emission current is such a high powered function of the temperature, all the electronic emission comes from the center of the filament.

The electron density of the primary emission beam is probably small compared with the plasma electron density. From Figure (5.1) the plate current is about 70 milliamperes at 10 microns gas pressure for a plasma electron density of 10^{12} electrons per cubic centimeter. The emission current is about a quarter of the plate current, as shown by Figure (5.16). The cross sectional area of the primary emission beam is not known but if it is assumed to be 1 square millimeter, the 600 volt emission electron density is about 7.5×10^{9} electrons per cubic centimeter.

The pulsed anode voltage

The anode voltage was applied in pulses to make it possible to use alternating current amplifiers in the detecting system and to minimize the positive ion bombardment of the filament. The A.C. amplifiers avoid some of the low frequency crystal noise of the crystal detector as well as the inherent instability of D.C. amplifiers. In the audio frequency range the noise temperature of a silicon crystal is inversely proportional to the frequency (117, p. 193).

The temperature of the filament changed slightly during the pulse as the heating from positive ion bombardment added to the continuous heating from the filament current. Since the filament temperature increases slightly during a pulse the plasma electron density also increases during a pulse. Usually the change in plasma electron density is small enough so that only one oscillation mode occurs during the pulse and it occupies most of the pulse length but sometimes the plasma electron density changes enough to have two different modes on the pulse.

The pulse repetition rate of the anode voltage was 30 per second. The pulse voltage could be varied continuously from zero to 900 volts and the pulse length from 50 to 900 microseconds. The plate voltage pulser could supply a peak current of 2 amperes at 800 volts or 4 amperes at 700 volts. The corresponding average plate currents are 12 and 24 milliamperes respectively. The pulse voltage

was displayed on a monitoring cathode ray oscilloscope by using a 10 to 1 resistance-capacitance voltage divider. The pulse height and length on the monitoring oscilloscope were calibrated by means of a Tektronix Type 514 oscilloscope. The plate current meter, whose resistance is about 100 ohms, had a 0.01 farad capacitor in parallel with it so as to read the average of the pulsed plate current. The plate current during a pulse was then the average value times the reciprocal of the duty cycle of the pulses. A typical duty used was 30 pulses per second times 200 microseconds per pulse = 1/167. The plate current was directly proportional to the pulse duration so that the current emitted while the plate voltage was zero contributed nothing to the plate current during a pulse.

The microwave interferometer system

The wavelengths of the electromagnetic waves radiated by the oscillating plasma electrons were measured by an interferometer system which consisted of a 14 by 18 inch horizontal aluminum interferometer plate above the gas discharge tube. This was driven at constant speed on a vertical track by a synchronous motor. A thick dipole receiving antenna was placed a few inches above the gas discharge tube. The interferometer plate reflected some of the electromagnetic radiation from the tube and formed standing waves in the region around the dipole detector. This standing wave pattern moved with the interferometer plate so that a succession of maxima and

minima of intensity moved past the dipole receiving antenna. The speed of the interferometer plate was about 0.4 centimeters per second.

The receiver

Figure (2.4) shows the dipole receiving antenna. It is constructed from a 1N26 crystal by turning off the crystal skirt on a lathe and inserting the stem of the crystal into a cylindrical piece of metal the same size as the body of the crystal. This makes a cylindrical dipole 0.55 centimeters in diameter and 1.75 centimeters long which is a broadband antenna because of its relative thickness.

The crystal dipole antenna receives and rectifies the signal which is then amplified and displayed on a cathode ray oscilloscope. A typical signal display is shown in Figure (2.5). As the standing wave pattern moves at constant speed past the receiving antenna the operator observes the maxima and minima of the pattern on the oscilloscope and writes a pip for every maximum or minimum observed by pulsing a graphic ammeter. After ten to twenty pips are recorded, the operator can measure the average distance between pips and the variations from this average. The wavelength is then calculated using the ratio of the interferometer plate speed to the speed of the graphic ammeter paper and the fact that the minima or maxima of the standing wave pattern are a half wavelength apart.

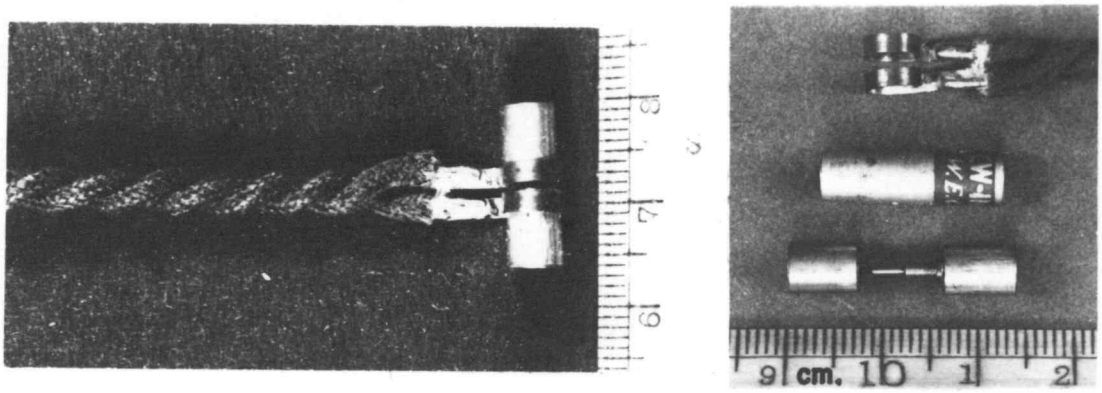

Figure (2.4)

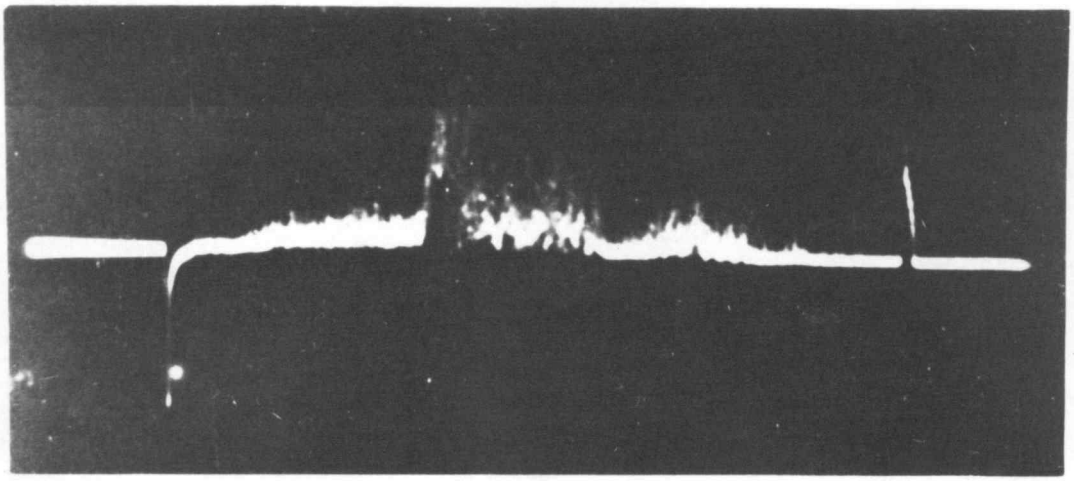

Figure (2.5)

The average uncertainty in the wavelength measurement when done carefully is about 0.5 millimeters; the root mean square deviation of the wavelength measurements is about 0.3 millimeters for an oscillation of wavelength equal to 25.4 millimeters, as shown in Figure (2.3).

The receiving amplifier gain was continuously variable from 40 to 1.6×10^7 but the range used was from 10^3 to 10^5. For the radiation intensity measurements the gain of the antenna was calculated and the gain of the amplifier calibrated with the Tektronix oscilloscope. The amplifier bandwidth was about 10 cycles per second to about 2 megacycles per second.

Figure (2.6) shows a schematic diagram of the experimental arrangement. Figure (2.7) is a photograph of the apparatus. The gas discharge tube is shown at (A) between the pole pieces of the magnet (B) which is on the vacuum system table (C). The interferometer plate on its vertical track is shown at (D). Below the battery charger at (E) is the bank of storage batteries supplying current to the magnet, the experimental tube filament, and the preamplifier filaments. The preamplifier is at (F) and the oscilloscopes are at (G) on the console table (H) which also contains most of the measuring equipment and control devices within reach of the operator. Footpedals on the floor under the table control the interferometer plate motion. A tank of gas is shown at (I) from which gas is allowed to flow into the vacuum system through the manually controlled leak at (J). The bay (K) contains power supplies and the plate voltage pulsing equipment. The graphic ammeter is at (L).

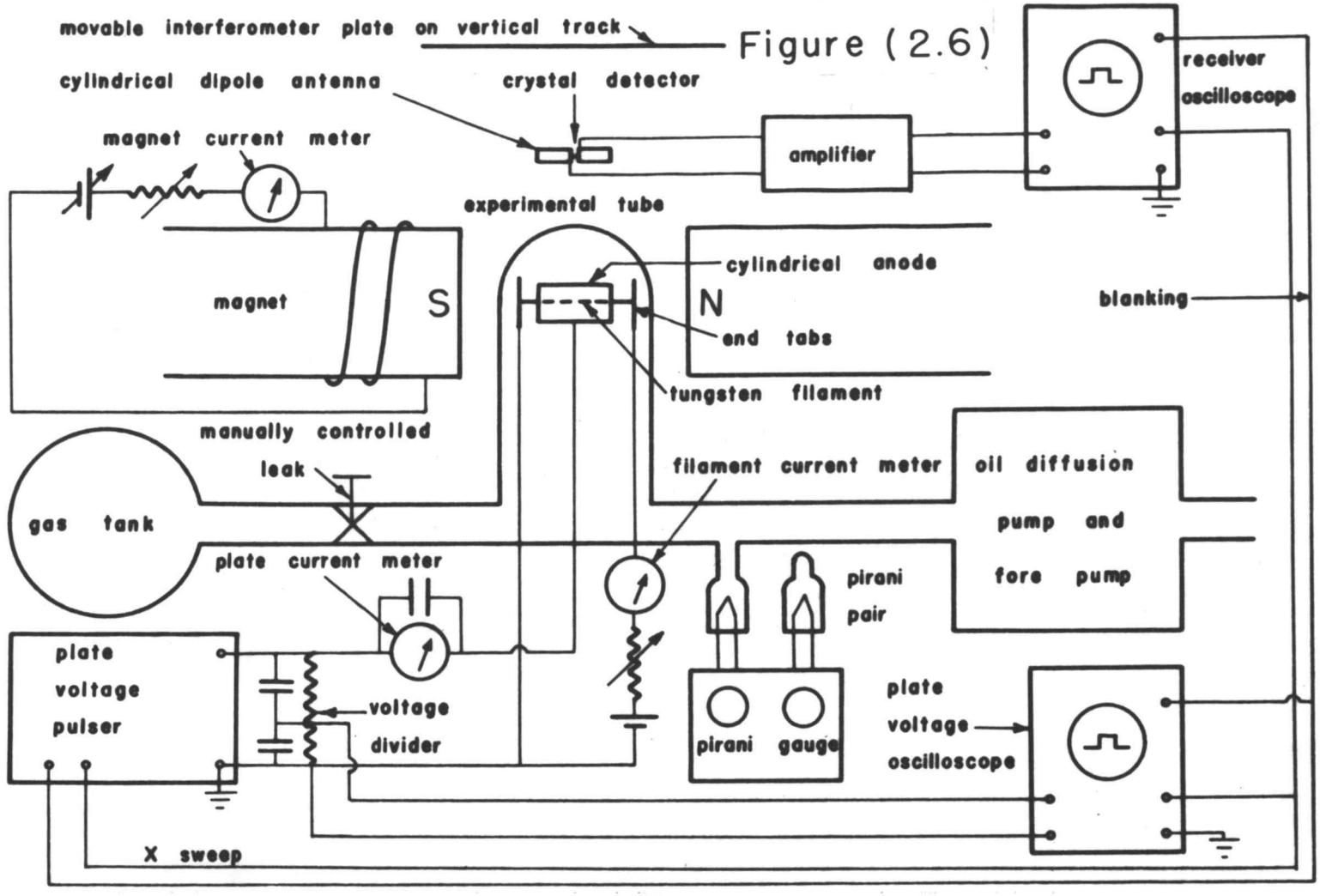
movable interferometer plate on vertical track
cylindrical dipole antenna
crystal detector
magnet current meter
amplifier
receiver oscilloscope
experimental tube
cylindrical anode
magnet
S
N
end tabs
blanking
tungsten filament
manually controlled
leak
filament current meter
oil diffusion pump and fore pump
gas tank
plate current meter
pirani pair
plate voltage pulser
voltage divider
pirani gauge
plate voltage oscilloscope
X sweep

Figure (2.6)

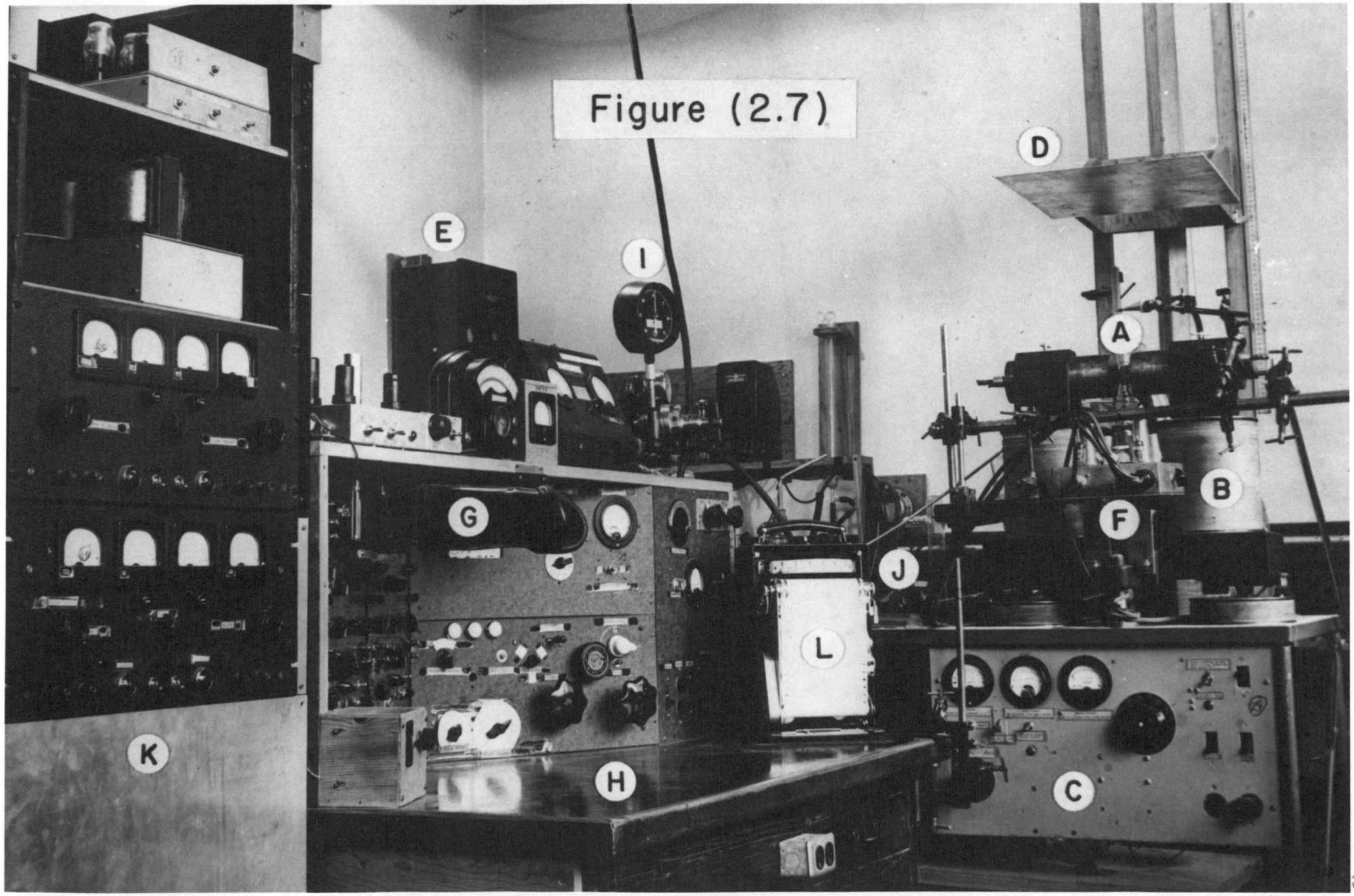
Figure (2.7)
A
B
C
D
E
F
G
H
I
J
K
L

STEADY STATE CHARACTERISTICS OF THE GAS DISCHARGE

Kinetic theory calculations for plasma electrons

Before considering the experimental observations of plasma oscillations let us first consider the steady state properties of the gas discharge upon which the plasma oscillations are superimposed. The plasma potential, plasma electron density and positive ion density are approximately constant throughout the plasma region. Let us make some kinetic theory order of magnitude calculations.

Probe measurements, which are discussed later, measured a plasma electron temperature T_- of about 154,600°K. At this temperature the average thermal energy eV_- of the plasma electrons is 20 electron volts and its thermal root mean square velocity $\left[\overline{v_-^2}\right]^{1/2}$ is 2.66×10^8 centimeters per second. The relation between these quantities is

$$eV_- = \frac{3}{2} kT_- = \frac{1}{2} m \overline{v_-^2}$$

$$= \frac{1}{2} m \left[\overline{v_x^2} + \overline{v_y^2} + \overline{v_z^2}\right] = \frac{1}{2} m \left[\overline{v_\perp^2} + \overline{v_{\parallel}^2}\right] \qquad (3.01)$$

where k is Boltzmann's constant, v_x, v_y, v_z are the components of the thermal velocity in the x, y, z directions respectively, and $v_\perp$ and $v_{\parallel}$ are the components of the thermal velocity perpendicular

and parallel to the magnetic field direction respectively. Let the magnetic field be in the z direction. Then

$$\overline{v_x^2} + \overline{v_y^2} = \overline{v_\perp^2} \quad \text{and} \quad \overline{v_z^2} = \overline{v_{//}^2}$$

An electron with thermal energy in a region containing a magnetic field, but no electric field, moves in a tight helical path around a magnetic flux line as shown in Figure (3.1). Because of the equipartition of energy, on the average, one third of the energy is in the translational motion in the magnetic field direction and two thirds of the energy is in the translational motion in a plane perpendicular to the magnetic field direction.

$$\frac{1}{2} kT_- = \frac{1}{2} m \overline{v_{//}^2} \tag{3.02}$$

$$kT_- = \frac{1}{2} m \overline{v_\perp^2} \tag{3.03}$$

The force on an electron in a magnetic field, but not in an electric field, is

$$\vec{f} = -e\vec{v}_- \times \vec{B} = \vec{f}_\perp \tag{3.04}$$

where $\vec{B}$ is the magnetic flux density and is in the z direction. Because of the vector product the force in the z direction $f_{//}$ is zero; the z component of the velocity $v_{//}$ remains unchanged. The

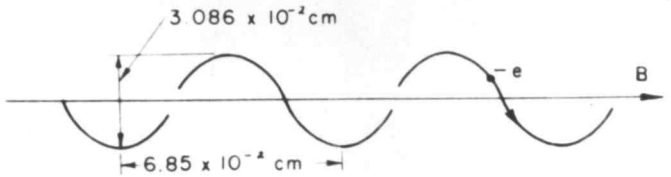

Figure (3.1)

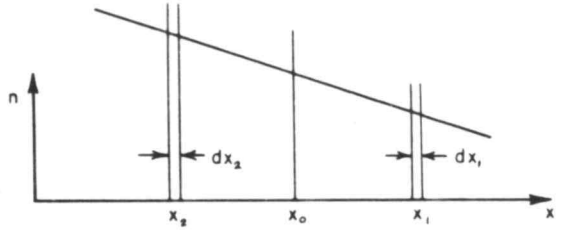

Figure (3.2)

Figure (3.3)

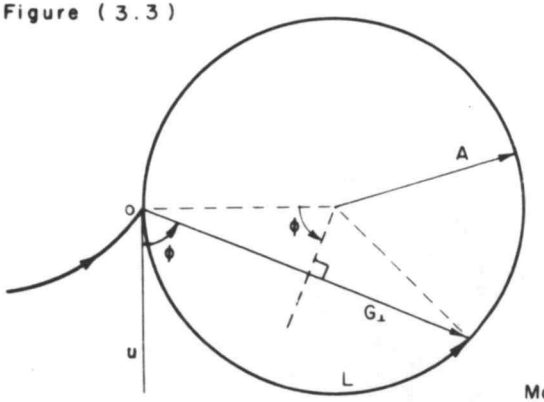

Magnetic flux
out of page

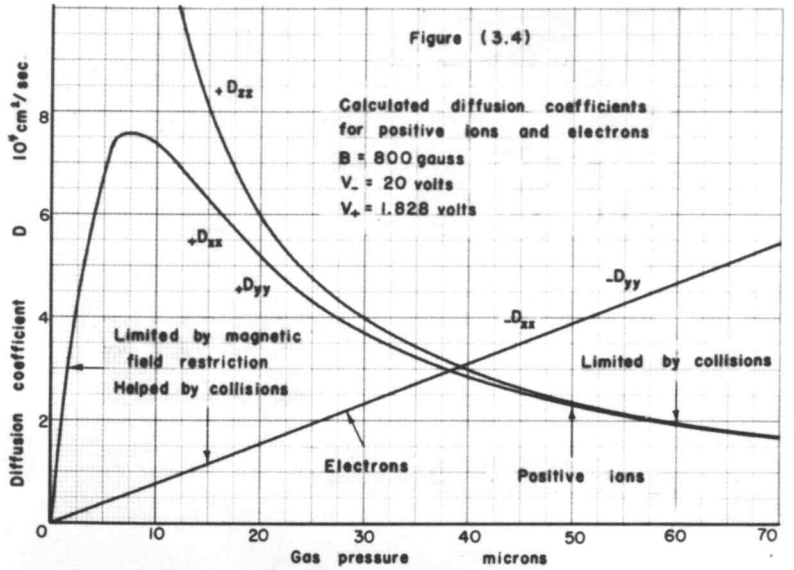

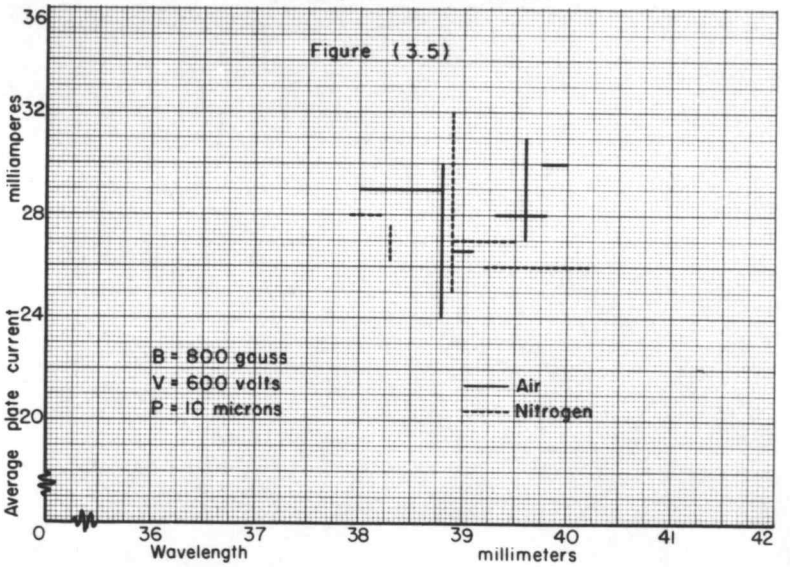

force in the x, y plane $\overrightarrow{f_\perp}$ causes the electron to rotate around an axis in the z direction with an angular frequency equal to the cyclotron angular frequency for electrons, ω_c.

$$|f_\perp| = mv_\perp \omega = ev_\perp B \tag{3.05}$$

$$\omega_c = \frac{eB}{m} \tag{3.06}$$

For a typical magnetic flux density of 8×10^{-2} webers per square meter, or 800 gauss, the cyclotron angular frequency for electrons is 1.407×10^{10} radians per second.

The radius $\sqrt{\overline{A^2}}$ of the helical paths of the plasma electrons with average energy is given by

$$\sqrt{\overline{A^2}} = \frac{\sqrt{\overline{v_\perp^2}}}{\omega_c} \tag{3.07}$$

where $\sqrt{\overline{v_\perp^2}} = \sqrt{\frac{2}{3}}\sqrt{\overline{v_-^2}} = 2.17 \times 10^8$ centimeters per second from equation (3.03). The radius $\sqrt{\overline{A^2}}$ of the average thermal circle is thus only 1.543×10^{-2} centimeters.

The mean free path of electrons L_- between collisions with neutral gas molecules of density n_g is given by the simple kinetic theory.

$$L_- = \frac{4}{n_g \pi D_m^2} \tag{3.08}$$

where D_m is the molecular diameter of the gas. Using 3.1×10^{-8} centimeters for the diameter of a nitrogen molecule as given by Spangenberg (120, p. 754), the electronic mean free path is 4.04 centimeters at a gas pressure of 10 microns.

The mean free time τ_- between collisions of the plasma electrons with gas molecules and the collision rate θ_- is given by

$$\tau_- = \frac{L_-}{v_-} = \frac{1}{\theta_-} \tag{3.09}$$

where for simplicity in the calculations no distinction is made between average velocity and root mean square velocity. The mean free time of the plasma electrons at 10 microns pressure is thus 1.52×10^{-8} seconds per collision and the collision rate 6.6×10^{7} collisions per second. A plasma electron makes 1.32×10^{4} collisions during a 200 microsecond pulse. Thus the average plasma electron makes 34 helix revolutions per collision.

The mean free path L_- of the plasma electrons is measured along the helical path. The distance traveled in the magnetic field direction $L_{\parallel}$ by the average plasma electron is

$$L_{\parallel} = \tau_- v_{\parallel} = \sqrt{\frac{1}{3}}\, L_- \tag{3.10}$$

The mean free path in the z direction is 2.33 centimeters.

The component of velocity in the z direction is reversed when the electron comes to the edge of the space charge sheath at the end

tabs. These reflections at the end tab space charge sheaths cause a plasma electron to move back and forth between the end tabs in a tight helical path around the same magnetic flux line until a collision with a gas molecule changes the axis of its helical path to another magnetic flux line which is at most the helical diameter (3.086×10^{-2} centimeters) away from the pre-collision axis. The progress of the electrons across the magnetic field thus is very much reduced by the field and becomes less than that of the slower and much heavier positive ions in the pressure range and magnetic flux density range used. Collisions with gas molecules let the plasma electrons progress across the magnetic field. The diffusion coefficient is thus a function of the magnetic flux density and the gas pressure.

A charged particle starting from rest in uniform magnetic and electric fields perpendicular to each other follows a cycloidal path. The displacement in the electric field direction for an electron is

$$y = -\frac{m}{e}\frac{E}{B^2}\left(1 - \cos\frac{eB}{m}t\right) \tag{3.11}$$

The average displacement is

$$\bar{y} = -\frac{m}{e}\frac{E}{B^2} = \frac{y_{max}}{2} \tag{3.12}$$

The drift velocity w is the average displacement times the collision rate which also equals the mobility times the electric field strength

$$w = \bar{y}\theta = \mu E \tag{3.13}$$

For a magnetic flux density of 800 gauss the drift velocity for electrons, below about two millimeters of Hg gas pressure, is

$$w = 58.7\ E/\left(\frac{\text{volts}}{\text{cm}}\right)\ P/(\text{microns})\ \frac{\text{cm}}{\text{sec}} \tag{3.14}$$

Without a magnetic field the simplest kinetic theory gives the drift velocity as

$$w = \frac{eE}{m\theta} = 2.66 \times 10^{8}\ \frac{E/\left(\frac{\text{volts}}{\text{cm}}\right)}{P/(\text{microns})}\ \frac{\text{cm}}{\text{sec}} \tag{3.15}$$

which yields about one half the experimental value. For example, $w = 5 \times 10^{6}$ centimeters per second for electrons in nitrogen at $\frac{E}{P} = 10$ volts/cm/mm of Hg as given by Rossi and Staub (112, p. 9). The electron mobility transverse to the magnetic field is thus reduced by a factor of the order of 50,000 for B = 800 gauss and P = 10 microns. Increasing the gas pressure increases the electron mobility with a magnetic field but decreases the mobility with zero magnetic field.

The relation between the diffusion coefficients D and the mobilities μ is

$$\frac{D_{xx}}{\mu_{xx}} = \frac{D_{yy}}{\mu_{yy}} = \frac{D_{zz}}{\mu_{zz}} = \frac{kT}{-e} \tag{3.16}$$

$$\frac{D_{xx_+}}{\mu_{xx_+}} = \frac{D_{yy_+}}{\mu_{yy_+}} = \frac{D_{zz_+}}{\mu_{zz_+}} = \frac{kT_+}{e} \tag{3.17}$$

so the mobilities are from equation (3.35)

$$\mu_{xx_-} = \frac{-e}{m_-} \frac{\theta_-}{\theta_-^2 + \omega_{c_-}^2} \tag{3.18}$$

$$\mu_{xx_+} = \frac{e}{m_+} \frac{\theta_+}{\theta_+^2 + \omega_{c_+}^2} \tag{3.19}$$

These vary in the same way with pressure as the diffusion coefficients shown in Figure (3.4).

Effective mean free paths

The mean square effective free path in the x direction $\overline{G_x^2}$, due to collisions with gas molecules and magnetic field restriction, is now calculated.

Figure (3.3) shows the projection of the helical path of an electron onto a plane perpendicular to the magnetic field. The electron suffers a collision at O and then starts out in a direction whose projection is in the direction U. The projection of its path describes this thermal circle of radius A until the next collision. The path length along the cyclotron orbit is s; $G_\perp$ is the distance

between the particle position projection and the position of the last collision and ϕ the angle between $G_\perp$ and the projection of the initial direction after the last collision.

From the geometry of the figure,

$$G_\perp^2 = 2A^2 (1 - \cos 2\phi) \tag{3.20}$$

and

$$s = 2A\phi \tag{3.21}$$

The electron projection travels along the thermal cyclotron orbit with constant velocity $v_\perp$ between collisions. The probability that an electron will travel a distance s or more is $\exp(-\frac{s}{L_\perp})$ where $L_\perp$ is the mean free path in the transverse plane due to collisions alone. The probability that an electron will travel a distance s and then suffer a collision in the next ds is

$$\exp(-\frac{s}{L_\perp}) - \exp(-\frac{s + ds}{L_\perp}) = \exp(-\frac{s}{L_\perp}) \frac{ds}{L_\perp} \tag{3.22}$$

The mean square of the effective free path in the transverse plane $\overline{G_\perp^2}$ is given by the square of the distance $G_\perp$ times the probability of having this effective free path integrated over the whole range of the path length and the thermal velocity distribution.

$$\overline{G_\perp^2} = \int_0^\infty \int_0^\infty G_\perp^2 \exp(-\frac{s}{L_\perp}) \frac{ds}{L_\perp} 2\beta^2 v_\perp \exp(-\beta^2 v_\perp^2) dv_\perp \tag{3.23}$$

From equations (3.20) and (3.21)

$$\overline{G_\perp^2} = \int_0^\infty \int_0^\infty \frac{2 v_\perp^2}{\omega_c^2} \left(1 - \cos \frac{\omega_c s}{v_\perp}\right) \exp\left(-\frac{s}{L_\perp}\right) \frac{ds}{L_\perp}$$

$$2 \beta^2 v_\perp \exp\left(-\beta^2 v_\perp^2\right) dv_\perp \qquad (3.24)$$

where $\beta^2 = \frac{m}{2kT_-}$. For a constant mean free time $\tau = \frac{L_\perp}{v_\perp}$ with respect to the velocity distribution, the integrals are easily evaluated. The solution is

$$\overline{G_\perp^2} = \frac{2 \overline{L_\perp^2}\ \overline{A^2}}{\overline{L_\perp^2} + \overline{A^2}} = \frac{2}{\frac{1}{\overline{A^2}} + \frac{1}{\overline{L_\perp^2}}} \qquad (3.25)$$

where

$$\overline{v_\perp^2} = \frac{1}{\beta^2} = \frac{2kT_-}{m} = \frac{2}{3}\ \overline{v_-^2} \qquad (3.26)$$

When the collision mean free path L is large compared with the mean radius of the thermal circle A, which may also be called the magnetic mean free path, the mean square effective free path $\overline{G_\perp^2}$ equals $\overline{2A^2}$ and when $A \gg L$, $\overline{G_\perp^2}$ equals $2\ \overline{L_\perp^2}$. The mean square effective transverse free path $\overline{G_\perp^2}$ has components in the x and y directions,

$$\overline{G_\perp^2} = \overline{G_x^2} + \overline{G_y^2} = 2\ \overline{G_x^2}\ . \qquad (3.27)$$

Diffusion coefficients

The collisions start the electrons off in a new random direction so the new helical axis is in a random direction. If there is an electron density gradient, more of the electrons in the higher density region are displaced by the collisions into the lower density region than are displaced by the collisions from the lower to the higher density region. A diffusion current then flows according to the equation

$$\vec{J}_- = + e \overrightarrow{\overrightarrow{D}}_- \nabla n_- \qquad (3.28)$$

where $\overrightarrow{\overrightarrow{D}}_-$ is the diffusion coefficient, which will now be calculated.

Referring to Figure (3.2), the number of particles per second which suffer a collision at position x_2 in a volume dx_1 dy dz an x distance $(x_1 - x_2)$ away from position x_2, is equal to the number of particles in the volume at position x_2, $\left[n\Big|_{x_o} - \frac{\partial n}{\partial x}\Big|_{x_o} (x_o - x_2) \right]$ dx_2 dy dz, times the collision rate θ times the probability that a particle will travel a distance $(x_1 - x_2)$ and then suffer a collision in dx_1, $1/4 \exp\left\{ - \frac{x_1 - x_2}{G_x} \right\} \frac{dx_1}{G_x}$, where G_x is the x component of the effective mean free path. One factor of 1/2 is introduced because only 1/2 of the particles on the average travel toward x_1, the other half traveling away from x_1 after a collision in dx_2. The other factor of 1/2 is the projected area of a unit surface at $x = x_o$ averaged over all angles of incidence. The net number of particles

per second transferring between positions x_1 and x_2 is this expression minus a similar expression representing the transfer of particles in the reverse direction. The total current density through position x_o is the integral of this expression with x_2 integrated from $-\infty$ to x_o and x_1 integrated from x_o to ∞, divided by the area dy dz, multiplied by the charge on the particles, -e for electrons, and averaged over the velocity distribution.

$$J_x = -e \int_{x_2=-\infty}^{x_o} \int_{x_1=x_o}^{\infty} \left\{ \left[n\Big|_{x_o} - \frac{\partial n}{\partial x}\Big|_{x_o} (x_o - x_2) \right] \right.$$

$$\left. - \left[n\Big|_{x_o} + \frac{\partial n}{\partial x}\Big|_{x_o} (x_1 - x_o) \right] \right\} \theta \, \frac{1}{4} \exp\left\{ - \frac{x_1 - x_2}{G_x} \right\} \frac{dx_1 dx_2}{G_x} \qquad (3.29)$$

$$= \int_{-\infty}^{x_o} \int_{x_o}^{\infty} e \frac{\partial n}{\partial x}\Big|_{x_o} \frac{\theta}{4} (x_1 - x_2) \exp\left\{ - \frac{x_1 - x_2}{G_x} \right\} \frac{dx_1 dx_2}{G_x} \qquad (3.30)$$

The solution of this equation is obtained by integrating by parts twice.

$$J_x = e \, \frac{\overline{G_x^2}\,\theta}{2} \, \frac{\partial n}{\partial x}\Big|_{x_o} \qquad (3.31)$$

where $\overline{G_x^2}$ is the mean square effective free path in the x direction.

Because of the magnetic field the medium is anisotropic to diffusion and the diffusion coefficient is a tensor. The quantity $\frac{\overline{G_x^2}\,\theta}{2}$ in equation (3.31) is the D_{xx} component of the diffusion coefficient tensor.

$$D_{xx} = \frac{\overline{G_x^2}\,\theta}{2}, \quad D_{yy} = \frac{\overline{G_y^2}\,\theta}{2}, \quad D_{zz} = \frac{\overline{G_z^2}\,\theta}{2} \tag{3.32}$$

The diffusion coefficient D_{xx} becomes

$$D_{xx} = \frac{\overline{G_\perp^2}\,\theta}{4} = \frac{1}{2}\,\frac{\overline{L_\perp^2}\;\overline{A^2}}{\overline{L_\perp^2} + \overline{A^2}}\,\theta_- = D_{yy} \tag{3.33}$$

When the collision mean free path is long compared with the helical path radius, the collisions help the diffusion across the magnetic field. When the collision mean free path is short compared with the helix radius, the diffusion across the field is hindered by the collisions.

The transverse collision mean free path $L_\perp$ is

$$L_\perp = \tau_- v_\perp = \sqrt{\frac{2}{3}}\; L_- = \frac{v_\perp}{\theta_-} \tag{3.34}$$

so D_{xx} can be written

$$D_{xx} = \frac{\overline{v_\perp^2}}{2} \frac{\theta_-}{\theta_-^2 + \omega_c^2} = \frac{1}{3} \overline{v_-^2} \frac{\theta_-}{\theta_-^2 + \omega_{c_-}^2} = D_{yy} \tag{3.35}$$

$$D_{zz} = \frac{\overline{G_\parallel^2}\,\theta_-}{2} = \overline{L_\parallel^2}\,\theta_- = \frac{1}{3} \overline{v_-^2}\, \frac{1}{\theta_-} \tag{3.36}$$

since

$$\overline{G_\parallel^2} = \int_0^\infty s^2 \exp\left\{ - \frac{s}{L_\parallel} \right\} \frac{ds}{L_\parallel} = 2\, \overline{L_\parallel^2} \tag{3.37}$$

From equation (3.08)

$$L_- = \frac{4kT}{\pi D_m^2 P} \tag{3.38}$$

and

$$\theta_- = \frac{v_-}{L_-} = \frac{v_- \pi D_m^2 P}{4kT} = 6.59 \times 10^6 \text{ P/(microns)} \frac{\text{collisions}}{\text{sec}} \tag{3.39}$$

Equation (3.35) becomes

$$D_{xx} = D_{yy} = \frac{1}{3} \frac{(2.66 \times 10^8 \text{ cm/sec})^2\, 6.59 \times 10^6 \text{ P}}{(6.59 \times 10^6 \text{ P collisions/sec microns})^2}$$

$$\frac{\text{collisions/sec microns}}{+ (1.407 \times 10^{10} \text{ radians/sec})^2} = 7.86 \times 10^2 \text{ P/(microns)} \frac{\text{cm}^2}{\text{sec}} \tag{3.40}$$

below a few millimeters gas pressure, and is plotted as a function of pressure, along with the diffusion coefficients for the positive ions, in Figure (3.4).

Negative ion formation

Let us consider the possibility of negative ion formation in the discharge. For electrons below about one electron volt an attachment process is

$$O_2 + e \rightarrow (O_2^-)^* \qquad (3.41)$$

where the negative molecular oxygen ion is vibrationally excited and must be stabilized by collision deactivation. The attachment probability for this process is about 1.2×10^{-4} attachments per collision at 0.5 electron volts as shown by Massey (87, pp. 58-63). A second attachment involving electrons with energies of one electron volt to about three electron volts is

$$O_2 + e \rightarrow (O_2^-)' \qquad (3.42)$$

which can be interpreted as arising from capture to a higher electronic state, or states, of O_2^- with subsequent collision stabilization. This process has an attachment probability of about 3.7×10^{-4} per collision at 2.0 electron volts.

A third attachment process which occurs for electrons with energies of about three electron volts to ten electron volts is

$$O_2 + e \rightarrow O^- + O \tag{3.43}$$

where the products are unexcited. This process has a cross section σ_c of about 8×10^{-19} square centimeters. A fourth attachment process occurring for electrons with energies from about ten electron volts to nineteen electron volts is

$$O_2 + e \rightarrow O^- + O' \ (^5S^o) \tag{3.44}$$

where the oxygen atom is in an excited state. The cross section σ_d is about 1.3×10^{-20} square centimeters. Above about nineteen electron volts some negative atomic oxygen ions are formed by the process

$$O_2 + e \rightarrow O^- + O^+ + e \tag{3.45}$$

with a cross section σ_e of about 2.2×10^{-19} square centimeters but this does not subtract from the plasma electron density.

For water vapor, attachment sets in at mean energies of about 0.1 electron volts and rises steadily with increasing energy up to about three electron volts above which the attachment coefficient remains approximately constant at about 10^{-3} attachments per collision. The process responsible for the high energy attachment

is probably

$$H_2O + e \rightarrow H + OH^- \tag{3.46}$$

For the 20 electron volt plasma electron energy distribution, process (3.43) yields the most attachments. The attachment rate is about

$$\gamma_{o_2} = \sigma_c \, v \, n_{o_2} = 6960 \text{ attachments per second} \tag{3.47}$$

for 5 electron volt electrons at 10 microns, where n_{o_2} is the number of oxygen molecules per cubic centimeter and σ_c the attachment cross section for process (3.43). At 22 degrees centigrade the saturated vapor pressure of water is 26.44 millibars or 2.61 percent of the gas molecules are water molecules. The attachment rate is

$$\gamma_{H_2O} = P_{H_2O} \frac{v}{L_{H_2O}} = 857 \text{ attachments per second} \tag{3.48}$$

for 5 electron volt electrons where P_{H_2O} is the attachment probability per collision with a water molecule and L_{H_2O} is the mean free path between collisions with water molecules. The attachment to water molecules occurs over a greater energy range than the attachment to oxygen molecules so the total attachments to water and oxygen are probably roughly the same.

The mean square displacement of the plasma electrons in a direction transverse to the magnetic field after a time t is given by

$$\overline{x^2} = D_{xx}\, t \tag{3.49}$$

where D_{xx} is the diffusion coefficient for electrons in a direction transverse to the magnetic field. After a time equal to the average life of an electron before attachment, $t = \frac{1}{\gamma} \approx \frac{1}{2\gamma_{o_2}}$ the root mean square displacement is 0.751 centimeters or about two times the plate radius for an electron distribution of 20 electron volts average energy and a magnetic flux density of 800 gauss.

Very few of the plasma electrons attach to electronegative molecules before being collected by the plate. This is shown experimentally by the oscillations with the same wavelengths, and therefore the same plasma electron densities, giving the same plate currents, within the experimental accuracy, for both air and commercial tank nitrogen as in Figure (3.5). The diffusion coefficients and mobilities are different for electrons and negative ions so the same plasma electron densities should give different plate currents if negative ion formation were appreciable. The ionization probabilities for air and nitrogen are the same above about 40 electron volts and nearly the same down to their ionization energies so the emission current required to give a certain ionization rate is about the same for both gases.

Since the angular cyclotron frequency for electrons is larger than the collision frequency below a few millimeters gas pressure equation (3.49) becomes

$$\overline{x^2} = \frac{1}{3} \frac{\overline{v_-^2}\,\theta_-}{\omega_c^2} \frac{1}{P'\theta_-'} \tag{3.50}$$

where P' is the attachment probability per collision and θ_-' the collision rate with electronegative molecules. Both θ_- and θ_-' are proportional to the pressure so the mean square displacement before attachment is not a function of the gas pressure below about a millimeter of mercury gas pressure. The root mean square displacement before attachment however decreases with increasing magnetic flux density and at higher flux densities electron attachment forming negative ions becomes appreciable. The negative ion formation subtracts from the plasma electron density.

In an encounter with a metal, a negative ion can lose its electron easily to the metal provided the work function of the metal is greater than the detachment energy of the ion. For in this case there is an unoccupied level for the electron in the metal, with energy equal to that of the level which it occupies in the ion, and the transfer will be a resonance phenomenon.

No reliable data on the recombination of electrons with positive ions are available. The approximate value of the recombination constant for electrons in argon is stated by Rossi and Staub (112, p. 14) to be $\beta = 2 \times 10^{-10}$ cubic centimeters per second. The values of β for other gases do not seem to differ materially from that relative to argon. For a plasma electron density of 10^{12} electrons per cubic centimeter this gives a recombination rate of 200 per

second. The recombination rate exceeds the attachment rate when the plasma electron density exceeds about 7×10^{13} electrons per cubic centimeter.

Kinetic theory calculations for positive ions

Measurements of the current to the end tabs during an oscillation give positive ion velocities of about 5×10^5 centimeters per second. This gives a positive ion average energy of 1.8 electron volts and a positive ion temperature of 14,120°K. The cyclotron angular frequency is 5.48×10^5 radians per second for atomic air ions in a magnetic flux density of 800 gauss. The radius of the helical path of a positive ion of average energy is 0.745 centimeters or about equal to the anode diameter. The mean free path of the neutral gas molecules is $L_g = \frac{L_-}{\sqrt{2}\,4}$. Using this value for the mean free path of the ions, the result is 0.715 centimeters so the magnetic field doesn't affect the positive and negative ion motions very much. The positive ion collision rate is 7.0×10^5 collisions per second or 140 collisions per 200 microsecond pulse.

The air atomic positive ion drift velocity is

$$w_i = 9.77 \times 10^5 \; \frac{E/(\frac{\text{volts}}{\text{cm}})}{P/(\text{microns})} \; \frac{\text{cm}}{\text{sec}} \qquad (3.51)$$

for gas pressures above about 10 microns of mercury. The positive

ion mobility is larger than the electron mobility for pressure less than 40 microns.

The positive ion diffusion coefficient in a direction transverse to the magnetic field is

$$D_{xx+} = \frac{\overline{v_+^2}\,\theta_+}{3(\theta_+^2 + \omega_c^2)} = D_{yy+}$$

$$= \frac{5.83 \times 10^{15}\ P/(\text{microns})}{4.9 \times 10^{9}\ P^2/(\text{microns})^2 + 3 \times 10^{11}}\ \frac{cm^2}{sec} \qquad (3.52)$$

$$D_{zz+} = \frac{\overline{v_+^2}}{3\theta_+} = \frac{1.19 \times 10^{6}}{P/(\text{microns})}\ \frac{cm^2}{sec} \qquad (3.53)$$

These diffusion coefficients are shown as a function of the gas pressure in Figure (3.4).

The gas temperature correction for the Pirani gauge

An error in the pressure measurements results when the Pirani gauge is calibrated at room temperature and then used at a higher gas temperature as in the arc discharge during an experiment. The gas at higher than room temperature causes the same cooling of the Pirani resistance wire in the vacuum system as the gas at a lower

pressure and temperature. The Pirani gauge thus reads too low a pressure for the heated gas.

The rate of heat loss from the Pirani resistance wire to the gas is equal to the product of the energy lost per collision of a gas molecule with the wire, which is proportional to the temperature difference between the wire and gas, and the number of collisions per second, which is proportional to the product of the velocity of the gas molecules and the gas density. By equating the rate of cooling of the resistance wire, at an absolute temperature T_2, by the gas at absolute room temperature T_o to that of the gas at a higher absolute temperature T_1, we obtain the ratio of the true pressure P_1, of the gas at the higher temperature, to the pressure reading P_o of the Pirani gauge calibrated at room temperature.

$$\frac{P_1}{P_o} = \frac{T_2 - T_o}{T_2 - T_1} \left[\frac{T_1}{T_o}\right]^{1/2} \tag{3.54}$$

The temperature of the Pirani resistance wire is about 400 degrees centigrade. The gas temperature during an experiment, with a typical value of plate current during a pulse of forty milliamperes, was about 60 degrees centigrade as measured by a thermometer inside the envelope about one inch away from the tube electrodes. For a gas temperature T_1 of 70 degrees centigrade, which corresponds to a peak plate current of about 160 milliamperes and a room temperature T_o of 22 degrees centigrade, the pressure ratio $\frac{P_1}{P_2}$ is 1.23.

A more fundamental quantity for the kinetic theory calculations is the gas density since it determines the mean free paths of the charged particles in the gas discharge. The ratio of the true gas density n_1, to the gas density n_o, calculated from the measured pressure P_o and the room temperature T_o, is

$$\frac{n_1}{n_o} = \frac{T_2 - T_o}{T_2 - T_1} \sqrt{\frac{T_o}{T_1}} \tag{3.55}$$

For a gas temperature of 70 degrees centigrade this gas density ratio is 1.06. The error in the mean free path calculations caused by using the measured pressure P_o and the room temperature T_o instead of the true pressure P_1 and the true temperature T_1 is thus of the same order of magnitude as other kinetic theory approximations.

From the equation of state

$$P_1 V = NkT_1 \tag{3.56}$$

where P_1 is the pressure exerted by N gas molecules in a volume V and with a gas temperature T_1, the molecular density of the gas is given by

$$n_g = \frac{N}{V} = \frac{P_1}{kT_1} \approx \frac{P_o}{kT_o} \tag{3.57}$$

For a typical measured pressure P_o of 10 microns of mercury at a room

temperature T_o of 295°K the molecular density is 3.28×10^{14} molecules per cubic centimeter.

Filament life tests

A filament life test showed that a tungsten filament 10 mils in diameter in a discharge in air at 100 milliamperes plate current during the pulses, 15 microns gas pressure, 800 gauss magnetic flux density and 600 volts pulsed plate voltage at a duty cycle of $\frac{1}{167}$ lasted 4.7 hours with the filament current changed continuously to maintain the plate current constant. The filament current required to give a constant emission current decreased linearly from 7.3 amperes at a rate of 1.36 amperes per hour. The filament burned out when the filament current decreased to 0.9 amperes.

Filament life tests made by a previous group (134, March-May 1949) showed that with a 5 mil tungsten filament in nitrogen with 100 volts d-c plate voltage, 15 microns pressure, 750 gauss, and 100 milliamperes plate current the filament lasted 0.85 hours. Spangenberg (120, pp. 35-38) shows that the life of the 10 mil filament should be about 5 to 6 times the life of the 5 mil filament for the same emission current. In the first case positive ions bombarded the filament only during the pulses with a duty cycle of $\frac{1}{167}$ and in the second case positive ions bombarded the filament continuously.

A 5 mil tungsten filament in air with 600 volts pulsed plate voltage, 15 microns pressure, zero magnetic field, and 25 milliamperes

plate current during the pulses lasted 2.1 hours. With zero magnetic field the emission electrons travel directly to the plate with little ionization. The plate current is then essentially the emission current. Twenty five milliamperes emission current compares with the 100 milliamperes plate current of the other life tests if the plate current is one quarter emission current and three quarters ionization current which is about the proportions shown in Figure (5.16).

It seems that any knocking-out of tungsten atoms, or groups of atoms, from the filament surface by the collisions of the air atomic positive ions with the filament surface does not have a large effect on the filament life. Positive ion bombardment may decrease the filament life by a factor of 2 or 3. A reason why the positive ion bombardment does not have a greater effect is that the bombardment occurs over the entire filament while the critical region for filament burn-out is the small hottest region in the middle of the filament. Calculated filament lifetimes defined as the time required for a 10 percent reduction in mass through evaporation give filament lives over a hundred times larger than those obtained experimentally even without positive ion bombardment because of the regenerative process leading to the filament failures, the attacking of the hot tungsten by water vapor, and the impairment of emission from tungsten by nitrogen necessitating a higher operating temperature.

One of the important effects of the presence of gas molecules in electronic devices is the chemical action at the electrodes. Tungsten, when hot, is effectively attacked even by traces of some gases, particularly water vapor. Emission from tungsten is impaired by other gases, especially nitrogen, but in the presence of mercury vapor and the noble gases it is unaffected. Mercury vapor has a lower ionization energy than the noble gases. Negative ions form but rarely in the noble gases or in mercury vapor.

PROBE MEASUREMENTS

Positive ion collection by the probe

The plasma electron temperature was measured by a probe, the circuit diagram of which is shown in Figure (4.2). The current i collected by the probe is measured by the microammeter G. From the variation of the probe current i, as a function of the voltage V on the probe, the electron temperature can be determined. The presence of the magnetic field complicates the interpretation of the data and makes the determination of certain desired quantities not accurate.

When the probe potential is strongly negative with respect to the plasma potential, which is near the plate potential, the probe collects only positive ions and repels all plasma electrons, as explained by Loeb (74, pp. 232-256). A positive ion space charge sheath thus forms around the probe. All of the positive ions which cross the sheath boundary fall down the potential energy hill and are collected.

The probe consists of a ten mil tungsten wire covered with glass except for the exposed tip, which is approximately spherical. The glass covering is to insulate the probe from the plate, through which the probe passes, and to define the collecting area of the probe tip. The probe tip was about halfway between the center of the plasma and one end-tab and at a radius of about 2 millimeters from the filament.

Figure (4.2)

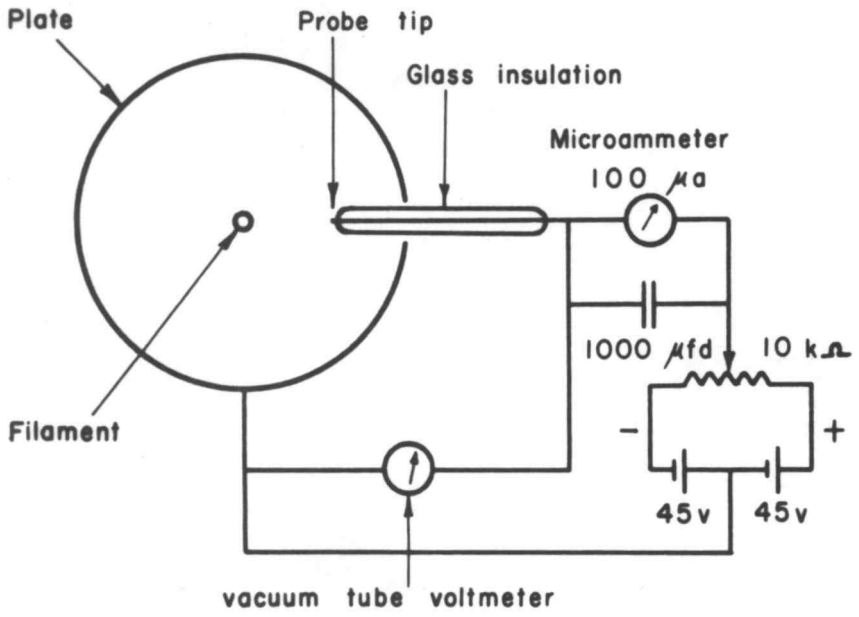

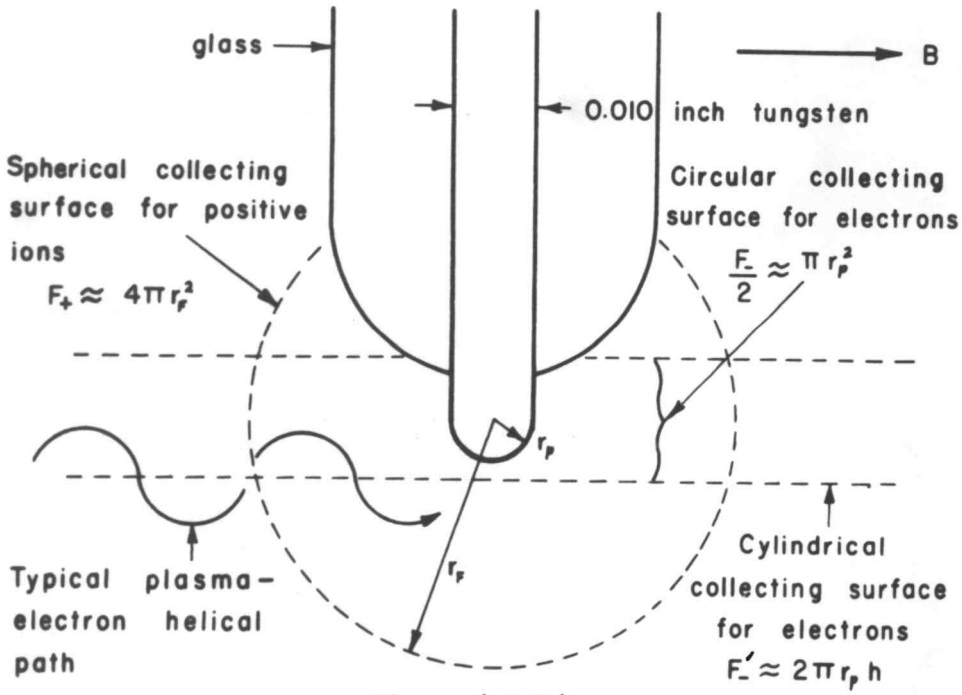

Figure (4.3)

The magnetic field does not bend the paths of the positive ions very much so that the collecting surface of the probe for positive ions is approximately the boundary between the probe space charge sheath and the plasma. This boundary is spherical with area $F_+ = 4\pi r_F^2$ where r_F is the radius of the outer edge of the space charge sheath. Owing to their heat motions the positive ions diffuse into the sheath across the area F_+ giving a positive probe current,

$$i_+ = 4\pi r_F^2 \frac{n_+ \overline{v_+} e}{4} . \tag{4.01}$$

The space charge limitation inside of the sheath also gives a current value

$$i_+ = \frac{4\epsilon}{9} \sqrt{\frac{2e}{M_+}} \frac{(V_B - V)^{3/2}}{(-\alpha^2)} \tag{4.02}$$

for positive ion flow inward between two concentric spherical electrodes, where $(-\alpha^2)$ is a correction factor depending on the ratio of r_F/r_p where r_p is the probe tip radius and V_B and V are the plasma and probe potentials respectively. Spangenberg (120, p. 825) gives $(-\alpha^2)$ as a function of r_F/r_p. The sheath radius r_F is such that these two current expressions are equal. The sheath thickness increases with increasing difference between plasma and probe potentials. The probe tip radius r_p is only approximately known but the radius of the collecting surface for positive ions r_F is a low

powered function of r_p so an uncertainty in knowing r_p is not reflected strongly into the accuracy of the positive ion current to the probe.

The factor $\frac{en_+\overline{v}_+}{4}$ in equation (4.01) can be evaluated by measuring the positive ion current I_{ET} to the end tabs, which collect only positive ions.

$$\frac{I_{ET}}{A_{ET}} = \frac{en_+\overline{v}_+}{4} \tag{4.03}$$

The average end tab current was 0.15 milliamperes and the end tab area, for both tabs together, was 0.883 square centimeters for a certain measurement so equation (4.01) becomes

$$i_+ = r_F^2 \; 2.138 \text{ milliamperes per square centimeter} \tag{4.04}$$

The constant in equation (4.02) can be evaluated and the equation becomes

$$i_+ = 1.455 \times 10^{-8} \frac{(V_B - V)^{3/2}}{(-a^2)} \quad \frac{\text{amperes}}{(\text{volts})^{3/2}} \tag{4.05}$$

Equations (4.04) and (4.05) together give the positive ion current to the probe as a function of the plasma-to-probe voltage difference.

Electron collection by the probe

As the probe voltage becomes more positive the more energetic plasma electrons can reach the probe tip surface against the retarding potential (V_B-V). The magnetic field greatly restricts the transverse motion of the plasma electrons so that only some of those plasma electrons with helical motions around magnetic flux lines which pass through the probe tip, or pass within the helical radius of the probe tip, can be collected. Figure (4.3) shows the collecting surfaces of the probe for positive ions and plasma electrons.

The electron current to the probe against the retarding potential is

$$i_- = F_- \frac{en_-\overline{v_{-\parallel}}}{2} \exp\left\{-\frac{e(V_B-V)}{kT_-}\right\} \qquad (4.06)$$

where F_- is the circular effective collecting area of the probe for electrons, $\overline{v_{-\parallel}}$ the average velocity of the plasma electrons in the z direction, k Boltzmann's constant, and T_- the electron temperature. The exponential factor gives the fraction of the plasma electrons that have energy greater than $e(V_B-V)$.

The total current $i_- + i_+$, and the positive ion current i_+, collected by the probe are shown in Figure (4.4). The difference of these two quantities gives the plasma electron current, i_-, to the probe. The natural logarithm of the electron probe current is, from equation (4.06)

$$\ln i_- = \ln \left[F_- \frac{e n_- \overline{v_{-\parallel}}}{2} \right] - \frac{e(V_B - V)}{kT_-} \tag{4.07}$$

This is shown by curve A in Figure (4.5), which is obtained from curve A in Figure (4.4). The slope of equation (4.07) with respect to the probe voltage V is

$$\frac{d \ln i_-}{dV} = \frac{e}{kT_-} \tag{4.08}$$

From Figure (4.5) the slope of the $\ln i_-$ curve for curve A is

$$\frac{1}{23.3 \text{ volts}} = \frac{e}{kT_-} \tag{4.09}$$

This gives an electron temperature

$$T_- = 270{,}000^\circ K \tag{4.10}$$

The corresponding average energy of the plasma electrons is

$$eV_- = \frac{3}{2} kT_- = \frac{3}{2} e \, 23.3 \text{ volts} = 35 \text{ electron volts} \tag{4.11}$$

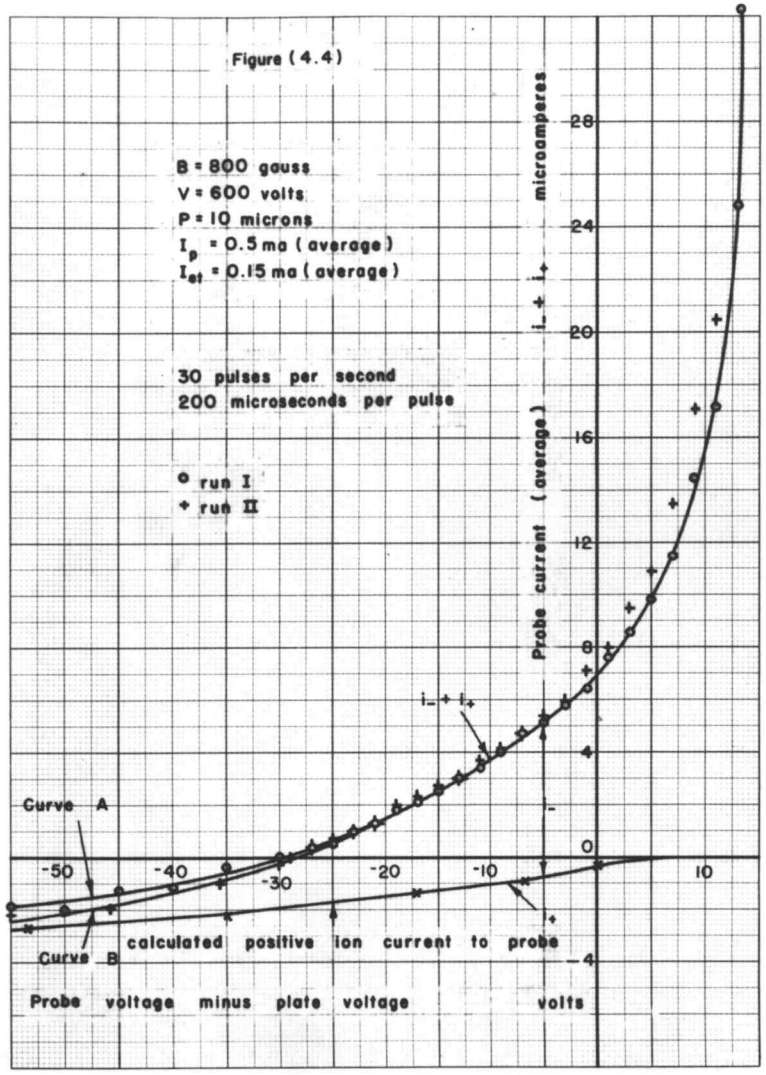
Figure (4.4)
B = 800 gauss
V = 600 volts
P = 10 microns
I_p = 0.5 ma (average)
I_{et} = 0.15 ma (average)
30 pulses per second
200 microseconds per pulse
o run I
+ run II
Probe current (average) $i_- + i_+$ microamperes
28
24
20
16
12
8
4
0
-4
$i_- + i_+$
i_-
i_+
Curve A
Curve B
-50
-40
-30
-20
-10
10
calculated positive ion current to probe
Probe voltage minus plate voltage volts

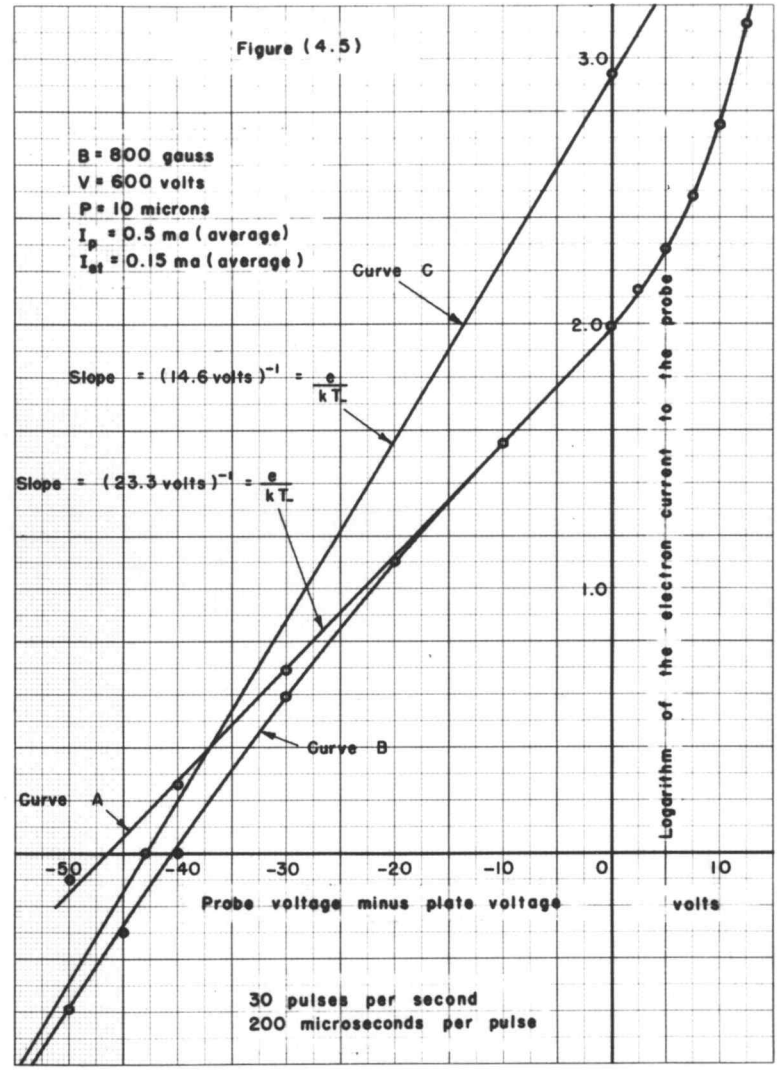
Figure (4.5)
B = 800 gauss
V = 600 volts
P = 10 microns
I_p = 0.5 ma (average)
I_{et} = 0.15 ma (average)
Curve C
Slope = $(14.6 \text{ volts})^{-1} = \frac{e}{kT_-}$
Slope = $(23.3 \text{ volts})^{-1} = \frac{e}{kT_-}$
Curve A
Curve B
3.0
2.0
1.0
Logarithm of the electron current to the probe
-50
-40
-30
-20
-10
0
10
Probe voltage minus plate voltage volts
30 pulses per second
200 microseconds per pulse

When the probe voltage becomes more positive than the plasma potential, the probe begins to repel the positive ions and a negative space charge sheath forms around the probe tip. The attraction of the positive probe for the plasma electrons increases the effective collecting area of the probe for electrons and gives a break in the ln i_- curve of Figure (4.5). This bend in the curve gives the plasma potential. The exact position of the bend in the curve is uncertain within several volts but shows that the plasma potential is close to the plate potential. As the probe voltage is increased further the electron current to the probe increases very rapidly and the readings soon become unstable because the large probe current distrubs the plasma balances.

From Figure (4.4), when the probe potential equals the plasma potential, the ratio of the electron and positive ion currents to the probe is

$$\left.\frac{i_-}{i_+}\right|_{V=V_B} = \frac{7.344}{0.344} = 21.35 \qquad (4.12)$$

From equations (4.01) and (4.06) this ratio is

$$\left.\frac{i_-}{i_+}\right|_{V=V_B} = F_- \frac{en_-\overline{v}_{-\parallel}}{2} \Big/ 4\pi r_F^2 \frac{en_+\overline{v}_+}{4} \qquad (4.13)$$

From Figure (3.1) an average plasma electron travels 6.85×10^{-2} centimeters in the z direction while making one helix rotation. If the probe tip were longer than this in the z direction, it would collect all the electrons with motions around flux lines passing within a helical radius of the probe tip. If the probe tip had infinitesimal length in the z direction, it would collect half of the plasma electrons with helical motions around magnetic flux lines which are tanget to the probe tip. The probe tip thickness is 2.54×10^{-2} centimeters so the circular effective collecting area of the probe tip has a radius a little larger than the probe tip radius. The probe collects electrons from both the plus and minus z directions so the effective collecting area for electrons becomes

$$F_{-} \approx 2 \times \pi r_p^{\,2} \tag{4.14}$$

Since the plasma electron and positive ion densities are approximately equal equation (4.13) becomes

$$\left.\frac{i_-}{i_+}\right|_{V=V_B} \approx \frac{\overline{v_{-\parallel}}}{\overline{v_+}} \tag{4.15}$$

The positive ion average velocity can be evaluated from equation (4.03) by measuring the end tab current during a plasma oscillation and calculating the positive ion density which gives the measured frequency of oscillation. This is shown later to be about 5×10^5

centimeters per second at the end tabs. The plasma electron velocity in the z direction is about 2.7×10^8 centimeters per second so the ratio $i_-/i_+ \Big|_{V=V_B}$ should be about 540. The positive ion current was evaluated by measuring the current to the end tabs so it is the electron current to the probe which is too low by a factor of about 25.

Interpretation of probe data in a magnetic field

Before an electron can travel around a flux line which passes through the probe tip, it must pass through the cylindrical surface F_-' in Figure (4.3) the area of which is

$$F_-' \approx 2\pi r_p h \tag{4.16}$$

where h is the length (about 1.8 cm) of the plasma region in the z direction. The electron current passing inward through this surface is

$$i_-' = e F_-' \frac{n_- \overline{v_{-\perp}}_{eff}}{\pi} = e F_-' n_- \frac{\theta \overline{G_\perp}}{\pi}$$

$$= e2\pi r_p h \frac{n_-}{\pi} \sqrt{\frac{2}{3}} \theta L_- \frac{A}{\sqrt{\frac{2}{3} L_-^2 + A^2}} \approx e2r_p h n_- \theta A \tag{4.17}$$

where $\overline{v}_{-\perp eff}$ is the average effective electron velocity transverse to the magnetic field. The net electron current passing inward through the surface F_-' is

$$i_{-\,net} = F_-' \, e \, (n_- - n_-') \frac{\overline{v}_{-\perp eff}}{\pi} \tag{4.18}$$

where n_- is the plasma electron density outside the cylindrical region enclosed by the surface F_-' and n_-' is the plasma electron density inside the region. This current must equal the electron current collected by the probe.

$$i_{-\,net} = F_- \, e \, n_-' \frac{\overline{v}_{\parallel}}{2} \exp\left\{ - \frac{e(V_B - V)}{kT_-} \right\} \tag{4.19}$$

Equating these two expressions and solving for the electron density inside the F_-' region

$$n_-' = \frac{n_-}{1 + \dfrac{\pi r_{p_-} L_- \omega_c}{2\sqrt{2}\, h \sqrt{\overline{v_-^2}}} \exp\left\{ - \dfrac{e(V_B - V)}{kT_-} \right\}}$$

$$= \frac{n_-}{1 + \dfrac{4.45 \times 10^8 \text{ cm/sec}}{\sqrt{\overline{v_-^2}}} \exp\left\{ - \dfrac{e(V_B - V)}{kT_-} \right\}}$$

$$= \frac{n_-}{f_1(T_-, V)} \tag{4.20}$$

Combining equations (4.19) and (4.20) we obtain the electron current to the probe as a function of the probe voltage.

$$i_- = 2\pi r_p^2 e \frac{\overline{v_\parallel}}{2} \frac{n_- \exp\left\{-\frac{e(V_B-V)}{kT_-}\right\}}{f_1(T_-,V)} \tag{4.21}$$

The natural logarithm of the electron probe current is

$$\ln i_- = \ln\left[\pi r_p^2 e \overline{v_\parallel} n_-\right] - \frac{eV_B}{kT_-} + \frac{eV}{kT_-} - \ln f_1(T_-,V) \tag{4.22}$$

and the derivative with respect to the probe voltage of $\ln i_-$ is

$$\frac{d \ln i_-}{dV} = \frac{e}{kT_-}\left[\frac{1}{1 + \frac{4.45 \times 10^6 \text{ m/sec}}{\sqrt{\overline{v_-^2}}} \exp\left\{-\frac{e(V_B-V)}{kT_-}\right\}}\right]$$

$$= \frac{e}{kT_- f_1(T_-,V)} \tag{4.23}$$

The slope of the $\ln i_-$ curve decreases with increasing probe voltage like curve B in Figure (4.5), which comes from curve B in Figure (4.4). Both curves A and B in Figure (4.4) are within the experimental accuracy of the probe measurements.

Equation (4.21) says that $f_1(T_-, V)$ times the measured electron current to the probe should be a purely exponential function of the probe voltage and that

$$\ln \left[i_-(V)\, f_1(T_-, V) \right]$$

should be a straight line with slope $\frac{e}{kT_-} = \frac{3e}{\overline{mv_-^2}}$. To evaluate the slope of this curve let us choose the two probe voltage values $V - V_B = 0$ and $V - V_B = -43$ volts. When the probe voltage is 43 volts negative with respect to the plasma voltage

$$\ln \left[i_-(V_B-43)\, f_1(T_-, V_B-43) \right]$$

is about zero as shown in Figure (4.5). When the probe potential equals the plasma potential, the electron current to the probe is

$$1 + \frac{4.45 \times 10^6 \text{ m/sec}}{\sqrt{\overline{v_-^2}}} \quad 7.344 \text{ microamperes.}$$

Then

$$\frac{d}{dV} \ln \left[i_-(V) f_1(T_-, V) \right] = \frac{e}{kT_-}$$

$$= \frac{\ln \left[i_-(V_B) f_1(T_-, V_B) \right] - \ln \left[i_-(V_B - 43) f_1(T_-, V_B - 43) \right]}{43 \text{ volts}}$$

$$= \frac{\ln \left[1 + \dfrac{4.45 \times 10^6 \text{ m/sec}}{\sqrt{\overline{v_-^2}}} \right] + \ln \left[7.344 \times 10^{-6} \right]}{43 \text{ volts}}$$

$$= \frac{3e}{m\overline{v_-^2}} \qquad (4.24)$$

The solution of this transcendental equation is $\sqrt{\overline{v_-^2}} = 2.78 \times 10^6$ meters per second so that $eV_- = \frac{3}{2} kT_- = 21.9$ electron volts. Curve C in Figure (4.5) shows the logarithm of the electron current to the probe for the case where the region F_-' is very long so that the plasma electron density inside the region is equal to the density outside the region.

The magnetic field restricts the electron flow across the field so that it is 1.6 times easier for the current, for electrons with 21.9 eV average energy, to flow in the magnetic field direction

through the small area F_- than across the magnetic field through the larger area F_-'. When the probe potential equals the plasma potential the density inside the F_-' region is 1/2.6 as high as the density in the rest of the plasma. As the electron density decreases the slight excess of positive ions gives the region a positive potential with respect to the surrounding plasma. As the potential of the region becomes about a volt higher than the plasma potential the region is denied to the less energetic positive ions, since the average positive ion energy is about 1.8 electron volts, so that the positive ion density decreases with the decreasing electron density. The small fraction of a percent more positive ions than electrons keeps the potential of the region about a volt higher than the plasma potential.

Compared to the average electron energy of a few electron volts in a glow or arc discharge, 21.9 eV is high. The emission electrons have energies of 600 electron volts and an ionizing collision is a violent occurrence with the detached electron getting on the average about half the difference of the bombarding electron energy and the ionization energy. A plasma electron can transfer a maximum of only $2m/M = 7.79 \times 10^{-5}$ of its energy to a molecule during an elastic collision. The ionization energy of nitrogen is 15.8 electron volts and that of oxygen 11.2 electron volts, so there is much ionization and excitation by the plasma electrons as well as the emission electrons.

From equation (4.21) the plasma electron density is 2.445×10^{11} electrons per cubic centimeter. From the plasma oscillation theory and data such as given in Figure (5.1) the plasma electron density is 1.18×10^{12} electrons per cubic centimeter, or 4.8 times the value determined by the probe measurement. The probe value is probably the least accurate of the two because of uncertainties in the probe tip collecting area, the plasma potential, and the fact that the probe disturbs the plasma. If the probe tip area were increased to define the probe tip area better, the probe would collect more current and disturb the plasma even more. If the average plasma electron energy were really less than the measured value, the measured plasma electron density would be higher and probably closer to the correct value.

From equation (4.03), using the positive ion density value from the plasma oscillation theory, the average positive ion velocity is 6×10^5 centimeters per second and the average energy of the positive ions 2.63 electron volts. If the probe value of positive ion density were used the positive ion average energy would be 61.1 electron volts which is much too large.

Probe measurement sources of error

Some difficulty was experienced with the tungsten metal evaporating from the filament to the probe, increasing the effective collecting area of the probe tip and finally making a leakage path

along the glass probe insulation to the plate. After a few probe current runs, the data would become meaningless. However, after a complete scrubbing of the glass probe insulator, the data would again be reproducible.

The probe measures the plasma electron density averaged over the time of the pulse. Positive ion bombardment of the filament during the pulse increases the filament temperature, and thus the emission current, so the plasma electron density is not constant during the pulse. The plate voltage pulses induced some transient voltages into the probe leads. With such a high energy distribution a large part of the plasma electrons have energies greater than the excitation and ionization energies of the air molecules. Inelastic collisions make the energy distribution of the plasma electrons non-Maxwellian. Another source of error in the probe measurements may be positive ions and photons from the plasma inducing secondary electron emission from negative probes. The secondary electron emission reduces the measured electron current to the probe. This may explain, or contribute to, the increase of the measured electron current to the probe as the probe becomes positive with respect to the plasma potential, as shown in Figure (4.5). Also, the probe area was not accurately known.

Positive ion current to the end tabs

Figure (5.4) shows the average plate current as a function of the gas pressure for an oscillation mode of frequency 1.168×10^{10} cycles per second shown in Figure (5.5). The theory requires that the plasma electron density be a constant value of 1.621×10^{12} electrons per cubic centimeter regardless of the pressure value.

The end tabs are the only electrodes which collect only a single type of particle. Bohm (50, pp. 77-86) shows that the potential at the space charge sheath boundary of a negative electrode is negative with respect to the potential in the interior of the plasma by an amount equal to one third the average energy of the plasma electrons divided by the electronic charge.

$$V_o = \frac{kT_-}{2e} \tag{4.25}$$

The velocity of positive ions at the sheath edge, if they fell through the whole potential difference V_o without a collision, would be

$$v_+ = \sqrt{\frac{2eV_o}{M_+}} = \sqrt{\frac{kT_-}{M_+}} \tag{4.26}$$

For an electron temperature of 154,600°K this velocity, for atomic nitrogen positive ions, is 9.66×10^5 centimeters per second.

The total number of positive ions from the plasma arriving at unit area of the sheath boundary per second is

$$\Gamma_+ = \frac{n_+ \overline{v_+}}{4} \tag{4.27}$$

as shown by Kennard (64, pp. 61-64). The positive ion current to the end tabs is thus the positive ion flow Γ_+ times the positive ion charge e, times the collecting area of the two end tabs $2\pi(r_2^2 - r_1^2)$ where r_2 is the radius of the cylindrical plate, 0.375 centimeters, and r_1 is the radius of the space charge sheath around the filament, about 0.1 centimeters.

Using the value of positive ion density equal to the calculated value of plasma electron density, 1.621×10^{12} electrons per cubic centimeter, corresponding to the plasma oscillation frequency of the mode, 1.168×10^{10} cycles per second, the calculated positive ion current to the end tab is 41 milliamperes during a pulse.

By connecting the end tabs to a separate lead through the glass envelope of the tube the current to the end tabs was measured. At 10 microns gas pressure the average plate current is 0.48 milliamperes as shown on Figure (5.4). The end tabs collected 0.14 milliamperes of this current and the filament the other 0.34 milliamperes. The end tab current divided by the duty cycle 1/167 equals the measured positive ion current of 23 milliamperes during a pulse.

The z component of the positive ion mean free path is 0.413 centimeters for a gas pressure of ten microns and the distance from

the center of the tube, where the emission electrons are ionizing the gas, to the end tabs, is one centimeter. Most of the positive ions thus do not fall through the total potential difference $V_o = 6.7$ volts without a collision and their average velocity at the end tab sheath is less than the value used in the calculation.

Using the value of positive ion density from the plasma oscillation theory the measured and calculated values of the positive ion current to the end tabs can be equated to obtain values for the average velocity and the temperature of the positive ions. The average velocity is 4.35×10^5 centimeters per second. The positive ion temperature is 10,700°K or 1.387 electron volts, which is not too high a value considering the very high E/p value of 666 volts per centimeter per millimeter of mercury.

Figure (5.6) shows the measured average plate current for the 7 kilomegacycle mode of Figure (5.3) as a function of the pressure. At 10 microns the average plate current is 0.26 milliamperes of which 0.06 milliamperes is collected by the end tabs and 0.20 milliamperes by the filament. The measured current to the end tabs during a pulse is 10 milliamperes.

Using the positive ion density value of 5.4×10^{11} electrons per cubic centimeter, corresponding to this mode, the calculated value of end tab current is 13.7 milliamperes during the pulse. Again the calculated value is higher than the measured value. Equating the measured and calculated values of the current to the

end tabs, the positive ion average velocity is 5.66×10^5 centimeters per second.

When the mean free paths are of the same order of magnitude as the dimensions of the discharge region the problem is more difficult to treat mathematically than if the particles make many collisions before being collected, and thus have a terminal velocity which is proportional to the small electric field in the plasma, or if the particles make practically no collisions before being collected and thus have an acceleration which is proportional to the electric field.

It should be emphasized that average velocity values for the positive ions obtained from measurements of the current to the end tabs are the average velocity values of the positive ions at the end tab sheath boundary and not the average velocity inside the plasma region. The measured positive ion average energies may be high by about one order of magnitude since there is a voltage drop of the order of kT_+/e between the plasma potential in the center of the plasma and the potential at the sheath edge which accelerates the positive ions toward the end tabs.

Boyd (22, p. 329) shows theoretically and experimentally that at pressures below 100 microns the saturation current to a negative probe is considerably greater than the random current of positive ions in the gas. It is very nearly equal to the value the conventional theory would give if the positive ions had a temperature equal to that of the electrons. His experiments with a small plane probe in the form of a grid, with a collector behind it, made it

possible to obtain probe characteristics in argon with the electron, ion, and secondary emission components separated from one another. Secondary emission from his platinum collector by photons and metastable particles amounted to about 10 percent of the saturation positive ion current with the greater portion being due probably to metastable argon atoms.

A floating double probe method (61, pp. 58-68) (62, pp. 1411-1412) (79, pp. 191-210) of measuring the electron temperature has the advantage that it disturbs the discharge much less than the single probe method. The double probes cannot collect any more electronic current than positive ion current. This gives the possibility of using larger plane probes so the collecting area is more accurately defined. The positive ion temperature is not given by the double probe method, however, and this quantity is needed to determine the electron and positive ion densities. In the single probe method the plasma density is determined from the measurement of saturated electron probe current and electron temperature. In the double probe method only the positive ion current saturates and so the positive ion temperature must be known to evaluate the positive ion density. The double probe method thus cannot be used in this problem to measure the plasma density.

WAVELENGTH OBSERVATIONS OF PLASMA OSCILLATIONS

Dependence of oscillation wavelengths on gas pressure and filament current

Oscillations are obtained for certain combinations of magnetic flux density, plate voltage, gas pressure, and filament current. If any one of these is varied while holding the other parameters constant, oscillations occur for certain discrete values of the variable and do not occur for intermediate values. About ten oscillation modes were obtained with a different frequency for each mode. The frequencies progress regularly from mode to mode and have corresponding free space wavelengths in the range of 1 to 10 centimeters.

For a given value of magnetic flux density each discrete wavelength requires a particular plasma electron density as predicted by the theory. This particular plasma density however may be produced by various combinations of gas pressure, plate voltage, and filament current.

Figure (5.1) is a typical set of data showing the measured free space wavelengths of the oscillations as a function of the gas pressure. It is seen that the wavelengths of the radiation are not direct functions of the gas pressure because any given oscillation mode can be obtained at any pressure from a few microns to about 150 microns.

Figure (5.1)

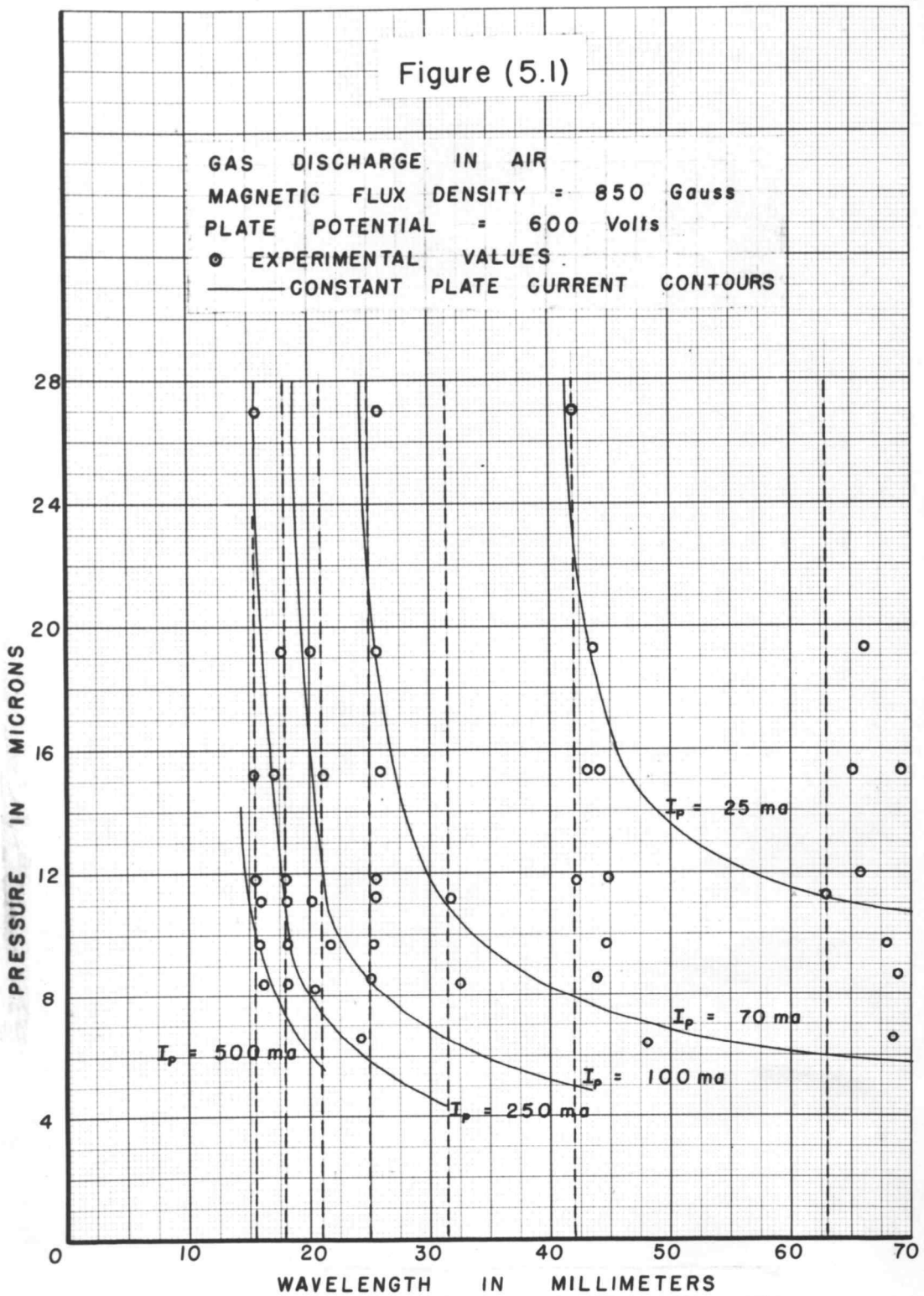
GAS DISCHARGE IN AIR
MAGNETIC FLUX DENSITY = 850 Gauss
PLATE POTENTIAL = 600 Volts
⊙ EXPERIMENTAL VALUES
——— CONSTANT PLATE CURRENT CONTOURS
PRESSURE IN MICRONS
WAVELENGTH IN MILLIMETERS
0
4
8
12
16
20
24
28
10
20
30
40
50
60
70
I_p = 25 ma
I_p = 70 ma
I_p = 100 ma
I_p = 250 ma
I_p = 500 ma

The data were taken by holding the gas pressure constant and increasing the filament current, and thus the emission current, obtaining the discrete oscillations, or modes, represented by the points progressing from right to left. Then a different gas pressure value was used and the emission current again increased from zero value. This process was repeated, thus giving the wavelengths as functions of the gas pressure and the emission current.

The data are not closely reproducible with respect to the filament current because of the wasting away of the filament by evaporation. They are, however, reproducible with respect to the plate current. Contours of constant plate current during a pulse are shown on the figure. Contours of constant emission current have the same shape as the plate current contours.

Contours of constant filament current have a similar but different shape than the emission current contours because the emission current is a function of the filament current and the gas pressure. The gas cools the filament giving less emission current at higher pressures as shown in Figure (5.2).

The wavelengths are not direct functions of the filament emission current because any certain oscillation mode can be obtained for any value of emission current, from a few milliamperes to a few hundreds of milliamperes, by using the appropriate gas pressure to yield the plasma electron density necessary for that particular mode.

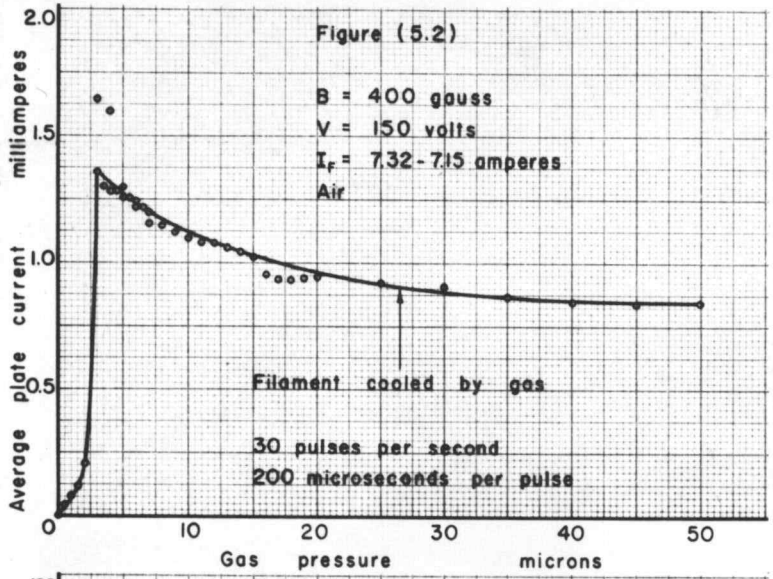
Figure (5.2)
B = 400 gauss
V = 150 volts
I_F = 7.32 - 7.15 amperes
Air
Filament cooled by gas
30 pulses per second
200 microseconds per pulse
Average plate current milliamperes
Gas pressure microns

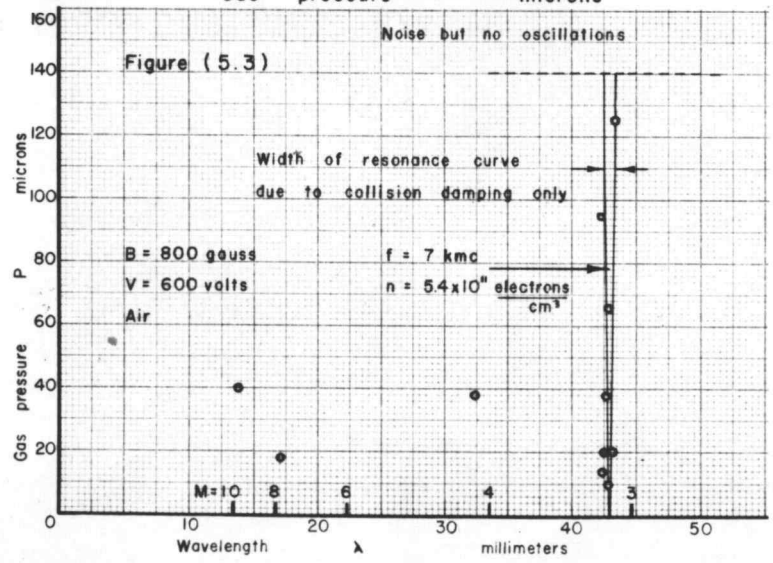
Figure (5.3)
Noise but no oscillations
Width of resonance curve due to collision damping only
B = 800 gauss
V = 600 volts
Air
f = 7 kmc
n = 5.4x10" electrons/cm³
M=10 8 6 4 3
Gas pressure P microns
Wavelength λ millimeters

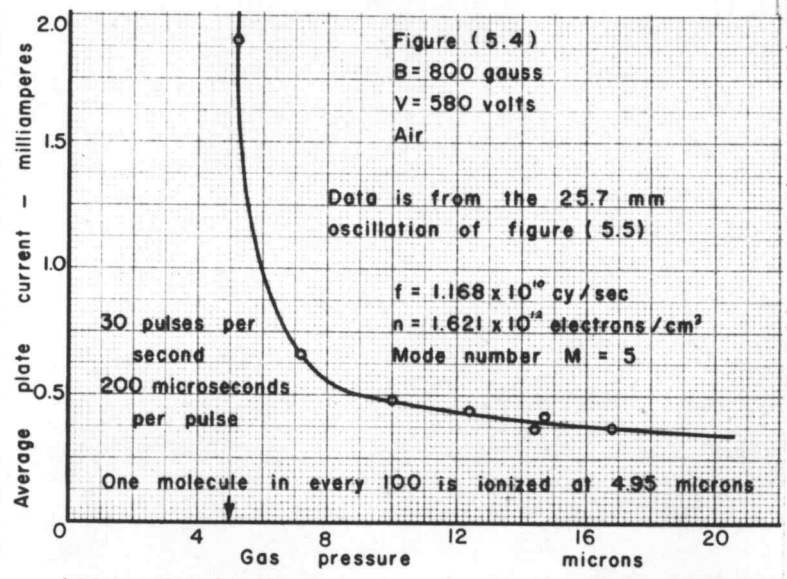
Figure (5.4)
B = 800 gauss
V = 580 volts
Air
Data is from the 25.7 mm oscillation of figure (5.5)
f = 1.168 x 10¹⁰ cy/sec
n = 1.62! x 10¹² electrons/cm³
Mode number M = 5
30 pulses per second
200 microseconds per pulse
One molecule in every 100 is ionized at 4.95 microns
Average plate current - milliamperes
Gas pressure microns

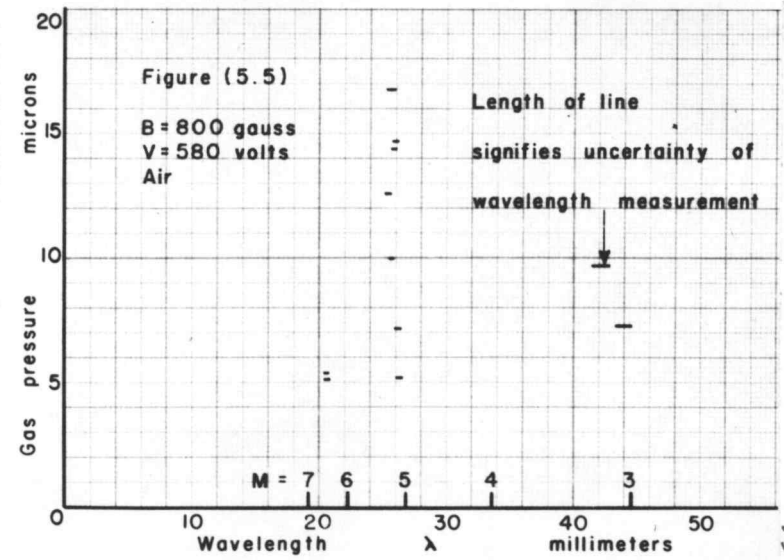
Figure (5.5)
B = 800 gauss
V = 580 volts
Air
Length of line signifies uncertainty of wavelength measurement
M = 7 6 5 4 3
Gas pressure microns
Wavelength λ millimeters

Increasing either the gas pressure or the filament current, and thus the emission current, increases the plasma electron density. An oscillation which is caused to cease, by say lowering the gas pressure, can be started again at the same frequency by increasing the filament current a suitable amount.

High pressure limit of oscillations

The high pressure limit of oscillation of a 7 kilomegacycle oscillation was 140 microns as shown in Figure (5.3). The collision rate for electrons at this pressure is 7.45×10^8 collisions per second. The plasma electrons thus make 9.4 oscillation cycles on the average before a collision disrupts the oscillation of a particular plasma electron. Collisions damp the plasma oscillations.

The selectivity, or quality factor Q, of the plasma oscillations is

$$Q = \frac{f_o}{\Delta f} = 2\pi \frac{\text{stored energy}}{\text{energy dissipated per cycle}} \qquad (5.01)$$

as shown by Goldman (48, pp. 135-139), where f_o is the resonant frequency of the plasma oscillations and Δf the frequency width of the resonance curve of the plasma at the half power level. The difference between the two frequencies higher and lower than the resonant frequency at which the impedance of the plasma differs from its resonant value by a factor of $\sqrt{2}$ is also equal to Δf.

The Q of the plasma for the 7 kilomegacycle oscillation at 140 microns gas pressure, considering collision damping only, is

$$Q = 2\pi \text{ (9.4 cycles per collision)} = 59 \qquad (5.02)$$

The plasma thus can be considered as a quite high quality resonant circuit even at this high pressure so collision damping is not the main factor which determines the high pressure limit of the plasma oscillations.

The electrons emitted by the filament have a velocity of 1.452×10^9 centimeters per second after falling through the 600 volts potential difference of the space charge sheath at the cathode. A magnetic flux density of 800 gauss bends the emission electrons in a circle of radius $R = \frac{v}{\omega_c} = 0.1033$ centimeters. The distance traveled by an emission electron on one loop into the plasma region is $2\pi R = 0.649$ centimeters per loop.

A 600 volt electron makes 5 ionizing collisions per centimeter per millimeter of mercury gas pressure in air as given by Finkelnburg (41, p. 95). At 140 microns of mercury gas pressure this is 0.7 ionizing collisions per centimeter. At this pressure then an emission electron makes 2.2 loops per ionizing collision on the average. After a collision the emission electron proceeds on in a new random direction. If about half of the collisions are ionizing and the rest exciting and elastic, the emission electron makes about one loop per collision at this pressure.

Some emission electrons give energy to the oscillating plasma electrons and some take energy from the plasma oscillation. A selection principle which allows the working emission electrons to give more energy to the plasma wave than the non-working emission electrons take from it requires that the emission electrons make more than one loop. This selection principle is discussed later when the excitation mechanism is considered. The factor which determines the high pressure limit of the plasma oscillations is thus the failure of the selection action.

The low pressure limit of the plasma oscillations occurs when there is insufficient ionization to form the plasma.

Dependence of plate current for a certain mode on the gas pressure

Let us see if the measured plate current variation with pressure is consistent with a constant plasma electron density for any certain mode. Figure (3.4) shows the variation of the diffusion coefficients and the mobilities of the charged particles with gas pressure. The plate collects all of the plasma electrons because the filament and the end tabs are about 600 volts negative with respect to the plasma potential.

Since the diffusion coefficient and mobility of the plasma electrons across the magnetic field to the plate are proportional to the gas pressure, a first thought might be that the plate current should be proportional to the pressure for a certain oscillation

mode. This is too simple a picture however. The plate also collects positive ions which subtract from the plasma electron current.

The plasma electron current plus the emission electron current that is scattered to the plate by collisions, minus the positive ion current collected by the plate, equals the net plate current. The plate current also equals the positive ion current to the end tabs, plus the positive ion current to the filament, plus the emission electron current from the filament, minus that part of the emission electron current which returns to the filament after one loop.

As the pressure is increased the positive ion mean free path and thus the mobility decreases. The positive ions then arrive at the end tab and filament space charge sheaths with a lower velocity so that the positive ion current is less at higher pressure for the same positive ion density.

The positive ion density is such that the rate of disposal of the ions I_+ equals the rate of ionization I of the gas.

$$I = I_+ \tag{5.03}$$

The disposal rate is proportional to the average ion velocity times the positive ion density. An expression for the average velocity of the positive ions is obtained by considering as a first approximation that the potential difference of $\frac{kT_-}{2e}$ between the center and edge of the plasma, a distance $\frac{h}{2}$ apart, produces a uniform electric field in the plasma region of magnitude $E = \frac{kT_-}{eh}$.

For high values of $\frac{E}{P}$, the ion drift velocity becomes large compared to the random velocity so that the energy gained from the field goes into increasing the ion drift energy. The average energy gained by the ion from the field is the force acting on the ion, $f = eE$, times the average distance $\bar{l}$ between collisions. The energy given by the ion to a gas molecule at a collision is half the ion energy, on the average, and in a steady state condition equals the energy gained from the field.

$$\frac{1}{2} M_+ (\overline{v_1^2} - \overline{v_o^2}) = eE\bar{l} \tag{5.04}$$

and

$$\overline{v_o^2} = \frac{1}{2} \overline{v_1^2} \tag{5.05}$$

where $\overline{v_1^2}$ and $\overline{v_o^2}$ are the mean square ion velocities before and after a collision.

The velocity in the electric field direction equals

$$v_x = v_{ox} + \frac{eE_x}{m} t = \sqrt{v_{ox}^2 + \frac{2eE_x}{M_+} l} \tag{5.06}$$

where v_{ox} is the average velocity in the field direction after a collision and is equal to $\frac{v_o}{\sqrt{2}}$. After a mean free time τ,

$$v_x(\tau) = v_{ox} + \frac{eE_x}{M_+}\tau = v_1 = \sqrt{2}\, v_o \tag{5.07}$$

so

$$\tau = \frac{M_+ v_o}{eE_x\sqrt{2}} \tag{5.08}$$

After a mean free path length $\bar{l}$

$$v_x(\bar{l}) = \sqrt{v_{ox}^2 + \frac{2eE_x}{M_+}\bar{l}} = v_1 = \sqrt{2}\, v_o \tag{5.09}$$

so

$$\bar{l} = \frac{3\, v_o^2\, M_+}{4\, e\, E_x} \tag{5.10}$$

The average ion drift velocity is

$$\overline{v_+} = \frac{\bar{l}}{\tau} = \frac{3}{4}\sqrt{2}\, v_o = \frac{3}{4}\sqrt{2}\sqrt{\frac{2eE_x\bar{l}}{M_+}} \tag{5.11}$$

The numerical factor depends on the method of averaging, but $\overline{v_+}$ is of the order of v_o.

$$\bar{l} = \frac{1}{S_m n_g} = \frac{kT_g}{S_m P} \tag{5.12}$$

where S_m is the collision cross section of gas molecules for ions, n_g the gas density, k Boltzmann's constant, T_g the gas temperature and P the gas pressure. The positive ion current is therefore

$$I_+ = \frac{A}{4} n_+ \overline{v_+} = \frac{A}{4} n_+ \frac{3}{4} \sqrt{2} \sqrt{\frac{2kT_- kT_g}{h M_+ S_m P}} = \frac{K_1 n_+}{\sqrt{P}} \tag{5.13}$$

where A is the area collecting the current.

A fraction K_2 of the ion current goes to the filament and end tabs. The rest goes to the plate. The plate current I_p equals the positive ion current to the filament and end tabs plus the net emission current I_e from the filament.

$$I_p = K_2 I_+ + I_e \tag{5.14}$$

The ionization current is proportional to the emission current I_e.

$$I = K_3 I_e \tag{5.15}$$

Putting equations (5.03), (5.13), and (5.15) into equation (5.14) yields

$$I_p = \frac{K_1 n_+}{\sqrt{P}} (K_2 + \frac{1}{K_3}) \tag{5.16}$$

The factor K_2 is shown later to be a function of the electrode geometry and a slow function of the pressure, being about 0.53 at 10 microns and approaching unity at high pressures. The factor K_3 is about 5.6 and is not a function of the pressure. K_3 is approximately

$$K_3 = \frac{0.0097\ \sqrt{V\ B\ d}}{(\text{volts gauss centimeters})^{1/2}} \tag{5.17}$$

where V is the plate voltage, B the magnetic flux density, and d the plate diameter.

The plate current varies with pressure in a manner similar to equation (5.16) for constant positive ion density, as shown by Figures (5.4) and (5.6). The measured functional relationship of the plate current and pressure for a certain oscillation mode is consistent with the theoretical requirement of constant positive ion density for the mode regardless of the pressure, current, and voltage. The quantitative check at 10 microns pressure also gives the correct order of magnitude for the positive ion density. The lengths of the lines in Figure (5.6) indicate the range of average plate current within which the 7 kilomegacycle mode is obtained.

Considering the currents through the boundary of the space charge sheath at the end tabs and filament, equation (5.14) is obtained for the plate current. A different expression is obtained for the plate current by considering the currents through the space charge sheath boundary at the plate. The plate current equals the

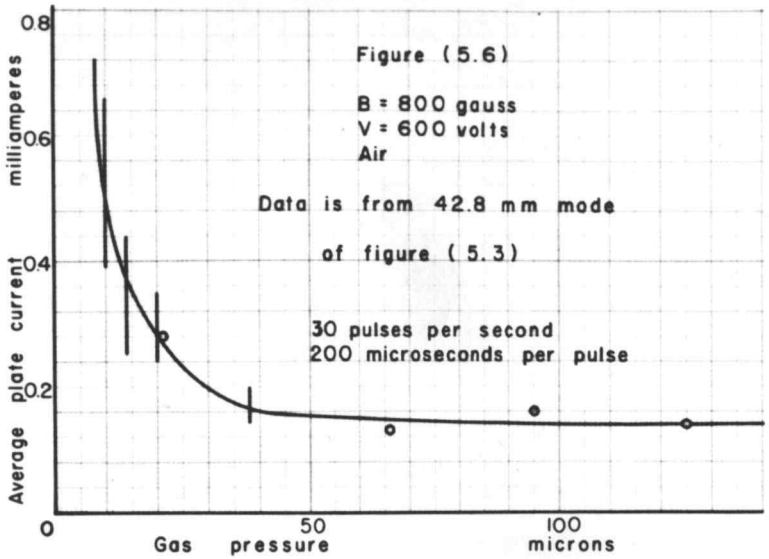
Figure (5.6)
B = 800 gauss
V = 600 volts
Air
Data is from 42.8 mm mode
of figure (5.3)
30 pulses per second
200 microseconds per pulse
Average plate current milliamperes
0.8
0.6
0.4
0.2
0
50
100
Gas pressure microns

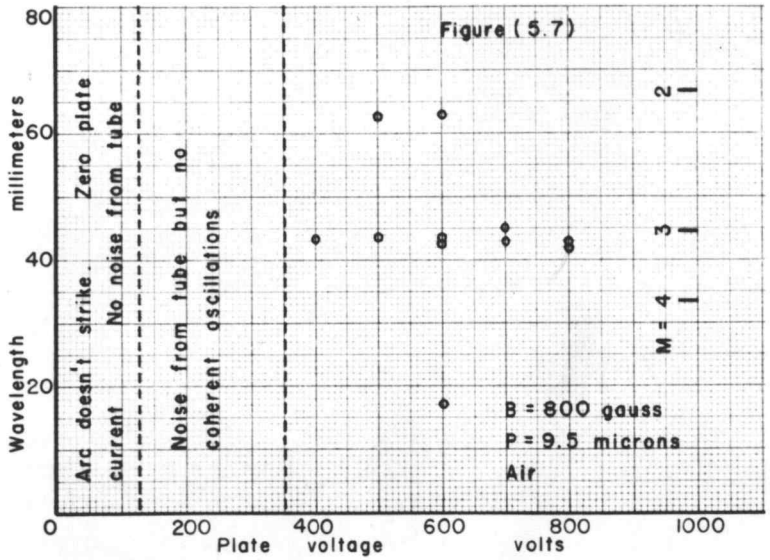
Figure (5.7)
Wavelength millimeters
80
60
40
20
0
Arc doesn't strike. Zero plate current
No noise from tube
Noise from tube but no coherent oscillations
M = 4 3 2 1
B = 800 gauss
P = 9.5 microns
Air
200
400
600
800
1000
Plate voltage volts

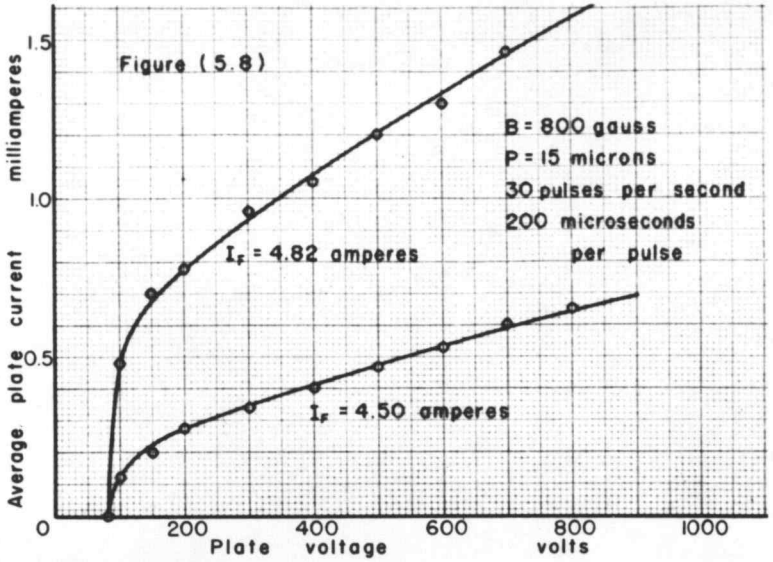
Figure (5.8)
Average plate current milliamperes
1.5
1.0
0.5
0
B = 800 gauss
P = 15 microns
30 pulses per second
200 microseconds per pulse
I_f = 4.82 amperes
I_f = 4.50 amperes
200
400
600
800
1000
Plate voltage volts

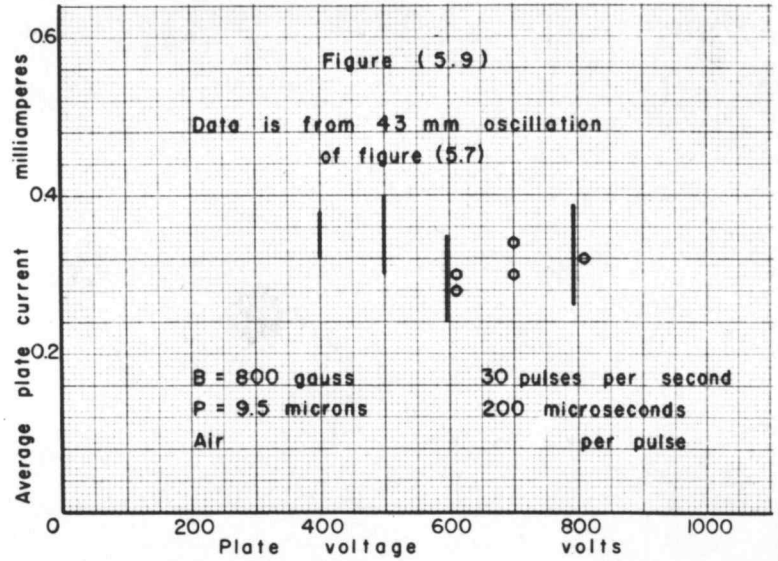
Figure (5.9)
Data is from 43 mm oscillation
of figure (5.7)
Average plate current milliamperes
0.6
0.4
0.2
0
B = 800 gauss
P = 9.5 microns
Air
30 pulses per second
200 microseconds per pulse
200
400
600
800
1000
Plate voltage volts

net emission current I_e plus the plasma electron current I_- minus that part of the positive ion current which is not collected by the end tabs and the filament $(1 - K_2)\, I_+$.

$$I_p = I_e + I_- - (1 - K_2)\, I_+ \tag{5.18}$$

The plate collects all the negative charges. Equating this expression to equation (5.14) we get, as a check,

$$I_+ = I_- \tag{5.19}$$

which is true because the ionization creates the positive ions and the plasma electrons at the same rate.

Dependence of plasma potential on gas pressure

The plasma potential is approximately equal to the plate potential. It may be a few volts more positive than the plate potential or a few volts more negative, depending upon the relative average energies of the positive ions and the plasma electrons, the magnetic flux density, the relative area of the plate compared with the areas of space charge sheath boundary at the end tabs and the filament, and the pressure.

If the plasma potential is a few volts negative with respect to the plate potential the plate collects all of the electrons arriving

at the sheath boundary but collects only a fraction K_4 of the total number of positive ions arriving at the sheath boundary which have sufficient energy to run up the potential hill in the sheath. Those positive ions which have less energy than that necessary to run over the potential hill and strike the plate run only part of the way up and then drop back into the plasma without being collected.

The positive ion current to the plate $(1 - K_2)\, I_+$ equals one fourth the positive ion density times the average velocity times the area of the plate A_p times the electronic charge times the fraction K_4 of those positive ions entering the sheath boundary that are collected.

$$I_+ (1 - K_2) = \frac{eA_p n_+ \overline{v_+} K_4}{4} = \frac{eA_p n_+ K_4}{4} \frac{\overline{L_+}}{\tau_+} \tag{5.20}$$

$\overline{L_+}$ is really the effective mean free path obtained by a suitable averaging of the transverse $\overline{L_{\perp_+}}$ and the parallel $\overline{L_{\parallel_+}}$ mean free paths over the angles of incidence. Since the transverse and parallel components of the positive ion mean free path are not too different, the ordinary kinetic theory mean free path $\overline{L_+}$ is used for the effective mean free path. One factor of one half comes from the fact that only half of the particles in a volume are going toward the plate and the other factor of one half comes from the projected area averaged over the angles of incidence.

The plasma electron current to the plate I_- equals 1/4 the plasma electron density times the plate area times the electronic

charge times the effective mean free path divided by the mean free time between collisions τ_-.

$$I_- = \frac{eA_p n_-}{4} \frac{\overline{G_{-\perp}}}{\tau_-} \tag{5.21}$$

where the transverse electronic mean free path $\overline{G_{-\perp}}$ is the effective mean free path because it is so very much smaller than that in the magnetic field direction.

Since $I_+ = I_-$ and $n_+ \approx n_-$ we have

$$\frac{\overline{L_+}}{\tau_+} \frac{K_4}{1-K_2} = \frac{\overline{G_{-\perp}}}{\tau_-} \tag{5.22}$$

The fraction of the positive ion current, K_2, that is collected by the end tabs and filament equals the ratio of the area of the sheath boundary at the end tabs and filament $A_{ET} + A_F$ to the total effective collecting area of the end tabs, filament, and plate. The effective area of the plate for positive ions is $A_p K_4$.

$$K_2 = \frac{A_{ET} + A_F}{A_{ET} + A_F + A_p K_4} \tag{5.23}$$

Putting this value of K_2 into equation (5.22) and solving for K_4 yields

$$K_4 = \frac{\overline{G_{-\perp}}}{\tau_-} \quad \frac{\tau_+}{L_+} \quad - \frac{A_{ET} + A_F}{A_p} \tag{5.24}$$

The transverse electronic mean free path $\overline{G_{-\perp}}$ equals the radius of the helical path $\sqrt{\overline{A^2}}$ for the range of pressures and magnetic flux densities used and is 1.543×10^{-2} centimeters for 800 gauss and 20 electron volts. The mean free time between electronic collisions τ_- is inversely proportional to the pressure and is $\frac{1.52 \times 10^{-7} \text{ sec}}{P/(\text{microns})}$. The effective collection velocity of the plasma electrons at the plate $\sqrt{\frac{\overline{A^2}}{\tau_-}}$ is then 1.017×10^5 P/(microns) centimeters per second. The values of positive ion average velocity previously calculated are about 5×10^5 centimeters per second. The plate area is approximately

$$A_p = \pi \; 0.75 \text{ cm } 2.0 \text{ cm} = 4.71 \text{ cm}^2 \tag{5.25}$$

The collecting area of the two end tabs is about

$$A_{ET} = 2 \frac{\pi}{4} (0.75 \text{ cm})^2 = 0.883 \text{ cm}^2 \tag{5.26}$$

The collecting area of the space charge sheath boundary at the filament having a radius of about one millimeter is approximately

$$A_F = \pi\ 0.2\ \text{cm}\ 2\ \text{cm} = 1.259\ \text{cm}^2 \tag{5.27}$$

Putting all these values into equation (5.24) we have

$$K_4 = \frac{1.017 \times 10^5 P/(\text{microns})}{5 \times 10^5} - \frac{1.259 + 0.883}{4.71} \tag{5.28}$$

As the pressure decreases, K_4 decreases, which means that the plasma potential decreases so that fewer of the positive ions have energy enough to penetrate the sheath at the plate. At 2.24 microns, K_4 is 0, no positive ions are collected by the plate, and the plasma potential sinks so far below the plate potential that the discharge goes over to another mode of operation without the positive column. This agrees with the break in the plate current versus pressure curve shown in Figure (5.2) at about 3 microns.

Because the plasma electrons travel back and forth freely in the magnetic field direction, the collecting area of a helical wire plate for electrons is the same as the area of a cylindrical sheet of the same diameter and length as the helix. When a collision knocks an electron into the space between the helical wires the z direction motion of the electron makes it strike the plate helix which captures it. The collecting area of the helical wire plate for positive ions is less than that for electrons because some of the positive ions can enter the region between the helix wires and

then come back into the plasma region without being collected. The fraction K_4 is thus the product of two factors K_5 K_6.

The factor K_5 may be called the opaqueness of the plate for positive ion collection. It is the ratio of the number of positive ions collected by the plate to the number which pass through the cylindrical surface at the inside of the helix when the plasma potential equals the plate potential.

The factor K_6 is the ratio of the number of positive ions with energy equal to, or greater than, the potential energy hill in the space charge sheath at the plate to the total number of positive ions. Because of the Boltzmann energy distribution of the positive ions

$$K_6 = \exp\left\{ - \frac{e(V_A - V_p)}{kT_+} \right\} \tag{5.29}$$

where V_A is the plate potential and V_p is the plasma potential. As K_6 approaches zero V_p approaches minus infinity very rapidly so that the transition between the discharge modes with and without the plasma region occurs in a very small pressure range.

For a low pitch helical plate K_5 was about seven tenths, therefore the plasma and plate potentials are equal ($K_6 = 1$) at 5.69 microns pressure. Above 5.69 microns pressure the plasma potential is more positive than the plate potential and the less energetic plasma electrons cannot reach the plate. The ratio K_7 of the number of plasma electrons with energy equal to or greater than the

potential energy hill in the space charge sheath at the plate, to the total number of plasma electrons is

$$K_7 = \frac{A_{ET} + A_F + A_p K_5}{A_p} \frac{}{v_+} \frac{\tau_-}{\bar{G}_{-\perp}}$$

$$= \frac{5.442}{4.71} \frac{5 \times 10^5}{1.017 \times 10^5 P/(\text{microns})}$$

$$= \exp\left\{ - \frac{e(V_p - V_A)}{kT_-} \right\} \qquad (5.30)$$

At the higher pressure limit of 140 microns the plasma potential is 42.8 volts more positive than the plate potential.

Dependence of oscillation wavelengths on plate voltage

Figure (5.7) shows the wavelengths of the oscillations obtained as a function of the plate voltage. For a gas pressure of 10 microns and a magnetic flux density of 800 gauss the arc strikes at about 125 volts. Below this voltage there is zero plate current and no electromagnetic noise radiation from the tube.

From about 125 volts to about 350 volts the tube generates electromagnetic noise radiation but no measured coherent oscillations. In this voltage range the diameter of the emission electron

orbits, which is proportional to the square root of the plate voltage, is smaller than the filament space charge sheath thickness for the low plasma electron density of the lower frequency modes so the emission electrons don't get out into the plasma region. The higher frequency modes, with higher plasma electron densities and smaller filament sheath thicknesses, probably can occur in this low voltage range but larger values of emission current are required to produce the same electron density as at higher voltages. Above about 350 volts the emission electron orbit radii are sufficient to give oscillations with the wavelengths indicated.

Figure (5.8) shows the variation of the plate current with plate voltage for constant pressure, magnetic flux density, and filament current. At 15 microns pressure the arc strikes at about 75 volts. As the voltage increases, the plate current, and therefore the plasma electron density, increases. As the plate voltage increases the emission electrons become more energetic. At an ionizing collision between an emission electron and a gas molecule, increasing the energy of the colliding emission electron increases the average energy of the electron knocked off from the molecule by the collision. The average energy of the electrons knocked off by the collisions determines the plasma electron temperature.

The emission electrons can transfer only a small amount of energy to the positive ions at an elastic collision because of the large difference in masses of the electrons and positive ions. However, the emission electrons can transfer a large amount of

energy to the electrons resulting from the ionization collision because their masses are the same.

The plasma electron temperature should increase with increasing plate voltage. The ionization energy of oxygen is 11.2 electron volts and of nitrogen 15.8 electron volts. The measured average plasma electron energy at 600 volts plate voltage was 20 electron volts. A large part of the plasma electrons are thus energetic enough to ionize the gas. Increasing the plasma electron temperature increases the ionization rate. This accounts for the increase in plate current with increasing voltage.

Figure (5.9) shows the average plate current for the 43 millimeter oscillation of Figure (5.7). The length of the lines indicates the range of plate currents in which the oscillation is obtained. The data points not written as lines are understood to have a similar range of plate current. The theory shows that the plate current for a certain oscillation mode is not a function of the plate voltage. Figure (5.9) is consistent with this prediction.

The plate current should be proportional to the square root of the electron temperature for a certain electron density as shown by equation (5.13). Since Figure (5.9) shows that the plate current for a certain oscillation mode is approximately constant for all values of plate voltage, the electron temperature is a low powered function of the plate voltage. The ionization rate is a high powered function of the electron temperature.

Dependence of oscillation frequencies on the plasma electron density

It is seen from Figure (5.1) that the measured wavelengths of the electromagnetic radiation from the plasma oscillations are approximately equal to integer submultiples of the cyclotron wavelength. The cyclotron wavelength is the wavelength in free space of an electromagnetic wave of the cyclotron frequency. This frequency, f_c, is

$$f_c = \frac{eB}{2\pi m} \tag{5.31}$$

in MKS units and is therefore a function only of the magnetic flux density. In Figure (5.1) the dotted lines represent calculated wavelengths corresponding to multiples of the cyclotron frequency.

Let us call the oscillation mode having a frequency approximately M times the cyclotron frequency the Mth mode. Figure (5.1) then shows oscillations in the second through the eighth mode. The intensities of the oscillations in the various modes are roughly equal, the lower frequencies being stronger.

Since $\omega = M\omega_c$, the dispersion relation can be written in terms of the mode number

$$\omega^2 = M^2 \omega_c^2 = \omega_c^2 + \omega_p^2 \tag{5.32}$$

The current to the end tabs is proportional to the positive ion

density which is in turn proportional to the square of the plasma angular frequency ω_p^2.

$$I_{ET} \sim n_+ \approx n_- \sim \omega_p^2 = (M^2 - 1)\,\omega_c^2 \qquad (5.33)$$

According to the theory the current to the end tabs should then be proportional to $(M^2 - 1)$. Figure (5.10) shows that this is so. The values for Figure (5.10) are from the same set of data as shown in Figure (5.1). The end tab current values are obtained from the plate current values and are shown in Figure (5.11). Figure (5.12) also shows the end tab current as a function of $(M^2 - 1)$ from the set of data shown in Figure (5.13).

It is seen in Figure (5.11) that a greater portion of the total current goes to the end tabs as the plate current increases. This is because the space charge sheath thickness decreases with increasing positive ion density so the collecting area for positive ions going to the filament decreases while the collecting area for positive ions going to the end tabs remains almost constant.

The values in Figure (5.13) marked by crosses were obtained with a cylindrical sheet anode. The other values are for a helical wire anode with end tabs farther apart. Oscillation frequencies approximately integer multiples of the cyclotron frequency were obtained with all combinations of electrode structures tried. Thus the oscillation frequencies are not critical functions of the electrode geometry or size. Some of the electrode structures tried

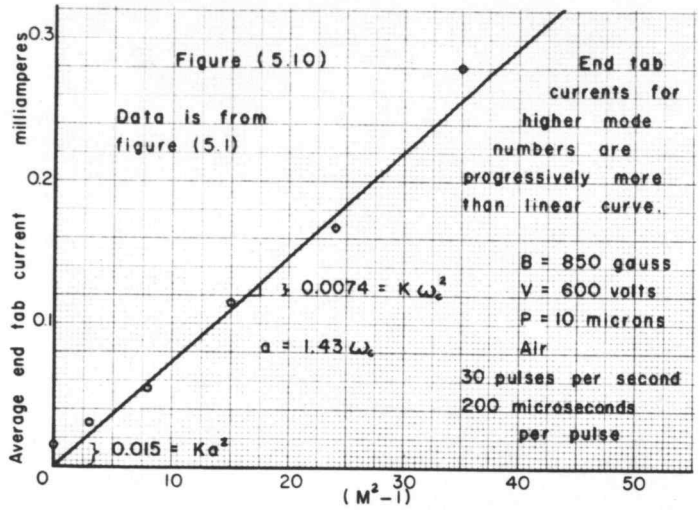
Figure (5.10)
Data is from figure (5.1)
End tab currents for higher mode numbers are progressively more than linear curve.
B = 850 gauss
V = 600 volts
P = 10 microns
Air
30 pulses per second
200 microseconds per pulse
} 0.0074 = K ω_c²
a = 1.43 ω_c
} 0.015 = Ka²
Average end tab current milliamperes
(M²-1)

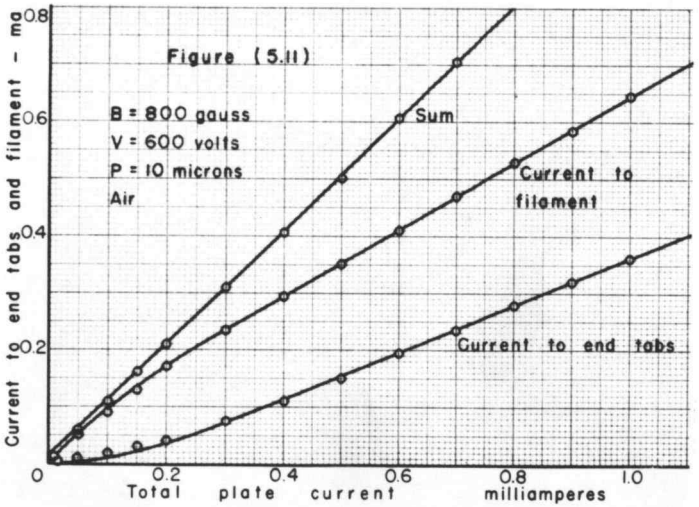
Figure (5.11)
B = 800 gauss
V = 600 volts
P = 10 microns
Air
Sum
Current to filament
Current to end tabs
Current to end tabs and filament - ma
Total plate current milliamperes

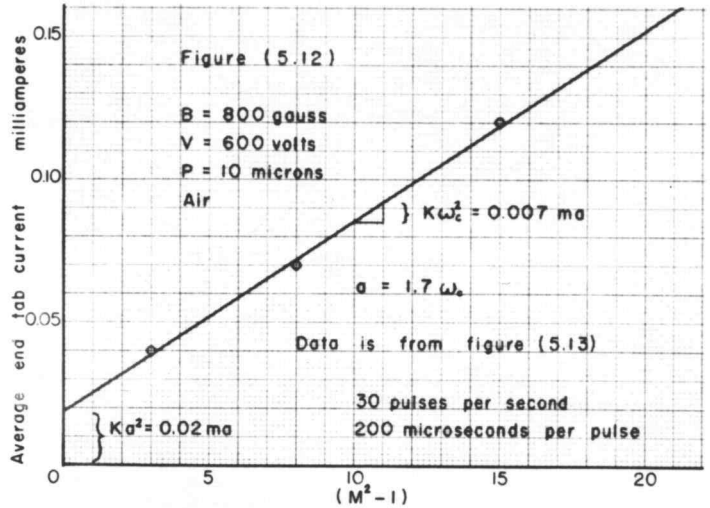
Figure (5.12)
B = 800 gauss
V = 600 volts
P = 10 microns
Air
} Kω_c² = 0.007 ma
a = 1.7 ω_c
Data is from figure (5.13)
30 pulses per second
200 microseconds per pulse
} Ka² = 0.02 ma
Average end tab current milliamperes
(M²-1)

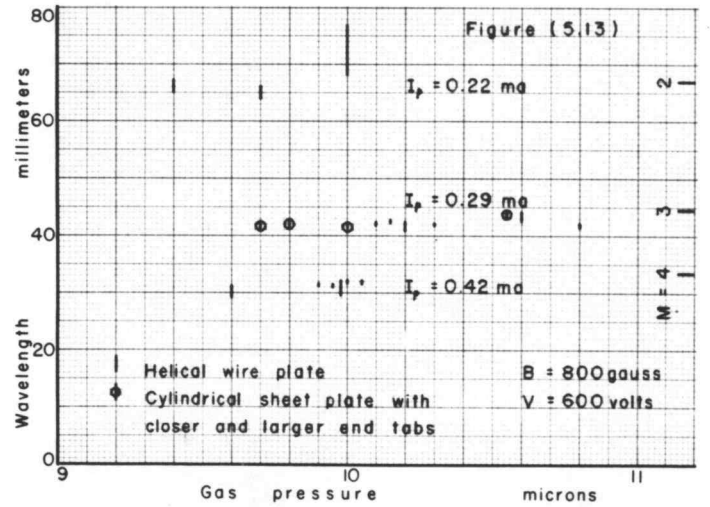
Figure (5.13)
I_p = 0.22 ma
I_p = 0.29 ma
I_p = 0.42 ma
M = 2
M = 3
M = 4
Helical wire plate
Cylindrical sheet plate with closer and larger end tabs
B = 800 gauss
V = 600 volts
Wavelength millimeters
Gas pressure microns

were helical wire anodes of various numbers of turns and various diameters, cylindrical sheet anodes of various diameters and lengths, various spacings and sizes of end tabs, and end tabs tilted at about a 45 degree angle to the filament direction.

The lengths of the lines in Figure (5.13) indicate the uncertainty of the wavelength measurements. During a measurement, the operator marks pips on the graphic ammeter paper for the signal minima observed on the cathode ray oscilloscope. The line lengths represent the maximum and minimum pip spacings.

Dependence of oscillation wavelengths on the magnetic flux density

Figure (5.14) shows a set of measured wavelengths of plasma oscillations as a function of the magnetic flux density with the anode voltage and gas pressure held constant. For a certain setting of magnetic flux density, the filament current, and thus the emission current, was increased to shift across the figure, horizontally from right to left passing through modes of regularly decreasing wavelengths. Increasing the emission current increases the plasma electron density which increases the plasma frequency.

Both the circles and the short fat lines represent experimentally observed oscillations. The lengths of the short fat lines represent the uncertainty of that wavelength measurement. The solid line curves represent the calculated wavelengths corresponding to frequencies which are integer multiples of the cyclotron frequency.

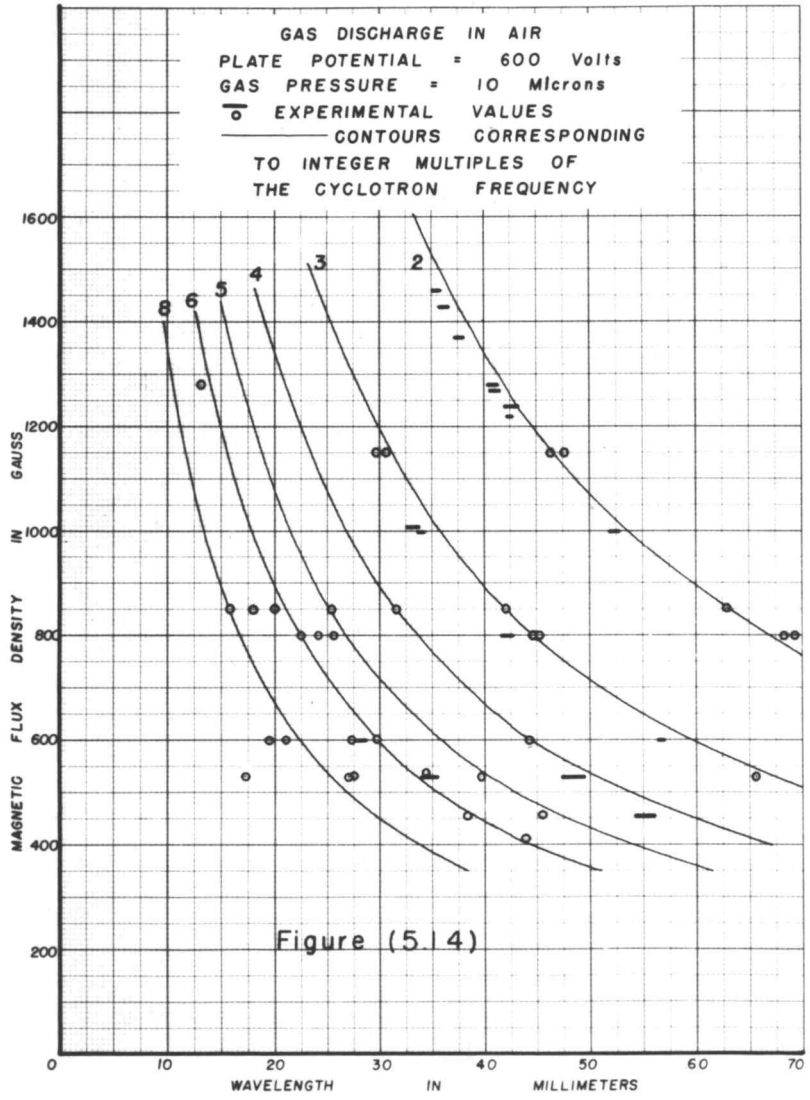
GAS DISCHARGE IN AIR
PLATE POTENTIAL = 600 Volts
GAS PRESSURE = 10 Microns
EXPERIMENTAL VALUES
CONTOURS CORRESPONDING TO INTEGER MULTIPLES OF THE CYCLOTRON FREQUENCY
MAGNETIC FLUX DENSITY IN GAUSS
WAVELENGTH IN MILLIMETERS
1600
1400
1200
1000
800
600
400
200
0
10
20
30
40
50
60
70
2
3
4
5
6
8

Figure (5.14)

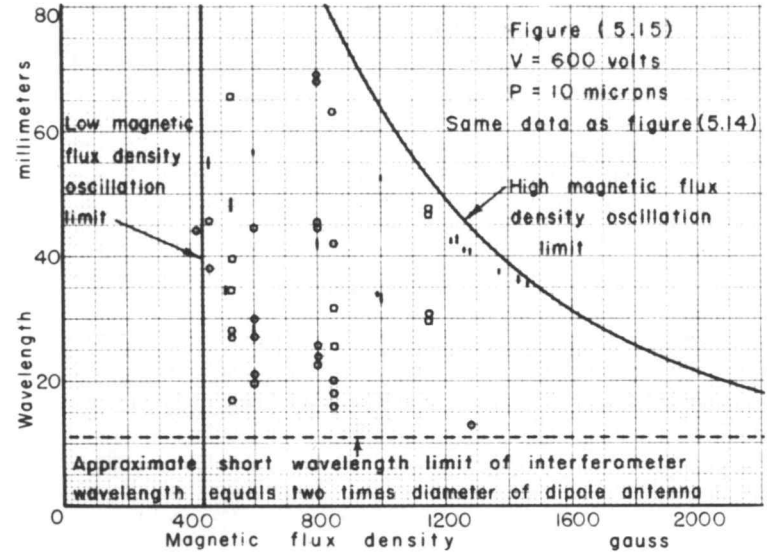
Figure (5.15)
V = 600 volts
P = 10 microns
Same data as figure (5.14)
Low magnetic flux density oscillation limit
High magnetic flux density oscillation limit
Approximate wavelength
short wavelength limit of interferometer equals two times diameter of dipole antenna
Wavelength millimeters
80
60
40
20
0
400
800
1200
1600
2000
Magnetic flux density gauss

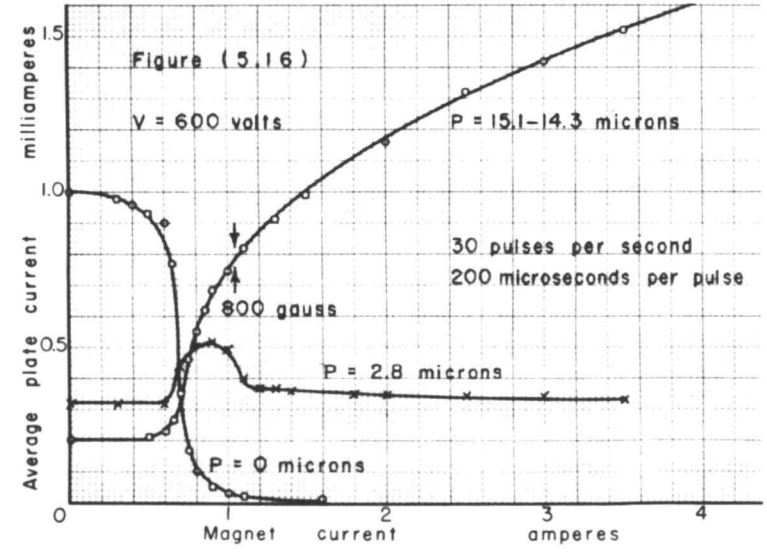
Figure (5.16)
V = 600 volts
P = 15.1-14.3 microns
30 pulses per second
200 microseconds per pulse
800 gauss
P = 2.8 microns
P = 0 microns
Average plate current milliamperes
1.5
1.0
0.5
0
1
2
3
4
Magnet current amperes

It is seen that the frequencies of the observed oscillations are approximately equal to integer multiples of the cyclotron frequency for the whole range of magnetic flux densities. The same frequencies were obtained for the different gases used (argon, nitrogen, and air).

For the lower oscillation modes, where the wavelengths of the modes are quite different in value, the interferometer completely resolves the modes. As is also shown in Figure (5.13), there are no wavelengths corresponding to half integer multiples of the cyclotron frequency. This is an important point which will be discussed further in a section on the excitation mechanism. For the higher numbered modes the resolution of the interferometer is insufficient to completely resolve the oscillations into their correct modes.

From Figure (5.14) the frequency is seen to be a continuously varying function over a frequency range of two or three to one by varying the magnetic flux density and one other variable, for example the filament current, in such a way that the oscillation stays in the same mode. For mode number two the wavelength can be continuously varied from about 100 millimeters to 35 millimeters. The wavelength range from about 10 millimeters to about 100 millimeters can be covered continuously by using several modes.

Magnetic flux density limits of oscillations

For small values of magnetic flux density the paths of the emission electrons are not bent much by the magnetic field and the emission current is intercepted by the anode. The anode diameter is about 7.5 millimeters so the magnetic flux density which would just cut off the emission current from reaching the 600 volt plate is about 440 gauss, which agrees well with Figure (5.14). The cut-off relation does not depend on the shape of the potential distribution between cathode and plate for it is derived from the energy relation. This imposes a lower limit on the frequency for each mode. The emission current must be cut off from the plate to obtain oscillations. The cut-off is quite sharp, going from strong oscillations to almost none in a range of about 50 gauss.

For large values of magnetic flux density the paths of the emission electrons are bent so much that the emission current stays entirely inside the space charge sheath at the filament and never gets out into the plasma region where the plasma electrons are. The emission electron beam passing through the same space occupied by the plasma electrons is a necessary condition for the excitation of these plasma oscillations.

As shown in Figure (5.14) mode two stops at about 1500 gauss. This cut-off at the cathode sheath is not as sharp as the cut-off at the plate. The space charge sheath thickness at the filament can be calculated from the space charge limited current equation in

cylindrical coordinates for zero magnetic field. Positive ions flow in the sheath from the cylindrical sheath boundary at the edge of the plasma region inward toward the cylindrical filament.

The space charge limited current I is

$$I = 2\pi \ell \frac{4\epsilon \sqrt{2e}}{9 \sqrt{M}} \frac{V^{3/2}}{r_o(-\beta^2)} \tag{5.34}$$

where ℓ is the length of the filament sheath, ϵ is the permittivity of free space, M is the mass of the positive ions, e is the positive ion charge, V is the potential drop across the sheath, r_o is the filament radius, $(-\beta^2)$ is a function of $\frac{r_1}{r_o}$ as given by Spangenberg (120, p. 178), and r_1 is the radius of the sheath boundary, all in MKS units. Kinetic theory gives the current of positive ions crossing the sheath boundary from the plasma region as

$$I = 2\pi r_1 \ell \frac{n_+ \overline{v_+} e}{4} \tag{5.35}$$

The radius of the sheath boundary is such that these two current relations are equal.

The wavelength of mode two, where it cuts off at 1500 gauss is about 35 millimeters. This corresponds to a frequency of 8.57 kilomegacycles and a positive ion density of 6.91×10^{11} positive ions per cubic centimeter.

The radius of the orbits of the 600 volts emission electrons in a magnetic flux density of 1500 gauss is 0.55 millimeters. Circular orbits for the emission electrons are quite good approximations to their actual orbits as shown by numerical-graphical trajectory plots of an emission electron in the cathode sheath. This is because the voltage gradient is large at the cathode so that the emission electrons acquire their velocities quickly and the instantaneous radius of curvature of their orbits is proportional to their instantaneous velocities.

If the average velocity of the positive ions were known accurately, the radius of the sheath boundary r_1 could be calculated from equations (5.34) and (5.35) and then the magnetic flux density value found which would just prevent the emission electrons from reaching the radius r_1. Since the positive ion average velocity is the least accurately known of the parameters in equations (5.34) and (5.35), the experimental cut-off value of 1500 gauss can be used to get a value for the positive ion average velocity. Since r_1 is about 1.1 millimeters $\frac{r_1}{r_o} = \frac{1.1 \text{ mm}}{0.127 \text{ mm}} = 8.69$.

Combining equations (5.34) and (5.35)

$$\overline{v_+} = 4 \frac{4\epsilon \sqrt{2e}}{9 \sqrt{M_+}} \frac{V^{3/2}}{r_o r_1 (-\beta^2) n_+ e}$$

$$= \frac{4 \times 1.455 \times 10^{-8} (600)^{3/2} \text{ amperes cm}^3}{1.27 \times 10^{-2} \text{cm } 0.11 \text{cm} (28.8) \ 6.91 \times 10^{11} \times 1.6 \times 10^{-19} \text{ coulombs}}$$

$$= 1.918 \times 10^5 \text{ centimeters per second} \qquad (5.36)$$

Let us consider the changes in this calculation which must be made to account for the effect of the magnetic field. The radius of curvature of the positive ions becomes large as they acquire higher velocities upon falling through the potential difference across the cathode sheath. The radius of curvature of a 300 volt positive ion, having fallen half way down the potential energy hill at the cathode, is 5.1 centimeters, so the space charge limited current through the cathode sheath is almost unaffected by the magnetic field.

The radius of the orbit R of a 1.918×10^5 centimeter per second positive ion in a magnetic flux density of 1500 gauss is 1.52 millimeters which is less than the transverse collision mean free path $\overline{L_\perp}$ of 5.84 millimeters. The magnetic field, bending the trajectories of the thermal positive ions, makes the effective mean free path less than the collision mean free path and so reduces the effective average velocity $\overline{v_{eff}}$ by the ratio

$$\frac{\overline{v_{eff}}}{\overline{v}} = \frac{R}{\sqrt{R^2 + \overline{L_\perp}^2}} = \left[\frac{\overline{v_\perp^2}}{\overline{v_\perp^2} + \overline{L_\perp^2}\,\omega_c^2} \right]^{1/2} \tag{5.37}$$

With an effective average velocity of 1.918×10^5 centimeters per second, from equation (5.36), and a cyclotron frequency ω_c for atomic air positive ions of 1.028×10^6 radians per second, for B = 1500 gauss, equation (5.37) becomes

$$\frac{1.918 \times 10^{5} \text{ cm/sec}}{\bar{v}}$$

$$= \frac{7.95 \times 10^{-7} \text{ sec } \bar{v}}{\left[(0.584 \text{ cm})^2 + (7.95 \times 10^{-7} \text{ sec } \bar{v})^2\right]^{1/2}} \qquad (5.38)$$

The positive root of this biquadratic equation is $\bar{v} = 4.0 \times 10^5$ centimeters per second which is in fair agreement with the values of the average positive ion velocity of 4.35×10^5 and 5.66×10^5 centimeters per second obtained from measurements of the current to the end tabs.

The cathode sheath thickness decreases with increasing plasma electron density so the cut-off value of magnetic flux density increases with decreasing wavelength. Combining equations (5.36) and (5.37) with the dispersion relation

$$\omega^2 = \omega_c^2 + \omega_p^2 = \frac{4\pi^2 c^2}{\lambda^2} = \frac{e^2 B^2}{m^2} + \frac{e^2 n_+}{\epsilon m} \qquad (5.39)$$

a relation is obtained between the wavelength limit of the electromagnetic radiation from the tube and the cathode sheath cut-off value of the magnetic flux density B_{max}.

$$\lambda = \frac{2\pi c m}{e B \sqrt{1 + \dfrac{8V\sqrt{\dfrac{m}{M}}\; e\sqrt{\dfrac{2}{3}\dfrac{\bar{v}^2 M^2}{e^2 B^2} + L_\perp^2}}{9 r_o (-\beta^2)\sqrt{\dfrac{2}{3}}\,\bar{v}^2 M}}} \tag{5.40}$$

in MKS units, which for the 600 volts plate voltage, 10 mil filament diameter, 10 microns gas pressure, and $\bar{v} = 4.0 \times 10^5$ cm/sec, becomes

$$\lambda = \frac{10.72 \times 10^{-3} \text{ meters}}{B_{max}\left[1 + \dfrac{1.371 \times 10^4}{(-\beta^2)}\right]\left(\dfrac{2.28 \times 10^{-7}}{B_{max}^2} + 3.505 \times 10^{-5}\right)^{1/2}\Bigg]^{1/2}} \tag{5.41}$$

with B in webers per square meter. The factor $(-\beta^2)$ is a function of $\frac{r_1}{r_o} = \frac{1.302}{B}$ (120, p. 178).

Figure (4.15) shows the limits of the oscillations due to the plate cut-off, the cathode sheath cut-off and the limits of the wavelength measurements due to the thickness of the dipole antenna. The thickness of the dipole antenna, 5.5 millimeters, becomes comparable to the half wavelength of the radiation for the higher frequencies. Figure (5.15) uses the same data as Figure (5.14). For the higher range of emission current, which should give

oscillations with free space wavelengths of the electromagnetic radiation shorter than 1.1 centimeters, there is plenty of radiation from the tube but the interferometer fails to measure any wavelengths.

Figure (5.16) shows the plate current as a function of the magnetic flux density with the other parameters held constant. At zero gas pressure the plate current is just the emission current, which is cut off from the plate at the higher values of magnetic flux density. For finite gas pressures the plate current increases with increasing magnetic flux density above the plate cut-off value. An ionizing collision by an emission electron can scatter the electron to the plate, for the lower flux density values, where it is collected before it has made many ionizing collisions. The higher magnetic fields bend the emission electron orbits so that more ionizing collisions are necessary to scatter the emission electrons to the plate.

In Figures (5.1), (5.3), (5.5), and (5.7) the odd mode numbers M have more oscillations measured than the even mode numbers. The odd M mode number oscillations seemed to be usually stronger than the even mode number oscillations. This could be due to a coupling to the electrode structure which acts as an antenna and reradiates part of the energy.

THE EXCITATION MECHANISM

Standing wave pattern in the tube

The emission electrons travel in approximately circular orbits from the cathode out into the plasma and back to the cathode again. They thus have velocity components in the plus and minus r directions and in the plus $\emptyset$ direction. To have a condition in which the emission electrons can feed energy to the longitudinal plasma waves the plasma wave phase velocity and the emission electron velocity must have components in the same direction.

Measurements of polarization inside the tube have been made (13$\frac{1}{4}$, April-June 1950). The data are shown in Figure (6.1) which indicates that the power coupled out of the tube when a coupling loop was inserted into the plasma region with the plane of the loop perpendicular to the filament was up to a thousand times greater than when the plane of the loop was parallel to the filament, or when a radial probe was inserted into the plasma region. This indicates that the electric field of the oscillations is in the $\emptyset$ direction. The longitudinal plasma waves are thus traveling in the plus and minus $\emptyset$ directions. Polarization measurements outside the tube are inconclusive because of the tube elements, acting as antennas, radiating the electromagnetic waves in a complex pattern.

To obtain radiation of a definite frequency, standing waves must form and build up until the radiation from this coherent oscillation

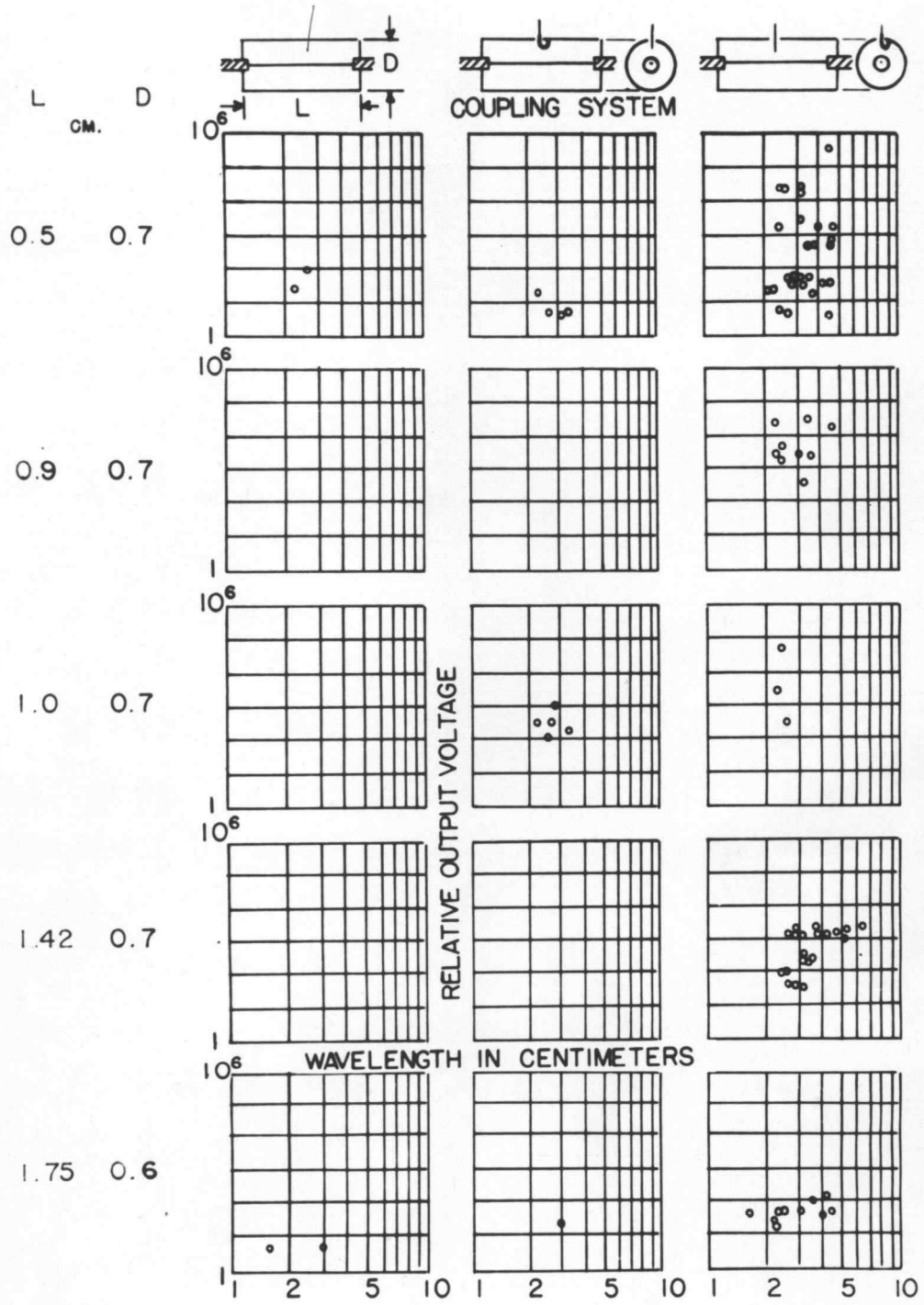
L
CM.
D
0.5 0.7
0.9 0.7
1.0 0.7
1.42 0.7
1.75 0.6
D
L
COUPLING SYSTEM
10^6
1
RELATIVE OUTPUT VOLTAGE
WAVELENGTH IN CENTIMETERS
1 2 5 10

Figure (6.1)

is appreciably larger than the transient oscillations which generate the incoherent noise radiation. Standing plasma waves in the ϕ direction may be resolved into two waves of equal amplitude, frequency, and wavelength traveling in the plus and minus ϕ directions. For the amplitude of the standing waves to be a single-valued function of position there must be an integer number of wavelengths around the circumference. This single-valuedness condition allows only oscillations with certain discrete frequencies.

The longitudinal plasma waves standing in the ϕ direction act like the anode structure of a multi-segment-anode magnetron and an exciting mechanism similar to the magnetron excitation mechanism explains the generation of oscillations.

Figure (6.2) shows the standing wave pattern in the plasma for four wavelengths around the circumference. The radial dotted lines are the nodes of the standing waves and the arrows show the direction of the plasma electron displacement in each internode region at a certain instant. The distance in the ϕ direction between adjacent nodes is equal to half the wavelength of the plasma waves. The plasma wavelength is thus proportional to the radial distance out to where the wavelength is measured.

It was shown in the first section that the frequency of the plasma oscillation is determined by the plasma electron density n and the magnetic flux density B. The oscillation frequency ν is constant throughout this region. The plasma wavelength λ_p is determined by the boundary conditions. The phase velocity of the

Figure (6.2)

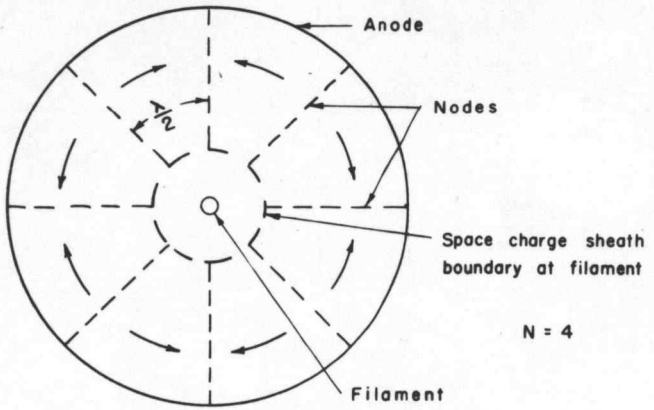

Figure (6.3) Magnetic flux out of page

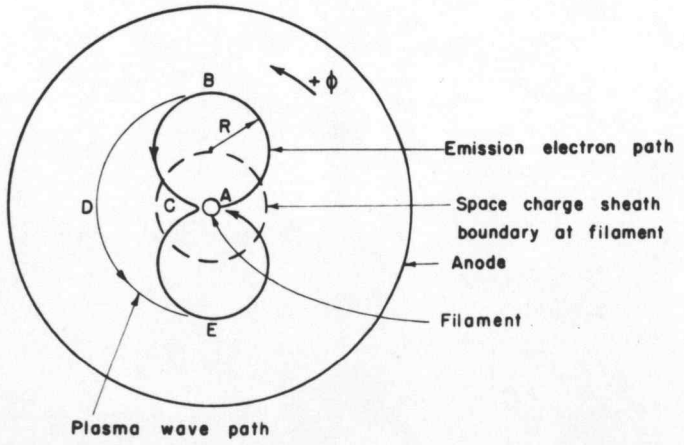

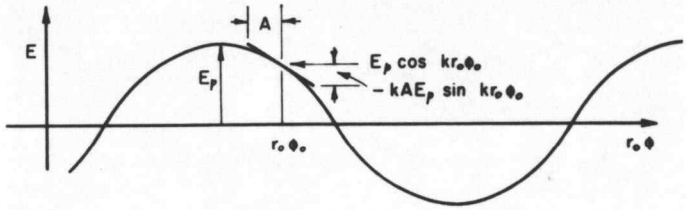

Figure (7.1)

Figure (7.2)

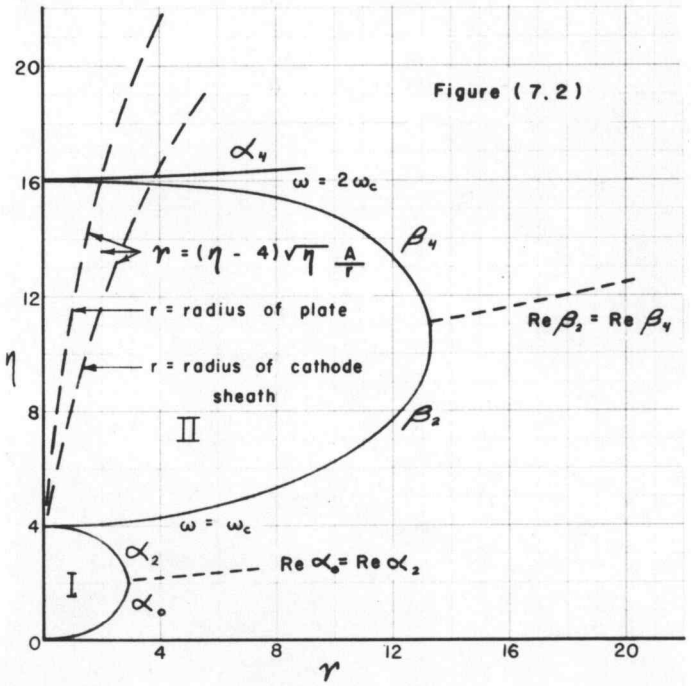

traveling plasma waves is $v_p = \lambda_p \nu$. The frequency is constant and the plasma wavelength is proportional to the radial distance r so the phase velocity is proportional to r.

Let us call an oscillation with N wavelengths around the circumference the Nth mode and later find the relation between the N and M mode numbers. The Mth mode is an oscillation with a frequency approximately equal to M times the cyclotron frequency. In the Nth mode

$$N\lambda_p = 2\pi r$$

or

$$\lambda_p = \frac{2\pi}{N} r \tag{6.01}$$

The phase velocity of the plasma waves at radius r is

$$v_p = \lambda_p \nu = \frac{2\pi\nu}{N} r \tag{6.02}$$

The traveling plasma waves are plane waves since a surface of constant phase is a plane. This plane contains the filament axis and rotates around this axis with constant angular velocity ω_ϕ.

$$\omega_\phi = \frac{v_p}{r} = \frac{2\pi\nu}{N} = \frac{\omega}{N} \tag{6.03}$$

Selection principle

Figure (6.3) shows an emission electron path. An electron thermally emitted from the filament at A falls down the potential energy hill in the cathode space charge sheath and enters the almost equipotential plasma region. The magnetic field bends its trajectory. In the plasma region its path is a circular arc.

Those electrons which are in an accelerating force field of the plasma wave when they are at position B take some energy from the plasma wave and when they arrive back at the filament at position C have more than enough energy to run up the potential energy hill at the filament sheath and be collected by the filament. These are the nonworking emission electrons. They only make one excursion into the plasma region.

Those electrons which are in a decelerating force field of the plasma waves when they are at position B give some of their energy to the plasma waves. These have insufficient energy to completely run up the potential energy hill at the filament sheath. They thus make more excursions into the plasma. These are the working electrons.

When the phase velocity of the plasma wave traveling in the plus $\emptyset$ direction is such that the wave travels the path B-D-E in the same time that the emission electron bunch travels the path B-C-E the emission electrons are in the same phase of the wave at E as at B and thus deliver more energy to the plasma wave.

If for simplicity we consider the filament and the space charge sheath at the filament to have infinitesimal thicknesses, the emission electron orbits become circles of radius R which the electrons travel at constant speed $v = \omega_c R$. The distance B-D-E that the plasma wave travels equals the distance B-C-E travelled by the emission electrons. If the phase velocity of the wave at radius 2R equals the velocity of the emission electrons a net energy is fed to the plasma wave and oscillations are possible. Thus

$$\frac{\omega}{N} 2R = v_p = v = \omega_c R \tag{6.04}$$

or

$$\omega = \frac{N}{2} \omega_c$$

but

$$\omega = M\omega_c \tag{6.05}$$

so the two mode numbers are related by $M = \frac{N}{2}$. The angular velocity of rotation, ω_ϕ, of the planes of constant phase around the filament axis is equal to

$$\omega_\phi = \frac{v_p}{2R} = \frac{\omega_c}{2} = \frac{eB}{2m} \tag{6.06}$$

or half the cyclotron angular velocity for electrons and is not a function of the plate voltage, gas pressure, or emission current.

From equations (6.03) and (6.06) we see that for every integer number N of plasma wavelengths around the circumference there exists a plasma electron density which gives an angular oscillation frequency ω such that $\frac{\omega}{N} = \omega_\phi = \frac{\omega_c}{2}$. Thus only discrete frequencies can be excited.

This magnetron excitation mechanism is available for exciting oscillations with frequencies equal to integer multiples of half the cyclotron frequency but oscillations are obtained experimentally which are integer multiples of the cyclotron frequency. This discrepancy is explained later where a refinement of the plasma oscillation theory shows that oscillations with even integer mode number N are unstable and tend to build up into oscillation while oscillations with odd integer mode numbers N are stable and do not tend to increase their amplitude.

The excitation mechanism depends upon the interaction between the emission electron beam and the plasma waves. The plasma waves modulate the emission electrons which in turn feed a net energy to the waves because of this modulation. Thus the plasma waves and the emission electron beam modulation grow or decay together. The collision damping of the plasma waves is sufficient to keep the oscillations from building up except when the plasma is unstable.

The resistance of the plasma oscillation R equals the sum of the collision damping resistance R_c, which is always positive, the plasma resistance R_p, which is negative for the growing wave and positive for the decaying wave when N is an even integer and

otherwise zero and is proportional to the oscillation amplitude, and the radiation resistance $R_r(a^2)$, which is always positive and proportional to the square of the oscillation amplitude.

$$R = R_c + R_r(a^2) \qquad \text{when N is not an integer} \qquad (6.07)$$

$$R = R_c - R_b(a) + R_r(a^2) \qquad \text{when N is odd} \qquad (6.08)$$

$$R = R_c \mp R_p - R_b(a) + R_r(a^2) \qquad \text{when N is even} \qquad (6.09)$$

The plasma resistance R_p is in general greater than the collision damping resistance R_c so when N is even, the oscillation resistance R is negative at zero oscillation amplitude and the oscillation builds up until the radiation resistance makes R go to zero. Then $R_b = R_c + R_r$ where in general R_r at maximum amplitude is much greater than R_c. When N is odd R is positive at zero amplitude and only becomes negative for a finite amplitude. If the beam current were large enough to supply a noise amplitude of this magnitude the tube would oscillate. Because of the finite charge of an electron in combination with its random emission, the mean square value of the fluctuating component $\overline{I_n^2}$ of a d.c. current I in the bandwidth Δf is

$$\overline{I_n^2} = 2eI\,\Delta f$$

in a temperature-limited state, up to frequencies for which transit times are important where the effective value of e must be revised (48, p. 224). The "starting current" for odd N in the plasma-magnetron oscillator tube is in general too high, however.

At 10 microns gas pressure a working emission electron makes 30.8 loops into the plasma on the average before suffering an ionizing collision while a nonworking emission electron makes only one loop. Thus spokes of negative charge build up in the decelerating phase of the plasma wave traveling in the plus ϕ direction and rotate with the traveling wave about the filament axis with an angular velocity equal to half the cyclotron angular velocity. These rotating space charge spokes of emission electrons give energy to the plasma wave traveling in the plus ϕ direction. The restoring forces in the plasma tending to make the plasma electrons return to their equilibrium positions couple the energy to the plasma wave traveling in the minus ϕ direction.

In polar coordinates the differential equations of motion of electrons in an axial magnetic field and a radial electric field are

$$\frac{d^2r}{dt^2} - r\left(\frac{d\phi}{dt}\right)^2 = -\frac{e}{m} r \frac{d\phi}{dt} B + \frac{e}{m}\frac{dV}{dr} \tag{6.10}$$

for the radial component of motion and

$$\frac{1}{r}\frac{d}{dt}\left(r^2 \frac{d\phi}{dt}\right) = r\frac{d^2\phi}{dt^2} + 2\frac{dr}{dt}\frac{d\phi}{dt} = \frac{e}{m}\frac{dr}{dt} B \tag{6.11}$$

for the angular component of motion. The solution of equation (6.11) using the initial condition that $\frac{d\phi}{dt} = 0$ when $r = r_c$, the cathode radius, is

$$\frac{d\phi}{dt} = \frac{\omega_c}{2}\left[1 - \frac{r_c^2}{r^2}\right] \tag{6.12}$$

When this relation is substituted into equation (6.10) a differential equation for the radial component of motion alone is obtained but it is difficult to solve because it is non-homogeneous and because V is a complicated function of r. The average value of the angular velocity of the emission electrons around the filament axis could be obtained if their radial position r were known as a function of time. Even if this is not known exactly, a qualitative discussion gives an approximate value for the average angular velocity of the emission electrons.

Since the emission electron orbits are approximately circular with a diameter about ten to thirty times the filament radius, the emission electrons spend most of the time at a large distance from the filament and the second term on the right hand side of equation (6.12) contributes only a small amount to the time average of $\frac{d\phi}{dt}$. The average angular velocity should thus be slightly less than half the cyclotron angular velocity. Equation (6.12) does not apply exactly because the plasma oscillations exert tangential forces on the emission electrons.

The measured wavelengths in all the figures except Figure (5.1) are slightly less than the integer submultiples of the calculated free space wavelength corresponding to the cyclotron frequency. In Figure (5.1) the measured wavelengths are slightly more than the calculated values but the magnetic flux density for this set of data was measured by a rotating coil fluxmeter. This fluxmeter was found later to read too high a magnetic flux density value. The calculated wavelengths were thus too low, so all the data give measured wavelengths consistently slightly less than the calculated values. The accuracy of the magnetic flux density calibration is probably only within a few percent and is not sufficient to say whether the plasma oscillation frequencies are exactly integer multiples or slightly higher or slightly lower than integer multiples of the cyclotron frequency.

PLASMA OSCILLATION THEORY

Plasma oscillations in a uniform static magnetic field with long wavelengths and thermal motions

Equation (1.49) gives the electric field that a plasma electron sees as its thermal helical motion takes it to different parts of the plasma standing wave. In a cylindrical coordinate system this electric field is in the tangential direction and is given by

$$\vec{E} = \vec{\epsilon}_{\phi} E_p(r,z) \cos k \left[r_o \phi_o + A \cos(\omega_c t + \alpha) \right] \cos \omega t \qquad (7.01)$$

where $r_o \phi_o$ is the ϕ coordinate of the center of the thermal circle, A is the radius of the thermal circle, α is the phase angle between the thermal motion and the plasma oscillation motion, and $k = \frac{2\pi}{\lambda_p}$ is the propagation constant.

The expansion of equation (7.01) is

$$\vec{E} = \vec{\epsilon}_{\phi} E_p \cos \omega t \left\{ \cos k r_o \phi_o \cos \left[kA \cos (\omega_c t + \alpha) \right] \right.$$

$$\left. - \sin k r_o \phi_o \sin \left[kA \cos (\omega_c t + \alpha) \right] \right\} \qquad (7.02)$$

Keeping only zero and first degree terms for $kA < 0.2$, equation (7.02) reduces to

$$\vec{E} = \vec{\varepsilon}_{\phi} E_p \cos \omega t \left[\cos k r_o\phi_o - kA \sin k r_o\phi_o \right.$$

$$\left. \cos (\omega_c t + \alpha) \right] \qquad (7.03)$$

or in complex notation

$$\vec{E} = \vec{\varepsilon}_{\phi} E_p \cos \omega t \text{ Real part of } \left\{ \left[1 + ikA \cos \right. \right.$$

$$\left. \left. (\omega_c t + \alpha) \right] \quad e^{ikr_o\phi_o} \right\} \qquad (7.04)$$

Equation (7.03) says that a plasma electron sees an electric field strength which varies periodically with time at the rate ω and is amplitude modulated at the rate ω_c. This is shown in Figure (7.1). Equation (7.03) approximates the actual variation of the electric field with distance by a linear variation.

The differential equation for the motion of an oscillating plasma electron is then, from equation (1.42),

$$\frac{d^2 s_\phi}{dt^2} + \omega_c^2 s_\phi + \frac{e}{m} E_p \cos \omega t \text{ Real part of}$$

$$\left\{ \left[1 + ikA \cos (\omega_c t + \alpha) \right] \quad e^{ikr_o\phi_o} \right\} = 0 \qquad (7.05)$$

Using equation (1.52), which gives the electric field strength resulting from a displacement of the plasma electrons,

$$\frac{en}{\varepsilon}\overline{s_\phi} = E_\phi = E_p \cos \omega t \cos k r_o \phi_o , \tag{7.06}$$

equation (7.05) becomes

$$\frac{d^2 s_\phi}{dt^2} + \left[\omega_c^{\,2} + \omega_p^{\,2} + ikA\,\omega_p^{\,2} \cos(\omega_c t + \alpha)\right] s_\phi = 0 \tag{7.07}$$

For infinite plasma wavelength, all the plasma electron oscillation displacements are the same so $\overline{s_\phi} = s_\phi$ but for a large but finite plasma wavelength the displacements s_ϕ of the individual electrons are slightly different from the average displacement $\overline{s_\phi}$, $\overline{s_\phi} \approx s_\phi$. The approximation that $\overline{s_\phi} = s_\phi$ is used in equation (7.07).

Amplitude modulation gives an imaginary coefficient of the periodic term while frequency modulation gives a real coefficient.

Equation (7.07) is recognized as Mathieu's equation

$$\frac{d^2 y}{dx^2} + (\eta + q \cos 2x)\, y = 0 \tag{7.08}$$

with the substitutions

$$2x = \omega_c t + \alpha \tag{7.09}$$

$$\eta = \frac{4(\omega_c^2 + \omega_p^2)}{\omega_c^2} \tag{7.10}$$

$$q = i\frac{4kA\,\omega_p^2}{\omega_c^2} = i\gamma \tag{7.11}$$

Mathieu's equation has received considerable study (88) but almost the entire work with Mathieu's equation is for real η and q. The characteristic numbers of integral order, a_n and β_n, of the Mathieu equation and the Mathieu functions, $ce_n(x,q)$ and $se_n(x,q)$ which are the solutions of Mathieu's equation, have been fairly completely tabulated for real η and q (130). The values of η, for a certain q, for which one of the two solutions of Mathieu's equation is periodic with period π or 2π are a_n and β_n. The factors a_n and β_n correspond to the functions $ce_n(x,q)$ and $se_n(x,q)$ respectively.

When q = 0 the solutions of the differential equation are $y = \cos\sqrt{\eta}\,x$ and $y = \sin\sqrt{\eta}\,x$. The Mathieu function $ce_n(x,q)$ becomes the cosine solution and the Mathieu function $se_n(x,q)$ becomes the sine solution when q = 0, and $\sqrt{\eta} = n$, with n an integer.

Our Mathieu equation has purely imaginary q and purely real η. A few of the characteristic numbers of integral order of the Mathieu equation for purely imaginary q and purely real η have been given by

Mulholland and Goldstein (95, pp. 834-840) and are shown in Figure (7.2) which shows the $\eta\gamma$ plane.

A formal solution of Mathieu's equation is

$$y_1(x) = e^{\mu x}\, \phi(x) \tag{7.12}$$

where $\mu = \alpha + i\,\beta$, with α and β real, is a function of η and q, and $\phi(x)$ is a periodic function of period π

$$\phi(x) = \sum_{r=-\infty}^{\infty} C_{2r}\, e^{i2rx} \tag{7.13}$$

When either α is not equal to zero or α equals zero, but β is non-integral, an independent solution is

$$y_2(x) = e^{-\mu x}\, \phi(-x) = y_1(-x) \tag{7.14}$$

because the Mathieu equation is unchanged by substituting -x for x.

By a continuation of the results for real η and q, when the parametric point (η,γ) lies inside a region such as I, II, etc. in Figure (7.2) α is zero and β is non-zero and the solutions are stable. The complete solution is

$$y(x) = A\sum_{r=-\infty}^{\infty} C_{2r}\, e^{i(2r+\beta)x} + B\sum_{r=-\infty}^{\infty} C_{2r}\, e^{-i(2r+\beta)x} \tag{7.15}$$

with $0 < \beta < 2$. The solution may also be written

$$y(x) = C \; ce_{2m+\beta}(x,q) + D \; se_{2m+\beta}(x,q) \tag{7.16}$$

where m is an integer. These are Mathieu functions of fractional order. If β is a rational fraction $\frac{p}{s}$, p and s being prime to each other, the solution is periodic with period $2s\pi$. When β is irrational, the solution is oscillatory but bounded and non-periodic.

When the parametric point (η,γ) lies outside a region such as I, II, etc. in Figure (7.2) α is non-zero and β is zero. The complete solution is then

$$y(x) = Ae^{\alpha x}\sum_{r=-\infty}^{\infty} C_{2r}\, e^{i2rx} + Be^{-\alpha x}\sum_{r=-\infty}^{\infty} C_{2r}\, e^{-i2rx} \tag{7.17}$$

If α is positive the first term of the solution approaches plus or minus infinity as x becomes infinite so the solution is unstable. If α is negative, instability arises from the second term. The solution may also be written in terms of the unstable Mathieu functions.

$$y(x) = C \; ceu_{2m+\alpha}(x,q) + D \; ceu_{2m+\alpha}(-x,q) \tag{7.18}$$

When the parametric point (η,γ) is on one of the characteristic curves in Figure (7.2) which divide the η,γ plane into stable and unstable regions both α and β are zero and the first solution is a periodic function of x of period π.

$$y_1(x) = \sum_{r=-\infty}^{\infty} C_{2r}\, e^{i2rx} \tag{7.19}$$

When the parametric point (η,γ) is on the α_{2m} characteristic curve the first solution is

$$y_1(x) = A\ \ ce_{2m}(x,q) \tag{7.20}$$

which is the even Mathieu function of integral order. When the parametric point (η,γ) is on the β_{2m} characteristic curve the first solution is

$$y_1(x) = A\ \ se_{2m}(x,q) \tag{7.21}$$

which is the odd Mathieu function of integral order. The second solutions corresponding to equations (7.20) and (7.21) are unstable. With imaginary q the solutions are complex in general which is expected because the differential equation is now complex.

The series of Mathieu show that for sufficiently small γ, α_{2m} and β_{2m} are real and α_o and α_2 become equal when $\gamma = 2.9376$. For larger values of γ, α_o and α_2 are conjugate complex numbers. Also β_2 and β_4, α_4 and α_6, β_6 and β_8, etc. behave in a similar way and α_{2m+1} and β_{2m+1}, are conjugate complex numbers for all values of γ.

From equations (6.04) and (7.10) and the dispersion relation

$$\eta = \frac{4\omega^2}{\omega_c^2} = N^2 \tag{7.22}$$

From equations (6.01), (6.04) and (7.11)

$$\gamma = (N^2 - 4)\, N \frac{A}{r} \tag{7.23}$$

where N is the number of standing plasma wavelengths around the filament, A is the radius of the thermal helix of the plasma electron (about 1.543×10^{-2} centimeters) and r is the radius corresponding to the plasma wavelength λ_p. Combining equations (7.22) and (7.23)

$$\gamma = (\eta - 4)\sqrt{\eta}\ \frac{A}{r} \tag{7.24}$$

which is shown as the dotted lines in Figure (7.2) for values of r equal to the plate radius and the radius of the cathode sheath and $A = A_{rms}$.

As the plasma electron density increases, η and γ increase along a curve between the dotted line curves. As the plasma electron density increases, the operating point (η,γ) passes through stable and unstable regions. The unstable regions occur in the vicinity of values equal to the square of even integers. Since $\eta = N^2$, $N = 2M$, and $M = \frac{\omega}{\omega_c}$ the unstable regions occur for integer M values, or for those values of plasma electron density which give an oscillation frequency which is an integer multiple of the cyclotron frequency.

An even number N of plasma wavelengths around the filament puts the operating point (η,γ) in an unstable region of the η,γ plane,

while an odd number puts the operating point (η,γ) in a stable region of the η,γ plane. Experimentally, oscillations occur for even N mode numbers so instability of the plasma electron oscillatory motion is a necessary condition for coherent oscillations.

When a plasma electron contributing to the organized plasma oscillation suffers a collision its oscillatory motion is destroyed and it starts out again with only its thermal motion. The rest of the plasma electrons in its vicinity are performing organized plasma oscillations so it sees an oscillating electric field which is the result of the plasma electron displacements. When the plasma electron density is such that the operating point (η,γ) is in an unstable region, the plasma electron motion is oscillatory and unstable so the oscillatory motion of this plasma electron which just suffered a collision increases in amplitude.

The oscillating plasma electron radiates electromagnetic energy with the same frequency as its oscillation frequency. The electromagnetic power radiated is proportional to the square of the amplitude of the plasma electron oscillation. The amplitude of the plasma electron oscillation is such that the plasma oscillations receive energy from the emission electrons at the same rate that radiation and collision damping take energy from the plasma oscillations.

When the plasma electron density is such that the operating point (η,γ) is in a stable region, there is no tendency for the

plasma oscillations to build up in amplitude so the oscillations only occur for even mode number N.

Gross (49, pp. 232-242) has derived exact expressions for the distribution function of the plasma electrons in a magnetic field from which can be obtained the dispersion relation of the plasma oscillations in a magnetic field. The distribution function contains an infinite series of Bessel functions of integer orders with argument kA. Each term of the infinite series contains the plasma oscillation frequency in the denominator so it is practical to obtain the dispersion relation only in certain limiting cases.

For $kA \ll 1$ his dispersion relation shows gaps at integer multiples of the cyclotron frequency in which steady state solutions are not possible. The magnitude of the frequency gap is, however, not easy to obtain from his distribution function. The Mathieu function derivation gives an unstable region at $\omega \approx 2\omega_c$ of width

$$\frac{\Delta\omega}{\omega} = \frac{(750)(5,308,416)}{(864,000)(32)} \left(\frac{A}{r}\right)^4 = 144.1 \left(\frac{A}{r}\right)^4 \qquad (7.25)$$

This expression is valid for $\gamma = 48 \frac{A}{r}$ less than about 0.1 but the γ for the tube range from about 2 to 4 for mode number M = 2 as shown in Figure (7.2). For γ greater than 0.1 the frequency width of the unstable region may be calculated by a rather lengthy iteration process as shown by McLachlan (88, pp. 48-56). For mode 2 and γ=3.2,

$$Q = \frac{\omega}{\Delta\omega} = \frac{8M^2}{\Delta\eta} = \frac{32}{\Delta\eta} = \frac{32}{16.050 - 15.912} = 232 \qquad (7.26)$$

and

$$\Delta f = \frac{\Delta\eta\,\omega_c}{16\pi M} = 19.3 \text{ megacycles per second} \qquad (7.27)$$

The reason for the band structure of a plasma is similar to that for a solid. In the solid state problem the electron travels in the space-periodic field of the lattice while in the plasma the electron travels in the time-periodic field, of period equal to the cyclotron period, due to the thermal rotation of the plasma electrons.

Plasma oscillations in a uniform static magnetic field with short wavelengths and thermal motions

As the plasma electron density increases the oscillation frequency increases, the plasma wavelengths decrease, and kA increases above the range where the Mathieu equation approximation is valid. The differential equation of motion of a plasma electron between collisions then becomes

$$\frac{d^2 s_\phi}{dt^2} + \omega_c^2 s_\phi + \frac{e}{m} E_p \cos \omega t \Big\{ \cos kr_o \phi_o \Big[J_o (kA)$$

$$- 2J_2 (kA) \cos 2 (\omega_c t + \alpha) + \cdots \Big] - \sin kr_o \phi_o$$

$$\Big[2J_1 (kA) \cos (\omega_c t + \alpha) - 2J_3 (kA) \cos 3$$

$$(\omega_c t + \alpha) + \cdots \Big] \Big\} = 0 \qquad (7.28)$$

by using the expansions of the trigonometric functions in terms of Bessel functions of the first kind.

$$\cos \Big[kA \cos (\omega_c t + \alpha) \Big] = J_o(kA) - 2J_2(kA) \cos 2$$

$$(\omega_c t + \alpha) + 2J_4(kA) \cos 4 (\omega_c t + \alpha) - \cdots \qquad (7.29)$$

$$\sin \Big[kA \cos (\omega_c t + \alpha) \Big] = 2J_1(kA) \cos (\omega_c t + \alpha) - 2J_3(kA)$$

$$\cos 3 (\omega_c t + \alpha) + 2J_5(kA) \cos 5 (\omega_c t + \alpha) - \cdots \qquad (7.30)$$

Combining the cosine terms,

$$\frac{d^2 s_\phi}{dt^2} + \omega_c^2 s_\phi + \frac{e}{m} E_p \Big\{ \cos kr_o \phi_o \Big[J_o(kA) \cos \omega t$$

$$- J_2(kA) \cos (\omega t + 2\omega_c t + 2\alpha) - J_2(kA) \cos (\omega t - 2\omega_c t$$

$$- 2\alpha) + \cdots \Big] - \sin kr_o \phi_o \Big[J_1(kA) \cos (\omega t + \omega_c t + \alpha)$$

$$+ J_1(kA) \cos (\omega t - \omega_c t - \alpha) - J_3(kA) \cos (\omega t + 3\omega_c t + 3\alpha)$$

$$- J_3(kA) \cos (\omega t - 3\omega_c t - 3\alpha) + \cdots \Big] \Big\} = 0 \qquad (7.31)$$

The solution for s_ϕ is an infinite sum of particular integrals

$$s_o = \sum_{m=-\infty}^{\infty} \Big[A_{2m} \cos kr_o \phi_o \cos (\omega t + 2m\omega_c t + 2m\alpha) - B_{2m+1}$$

$$\sin kr_o \phi_o \cos (\omega t + (2m + 1)\, \omega_c t + (2m + 1)\, \alpha) \Big] \qquad (7.32)$$

Substituting this solution into the differential equation, (7.31), and equating like terms, the coefficients are

$$A_{2m} = \frac{(-1)^m \frac{e}{m_e} E_p J_{2m}(kA)}{(\omega + 2m\omega_c)^2 - \omega_c^2} \qquad (7.33)$$

$$B_{2m+1} = \frac{(-1)^m \frac{e}{m_e} E_p J_{2m+1}(kA)}{(\omega + (2m+1)\omega_c)^2 - \omega_c^2} \qquad (7.34)$$

These coefficients are all finite except when the oscillation frequency is an integer multiple of the cyclotron frequency, $\omega = M\omega_c$. When M is an odd integer the A coefficient of the cos $\omega_c t$ term becomes infinite and, when M is even, the B coefficient of the cos $\omega_c t$ term becomes infinite. Thus stable solutions are possible except when the oscillation frequency is in the vicinity of an integer multiple of the cyclotron frequency.

The unstable frequencies come from having to use the equation for the conservation of the distribution function $f(x, y, z, v_x, v_y, v_z, t)$ in the whole phase space, when the plasma wavelength is finite, instead of the equation for the conservation of the distribution function $f(v_x, v_y, v_z, t)$ in the velocity dimensions of phase space (also called conservation of momentum or momentum transfer equations), when the plasma wavelength is infinite.

The resultant electric field due to the organized displacements of the plasma electrons is the vector sum of contributions to the electric field of all the individual plasma electrons in a certain small region. The phase angles α between the thermal motions of the individual plasma electrons and the plasma oscillations have a random distribution. The contributions of the components of the plasma electron motion involving cos $(\omega t + n\omega_c t + n\alpha)$ terms add to zero because

$$\int_0^{2\pi} \cos(\omega t + n\omega_c t + n\alpha)\, d\alpha = \begin{cases} 0 & , n \neq 0 \\ 2\pi \cos \omega t, & n = 0 \end{cases} \tag{7.35}$$

so only the cos ωt term of the individual plasma electron motions contributes to the oscillating plasma electric field.

The contributions to the electric field from the oscillating plasma electrons must be summed over all the plasma electron thermal velocities.

$$E_\phi = E_p \cos kx \cos \omega t = \frac{en}{\varepsilon} \overline{s_{\phi_\omega}}$$

$$= \frac{en}{\varepsilon} \overline{A_o \cos kx \cos \omega t}$$

$$= \frac{en}{\varepsilon} \frac{e}{m_e} \frac{E_p \cos kx \cos \omega t}{\omega^2 - \omega_c^2} \overline{J_o\left(\frac{k}{\omega_c} v_\perp\right)} \tag{7.36}$$

The distribution function of the thermal velocities in the plane transverse to the magnetic field is

$$f(v_\perp)\, dv_\perp = 2\beta^2 v_\perp \exp\left\{-\beta^2 v_\perp^2\right\} dv_\perp \tag{7.37}$$

where $\beta^2 = \frac{m_e}{2KT_-}$, m_e the electron mass, K Boltzmann's constant and T_- the electron temperature. This is the fraction of the plasma

electrons which have velocity components in the transverse plane between $v_\perp$ and $v_\perp + dv_\perp$.

The dispersion relation becomes

$$\omega^2 = \omega_c^2 + \omega_p^2 \int_0^\infty 2\beta^2 v_\perp J_o\left(\frac{k}{\omega_c} v_\perp\right) \exp\left\{-\beta^2 v_\perp^2\right\} dv_\perp \qquad (7.38)$$

This definite integral can be evaluated by expanding the zero order Bessel function in a power series

$$J_o\left(\frac{k}{\omega_c} v_\perp\right) = \sum_{m=0}^{\infty} \frac{\left[\frac{kv_\perp}{2\omega_c}\right]^{2m} \left[-1\right]^m}{(m!)^2} \qquad (7.39)$$

and integrating term by term.

$$\int_0^\infty v_\perp^{2m+1} \exp\left\{-\beta^2 v_\perp^2\right\} dv_\perp = \frac{m!}{2\beta^{2m+2}} \qquad (7.40)$$

so that the dispersion relation becomes

$$\omega^2 = \omega_c^2 + \omega_p^2 \sum_{m=0}^{\infty} \frac{(-1)^m}{m!} \left[\frac{k}{2\omega_c \beta}\right]^{2m} \qquad (7.41)$$

which is recognized as the series for exp $(-x^2)$. The new dispersion relation is then,

$$\omega^2 = \omega_c^2 + \omega_p^2 \exp\left\{ - \left(\frac{k}{2\omega_c \beta}\right)^2 \right\}$$

$$= \omega_c^2 + \omega_p^2 \exp\left\{ - \frac{k^2}{4\omega_c^2} \frac{2}{3} \overline{v_-^2} \right\}$$

$$= \omega_c^2 + \omega_p^2 \exp\left\{ - \frac{k^2 \overline{v_\perp^2}}{4\omega_c^2} \right\}$$

$$= \omega_c^2 + \omega_p^2 \exp\left\{ - \frac{k^2 \overline{A^2}}{4} \right\} \qquad (7.42)$$

For long plasma wavelengths $k \rightarrow 0$ and/or, for low plasma electron temperatures, $v_\perp \rightarrow 0$, and the new dispersion relation becomes the well known relation $\omega^2 = \omega_c^2 + \omega_p^2$.

The solution for s_ϕ when the oscillation frequency is in the vicinity of an integer multiple M of the cyclotron frequency contains an exponential factor

$$s_\phi = \sum_{m=-\infty}^{\infty} e^{\mp\mu t} \Big\{ \cos kr_o \phi_o \Big[A_{2m} \cos \Big((M + 2m)\, \omega_c t + 2m\alpha \Big)$$

$$+ C_{2m} \sin \Big((M + 2m)\, \omega_c t + 2m\alpha \Big) \Big]$$

$$- \sin kr_o \phi_o \Big[B_{2m+1} \cos \Big((M + 2m + 1)\, \omega_c t + (2m + 1)\, \alpha \Big)$$

$$+ D_{2m+1} \sin \Big((M + 2m + 1)\, \omega_c t\, (2m + 1)\, \alpha \Big) \Big] \Big\} \qquad (7.43)$$

The coefficients are

$$A_{2m} = \frac{(-1)^m \frac{e}{m_e} E_p J_{2m}(kA) \Big\{ \Big[(M + 2m)^2 - 1 \Big] \omega_c{}^2 - \mu^2 \Big\}}{\Big\{ \Big[(M + 2m)^2 - 1 \Big] \omega_c{}^2 + \mu^2 \Big\}^2 + 4\mu^2 \omega_c{}^2} \qquad (7.44)$$

$$C_{2m} = A_{2m} \left[\frac{\mp 2\mu\, (M + 2m)\, \omega_c}{\Big[(M + 2m)^2 - 1 \Big] \omega_c{}^2 - \mu^2} \right] \qquad (7.45)$$

$$B_{2m+1} = \frac{(-1)^m \frac{e}{m_e} E_p J_{2m+1}(kA) \Big\{ \Big[(M+2m+1)^2 - 1 \Big] \omega_c{}^2 - \mu^2 \Big\}}{\Big\{ \Big[(M+2m+1)^2 - 1 \Big] \omega_c{}^2 + \mu^2 \Big\}^2 + 4\mu^2 \omega_c{}^2} \qquad (7.46)$$

$$D_{2m+1} = B_{2m+1}\left[\frac{\mp 2\mu\,(M + 2m + 1)\,\omega_c}{\left[(M + 2m + 1)^2 - 1\right]\omega_c^{\,2} - \mu^2}\right] \tag{7.47}$$

The motions of the plasma electrons satisfy equation (7.43) as their oscillations start to build up after a collision. As their oscillation amplitudes get larger the electrons start to radiate electromagnetic energy and their oscillation amplitudes approach a constant value. This radiation damping is not taken into account by the differential equation of motion, equation (7.31).

The group velocity $\frac{\partial\omega}{\partial k}$ of the new dispersion relation,

$$\omega^2 = \omega_c^{\,2} + \omega_p^{\,2} \exp\left\{-\frac{k^2\,\overline{v_\perp^{\,2}}}{4\omega_c^{\,2}}\right\}$$

is

$$\frac{\partial\omega}{\partial k} = -\frac{\omega_p^{\,2}\,\overline{v_\perp^{\,2}}}{4\omega_c^{\,2}}\,\frac{k}{\omega}\exp\left\{-\frac{k^2\,\overline{v_\perp^{\,2}}}{4\omega_c^{\,2}}\right\} \tag{7.48}$$

so the product of the group velocity and the phase velocity $\frac{\omega}{k}$ is

$$v_{group}\,v_{phase} = -\frac{M^2 - 1}{4}\,\overline{v_\perp^{\,2}}_{\,thermal} \tag{7.49}$$

which is of the order of the mean square thermal plasma electron velocity. The group velocity is in the opposite direction to the phase velocity.

This is the same situation that exists in the backward-wave oscillator which is a microwave oscillator in which an electron stream interacts with a particular spacial harmonic of one of the transmission modes of a periodic structure of the type used in certain traveling wave amplifiers. While the driven harmonic has a phase velocity close to that of the electron stream and travels forward, the power flow of the transmission mode is in the opposite direction. Thus power absorbed by the circuit from the beam at any point flows backward and produces modulation of the beam.

The magnetic flux density and the plasma electron density are constant throughout the plasma region so that $\omega_c (= \frac{eB}{m})$ and $\omega_p (= \frac{e^2 n}{\epsilon m})$ are constant but the plasma wavelength is proportional to the radius r so the new dispersion relation says that the plasma oscillation frequency is a function of the radius. But the plasma oscillation frequency must be an integer multiple of the cyclotron frequency $\omega = M\omega_c$ for an unstable plasma and excitation. Therefore only a certain band of radius values can satisfy the dispersion relation.

Since

$$\exp\left\{-\frac{k^2 \overline{A^2}}{4}\right\} = \exp\left\{-\frac{M^2 \overline{A^2}}{r^2}\right\}, \tag{7.50}$$

as the plasma electron density is increased, first the large values

of r can satisfy the dispersion relation for mode M and the plasma is unstable at large r values. As the plasma electron density is further increased the plasma is unstable at smaller and smaller radii. If oscillations can build up in one region of the plasma, oscillations will be induced in the neighboring regions until the entire plasma is oscillating. This explains why a certain oscillation mode can be obtained over a considerable range of plate current, which is roughly proportional to ω_p^2, as shown in Figure (5.6), and why the end tab current values, which are proportional to ω_p^2, in Figure (5.10), are not exactly on the curve.

For small mode numbers M, $\exp\left\{-\frac{M^2\overline{A^2}}{r^2}\right\}$ is essentially unity for all r so the whole plasma region is either unstable or stable. For larger mode numbers the exponential function changes with the radius so the plasma is unstable only within a certain band of radius values.

The angular velocity of rotation about the filament axis of the planes of constant phase of the plasma traveling waves, $\omega_\phi = \frac{\omega}{2M}$, is now a function of the radius since ω is a function of the radius. The angular phase velocity is larger at larger radius values so the traveling plasma waves spiral inward toward the filament.

The new dispersion relation $\omega^2 = \omega_c^2 + \omega_p^2 \exp\left\{-\frac{k^2\overline{A^2}}{4}\right\}$ says that the plasma electron density must increase very much to get an increase in oscillation frequency when kA becomes large. Figure (7.3) shows the mode number M and the free space wavelength of the

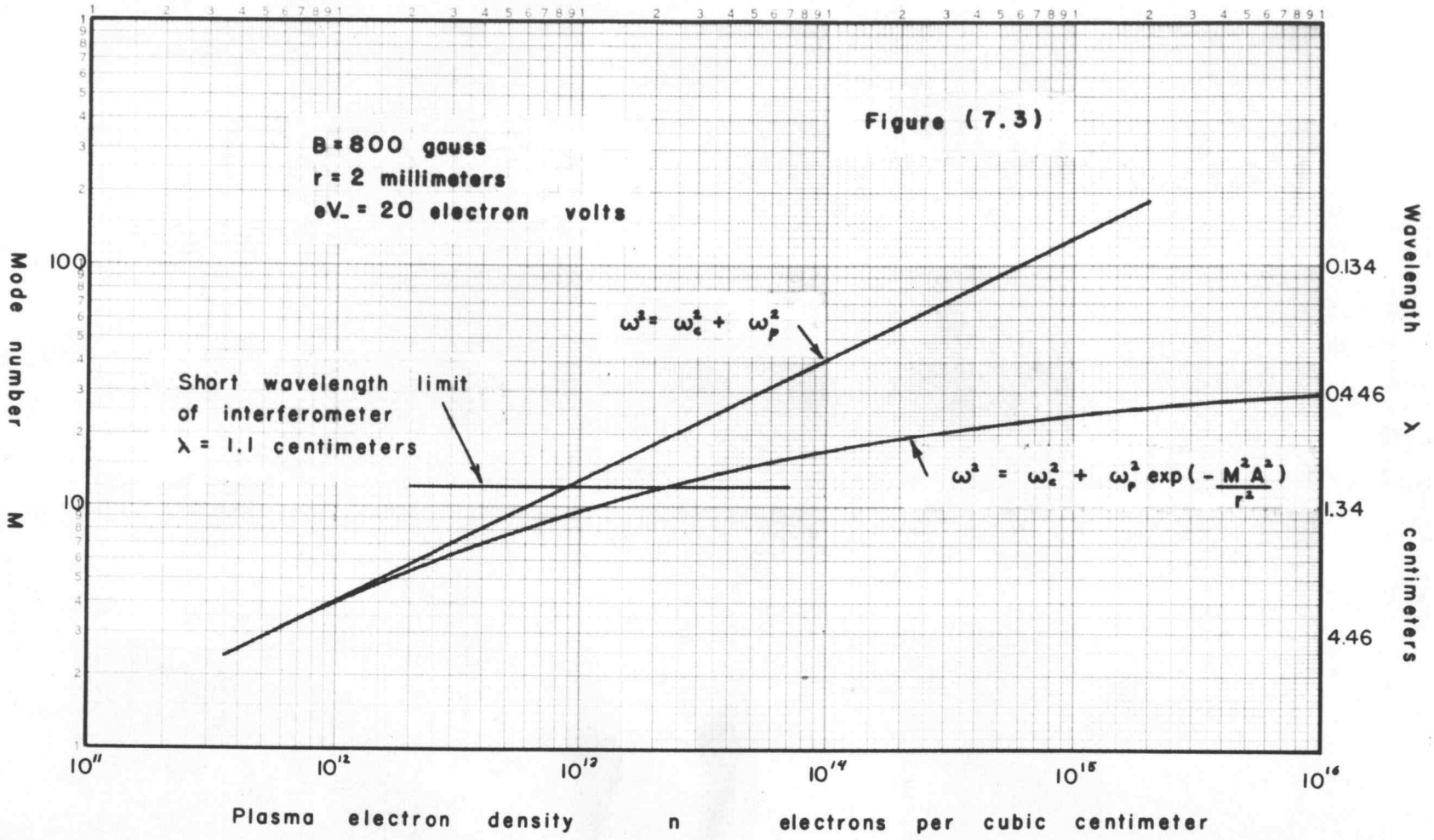
Figure (7.3)
B = 800 gauss
r = 2 millimeters
eV_ = 20 electron volts
$\omega^2 = \omega_c^2 + \omega_p^2$
Short wavelength limit
of interferometer
λ = 1.1 centimeters
$\omega^2 = \omega_c^2 + \omega_p^2 \exp(-\frac{M^2A^2}{r^2})$
Mode number M
100
10
0.134
0.446
1.34
4.46
Wavelength λ centimeters
10^{11}
10^{12}
10^{13}
10^{14}
10^{15}
10^{16}
Plasma electron density n electrons per cubic centimeter

electromagnetic radiation as a function of the plasma electron density for a radius of 2 millimeters, B = 800 gauss, and an average plasma electron energy of 20 electron volts. There is thus an upper oscillation frequency limit. The corresponding free space wavelength is about half a centimeter for the parameter values used in Figure (7.3). This high frequency cut-off was not given sufficient experimental investigation to show if this new dispersion relation is correct because the high frequency limit of the wavelength measurements occurs at a lower frequency than the dispersion relation cut-off as shown in Figure (7.3). In Figure (5.10) the end tab currents above about mode 6 were progressively higher than the linear curve, which holds for the dispersion relation $\omega^2 = \omega_c^2 + \omega_p^2$. This is in agreement with the new dispersion relation. The exponential factor would help to separate the modes, which are close together on a filament current scale, because the emission current is a steep function of the filament current.

Another limit on the maximum frequency attainable with this exciting mechanism is that the plasma electron density cannot be greater than the gas density. A pressure of about 100 microns has a density of 3.3×10^{15} molecules per cubic centimeter. With 30 percent ionization the plasma electron density would be 10^{15} electrons per cubic centimeter and the wavelength of the electromagnetic radiation would be about half a centimeter.

For long plasma wavelengths and large magnetic flux densities only the first two terms in the series expansion of the exponential

term in the dispersion relation need be retained and the dispersion relation then becomes

$$\omega^2 = \omega_c^2 + \omega_p^2 \left[1 - \frac{k^2 v_\perp^2}{4\omega_c^2} + \cdots \right]$$

$$= \omega_c^2 + \omega_p^2 - \frac{\omega_p^2}{\omega_c^2} \frac{KT}{2m} k^2 \qquad (7.51)$$

which agrees with Gross' dispersion relation (49, p. 239) for $\omega_c^2 \gg \frac{KT}{m} k^2$ and $\omega_c^2 \gg \omega_p^2$ for a Maxwellian velocity distribution. The dispersion relations disagree for the other cases, for example when $\omega_p^2 \gg \omega_c^2$, probably because it is difficult to extract the dispersion relation from Gross' distribution function.

There is heavy damping of plasma waves with wavelengths shorter than 2π times the Debye length. There is a little variation among authors on the exact definition. The definition here differs from Debye and Huckel's by a factor $\sqrt{2}$.

$$\lambda_D = 2\pi \left[\frac{KT\,\varepsilon}{ne^2} \right]^{1/2} \qquad (7.52)$$

At this wavelength the phase velocity of the plasma wave equals the root mean square of the thermal velocity component in the direction

of the wave propagation. The random thermal motions disrupt waves with slower phase velocities.

$$\lambda_D f_p = \left[\frac{KT_- \varepsilon}{ne^2}\right]^{1/2} \left[\frac{ne^2}{\varepsilon m}\right]^{1/2} = \left[\frac{KT_-}{m}\right]^{1/2} = \sqrt{\overline{v_x^2}} \qquad (7.53)$$

The plasma wavelength in the tube equals

$$\lambda_p = \frac{\omega_c r}{2f} \qquad (7.54)$$

so the plasma wavelength equals the Debye cut-off wavelength

$$\lambda_p = \frac{1.407 \times 10^{10} \text{ radians/sec } r}{2f}$$

$$= \frac{1.535 \times 10^{8} \text{ cm/sec}}{f_p} = \lambda_D \qquad (7.55)$$

when $r = 2.182 \times 10^{-2} \frac{M}{(M^2-1)^{1/2}}$ centimeters for B = 800 gauss and $eV_- = 20$ electron volts. This is a much smaller radius than the cathode sheath thickness of about one to two millimeters, except for M = 1, so the damping at the Debye cut-off wavelength is not a limit of the plasma oscillations. As the plasma electron density increases the plasma wavelengths decrease because of the constant angular velocity type of excitation, but the Debye cut-off wavelength also decreases with increasing plasma electron density and the ratio of

the phase velocity of the plasma wave to the average thermal velocity remains approximately constant with changing plasma electron density. For M = 1 the electron density is zero so plasma oscillations are not possible.

The power of the electromagnetic waves radiated by an accelerating charge is proportional to the square of its acceleration or, for a harmonically varying charge, to the square of its displacement as shown by Stratton (122, pp. 434-476). The average power radiated by a single plasma electron due to its motion in the ϕ direction is then

$$P = \frac{\omega^4 \mu e^2}{6\pi c} \frac{1}{\tau} \int_0^{\tau} s_\phi^2 \, dt = \frac{\omega^2 \mu e^2}{6\pi c} \overline{s_\phi^2} \tag{7.56}$$

$$P = \sum_{m=-\infty}^{\infty} \left[\frac{(\omega + 2m\omega_c)^4 \mu e^2}{12 \pi c} A_{2m}^2 \cos^2 kr_o\phi_o \right.$$

$$\left. + \frac{(\omega + (2m + 1)\omega_c)^4 \mu e^2}{12 \pi c} B_{2m+1}^2 \sin^2 kr_o\phi_o \right] \tag{7.57}$$

from equation (7.32) since

$$\frac{1}{\tau} \int_0^{\tau} \cos \left[(M + n)\omega_c t + n\alpha\right] \cos \left[(M + m)\omega_c t + m\alpha\right] dt$$

$$= \begin{cases} 0 \text{ when } m \neq n \\ \\ \frac{1}{2} \text{ when } m = n \end{cases} \tag{7.58}$$

so the cross product terms vanish. Averaging over all values of ϕ_o the power becomes

$$P = \frac{\mu e^2}{24\pi c} \sum_{m=-\infty}^{\infty} \left[(\omega + 2m\omega_c)^4 \, A_{2m}^2 \right.$$

$$\left. + (\omega + (2m+1)\,\omega_c)^4 \, B_{2m+1}^2 \right] \tag{7.59}$$

The plasma electrons thus radiate electromagnetic energy with not only the plasma oscillation frequency ω but also the sideband frequencies $\omega \pm m\omega_c$ which are the cyclotron frequency apart. The power radiated by a group of charges oscillating together in phase is proportional to the square of the total charge $(N_e e)^2$ where N_e is the number of charges oscillating together in phase. The power radiated by a group of charges oscillating together but with random phases is equal to the sum of the powers radiated by the individual electrons. The plasma electrons are oscillating in phase with the fundamental frequency and are oscillating with random phases with the sideband frequencies.

Using equations (7.33) and (7.34) the power in the fundamental is

$$P_o = \frac{\omega^4 \mu (N_e e)^2}{24\pi c} \left[\frac{\frac{e}{m} E_p \overline{J_o(kA)}}{\omega^2 - \omega_c^2} \right]^2 4M \qquad (7.60)$$

while the power in the first upper and lower sidebands are

$$P_{+1} = \frac{\mu e^2 N_e (\omega + \omega_c)^4}{24\pi c} \left[\frac{\frac{e}{m} E_p \overline{J_1(kA)}}{(\omega + \omega_c)^2 - \omega_c^2} \right]^2 4M \qquad (7.61)$$

$$P_{-1} = \frac{\mu e^2 N_e (\omega - \omega_c)^4}{24\pi c} \left[\frac{\frac{e}{m} E_p \overline{J_1(kA)}}{(\omega - \omega_c)^2 - \omega_c^2} \right]^2 4M \qquad (7.62)$$

For the higher mode numbers, for example when $\omega \geq 10\ \omega_c$

$$\frac{(\omega + \omega_c)^4}{(\omega + \omega_c)^2 - \omega_c^2{}^2} \approx 1 \qquad (7.63)$$

so the ratio of the fundamental power to the power in one of the closest sidebands is

$$\frac{P_o}{P_{+1}} = \left[\frac{\overline{J_o(kA)}}{\overline{J_1(kA)}} \right]^2 N_e \qquad (7.64)$$

N_e is about 10^9 to 10^{12} so the sideband power is entirely negligible compared with the fundamental power.

Plasma oscillations with thermal motions and with zero magnetic field

Let us consider the Hartree consistent field approximation applied to a plasma with zero magnetic field. The differential equation of motion of a plasma electron is

$$\frac{d^2s}{dt^2} = -\frac{e}{m} E_p \cos \omega t \cos kx \tag{7.65}$$

where x is the x coordinate of the plasma electron due to its thermal motion.

$$x_{thermal} = v_x t + \alpha \tag{7.66}$$

so the motion equation becomes

$$\frac{d^2s}{dt^2} + \frac{e}{m}\frac{E_p}{2}\Big[\cos(\omega t + kv_x t + k\alpha)$$

$$+ \cos(\omega t - kv_x t - k\alpha)\Big] = 0 \tag{7.67}$$

The solution for the plasma oscillation motion due to the electric field $E = E_p \cos \omega t \cos kx$ is

$$s = \frac{eE_p}{m2}\left[\frac{\cos(\omega t+kv_x t+k\alpha)}{(\omega + kv_x)^2} + \frac{\cos(\omega t-kv_x t-k\alpha)}{(\omega - kv_x)^2}\right] \tag{7.68}$$

The electric field produced by the electron displacements at a position x_o is

$$E(x_o,t) = \frac{en}{\varepsilon} \bar{s}(x_o,t) \tag{7.69}$$

where $\bar{s}$ is the average of the electron displacements at position x_o and time t. Those plasma electrons are at position x_o at time t which have values of a and v_x that satisfy

$$x_o = v_x t + a \tag{7.70}$$

The electron displacements are then summed over the thermal velocity distribution in the x direction.

$$f_x(v_x)\, dv_x = \frac{\beta}{\sqrt{\pi}} \exp\left\{-\beta^2 v_x^2\right\} dv_x \tag{7.71}$$

where $\beta^2 = \frac{m_e}{2KT_-}$. This is the fraction of the plasma electrons which have velocity components in the x direction between v_x and $v_x + dv_x$.

$$E(x_o,t) = \frac{\beta e^2 n E_p}{\sqrt{\pi}\,\varepsilon m 2}\left[\cos(\omega t + kx_o)\int_{-\infty}^{\infty}\frac{\exp\left\{-\beta^2 v_x^2\right\} dv_x}{(\omega + kv_x)^2}\right.$$

$$\left. + \cos(\omega t - kx_o)\int_{-\infty}^{\infty}\frac{\exp\left\{-\beta^2 v_x^2\right\} dv_x}{(\omega - kv_x)^2}\right] \tag{7.72}$$

These are improper integrals for real frequencies and wavelengths. When the phase velocity $\frac{\omega}{k}$ is much larger than the average thermal velocity $\overline{v_x}$, the integrand can be expanded in a power series about $\frac{kv_x}{\omega} = 0$ and only the first four terms retained as shown by Bohm and Gross (18, pp. 1851-1864). The integrals become

$$\frac{1}{\omega^2} \int_{-\infty}^{\infty} \exp\left\{-\beta^2 v_x^2\right\} \left[1 \mp 2\frac{kv_x}{\omega} + 3\frac{k^2 v_x^2}{\omega^2} \mp 4\frac{k^3 v_x^3}{\omega^3} + \cdots\right] dv_x \tag{7.73}$$

The terms with odd powers of v_x are odd functions of v_x so their integral is zero. The integration of equation (7.72) with k small is

$$E(x_o, t) = \frac{\omega_p^2}{\omega^2} E_p \cos\omega t \cos kx_o \left[1 + 3\frac{k^2}{\omega^2}\frac{KT_-}{m}\right] \tag{7.74}$$

so that the dispersion relation for small k is

$$\omega^2 = \omega_p^2 + \frac{3KT_-}{m} k^2$$

or

$$\omega^2 = \omega_p^2 + \overline{v_-^2}\, k^2 \tag{7.75}$$

The product of the group velocity $\frac{\partial\omega}{\partial k}$ and the phase velocity $\frac{\omega}{k}$ is

$$v_{group}\, v_{phase} = \overline{v_-^2} \tag{7.76}$$

There is some evidence that the moving striations in the positive column of a glow discharge move with a velocity equal to the group velocity given by this equation. There is other evidence, however, that the striations are positive ion oscillations (70, pp. 356-368).

The integrals in equation (7.72) are proper integrals if either the frequency or the wavelength is complex. Amplifiers amplify real frequencies so when wave amplifiers are in an unstable region the wavelength is complex and the signal amplitude increases with distance. For example in the traveling wave tube the signal increases with distance down the length of the tube. Oscillators are amplifiers with the output fed back to the input. The single-valuedness in space condition restricts the wavelengths to real values so in an unstable region the frequency is complex and the signal amplitude increases with time. The increase with time continues until a nonlinear effect limits the amplitude.

Thus in our plasma magnetron oscillator the wavelengths are real and the frequencies complex, $\omega = \omega \pm i\mu$.

For an oscillating electric field in the plasma region of

$$E = E_p e^{\pm\mu t} \left[\cos(\omega t - kx) + K_o \sin(\omega t - kx)\right] \tag{7.77}$$

the oscillatory motion of a plasma electron with an x component of velocity v_x and an x position due to its thermal motion $x = v_x t + \alpha$ is described by

$$s = e^{\pm\mu t}\left[K_1 \cos(\omega t - kx) + K_2 \sin(\omega t - kx)\right] \tag{7.78}$$

The K_1 and K_2 are determined from the differential equation of motion

$$\frac{d^2 s}{dt^2} = -\frac{eE_p}{m} e^{\pm\mu t}\left[\cos(\omega t - kv_x t - k\alpha)\right.$$

$$\left. + K_o \sin(\omega t - kv_x t - k\alpha)\right] \tag{7.79}$$

and are

$$K_1 = \frac{eE_p}{m} \frac{\left[(\omega - kv_x)^2 - \mu^2\right] \pm K_o\, 2\mu\,(\omega - kv_x)}{\left[(\omega - kv_x)^2 + \mu^2\right]^2} \tag{7.80}$$

$$K_2 = \frac{eE_p}{m} \frac{\mp 2\mu\,(\omega - kv_x) - K_o\left[(\omega - kv_x)^2 - \mu^2\right]}{\left[(\omega - kv_x)^2 + \mu^2\right]^2} \tag{7.81}$$

The electric field produced by the electron displacements at a position x_o and time t is proportional to the electron displacements averaged over the velocity distribution

$$E(x_o,t) = \frac{\beta\,\omega_p^{\,2}\,E_p\,e^{\mp\mu t}}{\sqrt{\pi}}\Bigg[\cos(\omega t - kx_o)$$

$$\int_{-\infty}^{\infty}\frac{\left[(\omega - kv_x)^2 - \mu^2\right] \pm K_o\,2\mu\,(\omega - kv_x)}{\left[(\omega - kv_x)^2 + \mu^2\right]^2}$$

$$\exp\left\{-\beta^2 v_x^{\,2}\right\}dv_x + \sin(\omega t - kx_o)$$

$$\int_{-\infty}^{\infty}\frac{\mp\,2\mu\,(\omega - kv_x) + K_o\left[(\omega - kv_x)^2 - \mu^2\right]}{\left[(\omega - kv_x)^2 + \mu^2\right]^2}$$

$$\exp\left\{-\beta^2 v_x^{\,2}\right\}dv_x\Bigg] \qquad (7.82)$$

Let us for simplicity write

$$F_1 = \frac{\omega_p^{\,2}\,\beta}{\sqrt{\pi}}\int_{-\infty}^{\infty}\frac{(\omega - kv_x)^2 - \mu^2}{\left[(\omega - kv_x)^2 + \mu^2\right]^2}\exp\left\{-\beta^2 v_x^{\,2}\right\}dv_x \qquad (7.83)$$

$$F_2 = \frac{\omega_p^{\,2}\,\beta}{\sqrt{\pi}}\int_{-\infty}^{\infty}\frac{2\mu\,(\omega - kv_x)}{\left[(\omega - kv_x)^2 + \mu^2\right]^2}\exp\left\{-\beta^2 v_x^{\,2}\right\}dv_x \qquad (7.84)$$

The equation (7.82) becomes

$$E(x_o,t) = E_p e^{\pm\mu t}\left[\cos(\omega t - kx_o)(F_1 \pm K_o F_2)\right.$$

$$\left. + \sin(\omega t - kx_o)(\mp F_2 + K_o F_1)\right] \tag{7.85}$$

When we try to equate this field to the originally assumed field, we obtain the relations

$$1 = F_1 \pm K_o F_2 \tag{7.86}$$

$$K_o = \mp F_2 + K_o F_1 \tag{7.87}$$

By eliminating K_o from these equations the relation

$$F_2^2 + (1 - F_1)^2 = 0 \tag{7.88}$$

is obtained. The integrals F_1 and F_2, however, are real so the only values that satisfy the equation (7.88) exactly are $F_2 = 0$, $F_1 = 1$. If the velocity distribution is Maxwellian, the integral F_2 is small but not zero and F_2 approaches zero only when μ approaches $\pm$ infinity, or 0, but when $\mu = 0$, F_1 becomes infinite. This approach then of moving the pole off the real v_x axis is not completely successful because the actual velocity distribution is not known. In a linear theory the poles at $v_x = \frac{\omega}{k} \pm i\frac{\mu}{k}$ do not interact. It is expected

that the velocity distribution becomes slightly non-Maxwellian and is such a distribution that the integral F_2 becomes zero. The definite integrals are now finite because the second order pole has been removed from the real v_x axis. The dispersion relation is

$$1 = \frac{\beta \omega_p^2}{\sqrt{\pi}} \int_{-\infty}^{\infty} \frac{(\omega - kv_x)^2 - \mu^2}{\left[(\omega - kv_x)^2 + \mu^2\right]^2} \exp\left\{-\beta^2 v_x^2\right\} dv_x \qquad (7.89)$$

For a certain wavelength this is one relation with two unknowns, ω and μ.

The dispersion relation is difficult to solve but some qualitative information can be obtained by considering the function in the complex v_x plane. The integrand has two second order poles at $v_x = \frac{\omega}{k} \pm i \frac{\mu}{k}$ and two essential singularities at $v_x = \pm i \infty$.

When $\frac{\omega}{k} >> \frac{1}{\beta}$ the exponential factor is very small in the vicinity of the poles and the poles can be close to the real v_x axis and $\frac{\mu}{k}$ is very small. The dispersion relation, equation (7.89), is written as

$$k^2 = \omega_p^2 f_1 \left(\frac{\mu}{k}, \frac{\omega}{k}, \beta\right) \qquad (7.90)$$

For a certain plasma electron density (ω_p), temperature (β), and wavelength (k), the poles at $\frac{\omega}{k} \pm i \frac{\mu}{k}$ move as the frequency is changed in such a way that the function $f_1 \left(\frac{\mu}{k}, \frac{\omega}{k}\right)$ remains constant.

The damping or growth factor μ thus increases as the frequency decreases since $f_1\left(\frac{\mu}{k}, \frac{\omega}{k}\right)$ increases as $\frac{\mu}{k}$ and $\frac{\omega}{k}$ decrease. For a smaller wavelength (larger k) the constant k pole position contour in the complex plane is closer to the real v_x axis. The plasma thus seems to be unstable for all frequencies and wavelengths, being more unstable at small $\frac{\omega}{k}$.

The theory so far is a first approximation to the consistent field. The frequency seen by a plasma electron moving with a thermal velocity component in the x direction of v_x is $\omega - kv_x$. Electrons traveling with x velocity of $v_x = \frac{\omega}{k}$ see a d.c. field and so feel a force of the same sign for a long time. In the first approximation they either accept from, or give to, the wave a large amount of energy. But when they accept, or give up, some energy they no longer travel with an x velocity equal to the wave velocity.

The Maxwellian electron velocity distribution in low-pressure arcs behaves as if it had a very short relaxation time and length. Langmuir (43, p. 74) has shown experimentally that local disturbances are smoothed out almost completely within distances in which the probability of collision with gas molecules can be as small as one hundredth, provided only that the electron concentration is of the order of 10^9 electrons per cubic centimeter or more.

This suggests a very strong energy interchange between electrons but theoretical calculations show the electron-electron interaction to be at least three orders of magnitude smaller than values needed to account for the experimental results. A possible explanation is

that random plasma oscillations in the always unstable plasma give rise to macroscopic turbulence which assists in maintaining the electron velocity distribution Maxwellian. This is an interaction among the electrons only but on a macroscopic scale.

Collisions of the electrons with gas molecules continually extract the electrons from the velocity range near the wave velocity and replenish the supply with new electrons. The consistent field approach is unable adequately to describe the interaction between the plasma wave and the electrons near the wave velocity, which are trapped in a potential trough of the wave, unless the actual velocity distribution is known.

RADIATION INTENSITY OBSERVATIONS

Power radiated by the tube

The intensity of the electromagnetic radiation was measured by using the Tektronix oscilloscope for the receiver and calculating the gain of the dipole antenna. Figure (8.1) shows the equivalent circuit of a center-loaded receiving antenna oriented to lie in an equiphase plane of a linearly polarized electric field as shown by King and Harrison (66, pp. 18-34).

Here Z_L is the load impedance and Z_a the self impedance of the antenna as seen by a generator connected in place of the load. The electromotive force in the equivalent series circuit has the magnitude

$$V_e = 2\, h_e\, E \cos \Psi \tag{8.01}$$

where h_e is the "effective" half-length of the antenna, E is the incident electric field strength, and Ψ is the angle between the antenna direction and the polarization direction.

For an indefinitely thin antenna the effective half-length is given by

$$h_e = \frac{\lambda}{2\pi} \tan\left(\frac{kh}{2}\right) = \frac{1 - \cos kh}{k \sin kh} \tag{8.02}$$

Figure (8.1)

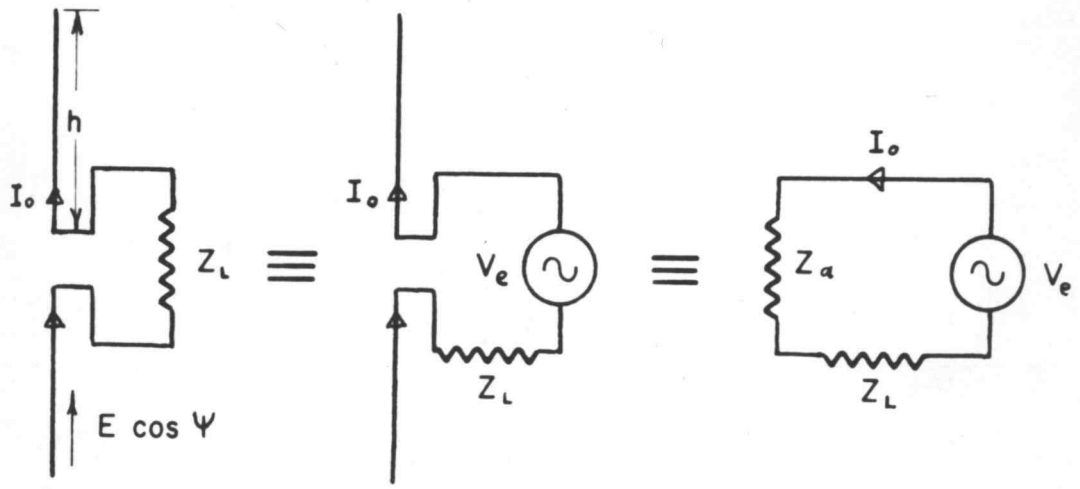

where h is the actual half-length of the antenna (8.75 mm). This is a good approximation even for thick antennas for lengths sufficiently below $h = \frac{\lambda}{2}$. When $h \approx \frac{\lambda}{2}$, the effective half-length was obtained from the curves of King and Harrison.

The load on the antenna is the 1N26 crystal. The forward resistance of the crystal, R_f, is 305 ohms and $R_b = 59{,}000$ ohms is its back resistance. The antenna impedance $|Z_a|$ is about 82.5 ohms for a $\frac{h}{\lambda}$ value of $\frac{8.75 \text{ mm}}{33.5 \text{ mm}} = 0.261$. The direct current component of the voltage into the amplifier, V_{in} equals $\frac{1}{\pi}$ times the difference of the forward and back voltages across the crystal.

$$V_{in} = V_e \frac{\dfrac{R_b}{R_b + |Z_a|} - \dfrac{R_f}{R_f + |Z_a|}}{\pi}$$

$$= V_e \frac{0.998 - 0.787}{\pi} = \frac{0.211}{\pi} V_e \qquad (8.03)$$

The self impedance Z_a of the cylindrical dipole antenna is obtained by extrapolating the values of input resistance and reactance for thinner cylindrical dipole antennas to the case of the thick antenna. Ramo and Whinnery (107, pp. 489-491) show how the input impedance Z_a of a cylindrical antenna varies with the wavelength. The average characteristic impedance of a cylindrical antenna is

$$Z_o = 120 \left(\ln \frac{2h}{a} - 1\right) \qquad (8.04)$$

where a is the radius. For the antenna of length 2h = 1.75 centimeters and diameter 2a = 0.55 centimeters, Z_o = 102 ohms. The value of Z_a, for λ = 33.5 millimeters, extrapolated from the values for the higher average characteristic impedances of thinner cylindrical antennas, to the value of 102 ohms is about $Z_a = 80 + j20$. Thus $|Z_a| = 82.5$.

The deflection on the oscilloscope alternated between about 0.4 centimeters and zero as the interferometer reflector moved. Since half of this amplitude was from the direct radiation from the tube and the sensitivity of the oscilloscope was 30 millivolts per centimeter, the direct current component of the voltage into the amplifier from the direct radiation was about V_{in} = 6 millivolts. From equation (8.03),

$$V_e = \frac{\pi \, 6mv}{0.211} = 89.3 \text{ millivolts} \qquad (8.05)$$

The radiation from the tube is divergent. The standing wave pattern between the tube and the interferometer reflector plate, a distance X away from the tube and moving with velocity v, is the same as would be obtained from the tube and a "mirror image" tube, a distance 2X away from the tube and moving with velocity 2v, and no reflector plate. The maxima and minima of the electric field

strength at the antenna position converge toward the direct radiation value as the interferometer plate moves away from the tube and antenna.

A convenient rule for determining the limiting range R between the near field (Fresnel) and far field (Fraunhofer) conditions for a receiving antenna and an isotropic radiator is

$$R = \frac{D^2}{\lambda} \tag{8.06}$$

where D is the aperture diameter of the receiving antenna and λ is the free space wavelength of the electromagnetic radiation. If the length of the dipole receiving antenna, 1.75 centimeters, is taken as the aperture diameter, and the distance R between the plasma region and the receiving antenna is about three inches, far field conditions exist for wavelengths longer than about 0.4 centimeters. For shorter wavelengths the received power is reduced.

The effective half-length h_e of the antenna for 33.5 millimeter radiation is

$$h_e = \frac{33.5 \text{ mm}}{2\pi} \tan \frac{\pi\, 8.75 \text{ mm}}{33.5 \text{ mm}} = 5.72 \text{ mm} \tag{8.07}$$

The measured electric field strength at the antenna, from equation (8.01) is

$$E_{rms} = \frac{V_e}{2\sqrt{2}\, h_e} = \frac{8.93 \times 10^{-2}\ v}{2\sqrt{2}\ 5.72 \times 10^{-3}\ m}$$

$$= 5.51\ \frac{\text{volts}}{\text{meter}} \qquad (8.08)$$

By comparing the radiation pattern from the standing plasma waves with the pattern from a circular antenna with an integer number N of standing waves around the ring, an estimate can be made of the gain of the radiator in the direction of the dipole receiving antenna. A ring antenna (for $N \geq 1$) has zero gain in the direction perpendicular to the plane containing the ring. An estimate of the gain G in the plane transverse to the magnetic field for $M = 4$ ($N = 8$) is taken to be

$$G = 2.75 \qquad (8.09)$$

by extrapolating from Knudsen's data for lower values of N (67, p. 690). The gain is the ratio of the radiated power density in a certain direction to the radiated power density averaged over all directions.

The capacitance of the cable between the crystal dipole antenna and the amplifier input was 152.7 μμf and the input capacitance of the amplifier was 40 μμf. The receiver bandwidth is then

$$B = \frac{1}{2\pi\,(305\Omega)\;192.7\;\mu\mu f} = 2.715 \text{ megacycles per sec.} \quad (8.10)$$

The rest of the amplifier is broader band than this.

The bandwidth of the video receiver is small compared to the bandwidthΔf of the signal radiated by the tube so there is a loss of sensitivity of the receiver. The loss of sensitivity in voltage is

$$\alpha = \frac{3\,(2B)}{2\,\Delta f} = \frac{3BQ}{f} \quad (8.11)$$

(93, p. 414), using the relation that a video bandwidth is equivalent to half an i.f. bandwidth. The crystal detector is a linear detector at high signal levels so the ratio of the measured to the actual field strengths is α.

The antenna was three inches from the plate of the tube. The power radiated, from equations (8.08), (8.09), (8.10), and (8.11), is

$$P_r = \frac{E_{rms}^{\,2}\, f^2\, 4\pi r^2}{9B^2\, Q^2\, Z_o\, G} = \frac{2.58 \times 10^3}{Q^2} \text{ watts} \quad (8.12)$$

$$= \frac{K_1}{Q^2} \quad (8.13)$$

where Z_o is the intrinsic impedance of free space (376.7 ohms) and r is the distance from the source at which the measured electric field strength has the value E_{rms}.

The quality factor Q of the plasma, considering the radiation damping is

$$Q = 2\pi \frac{\text{energy stored}}{\text{energy radiated per cycle}}$$

$$= \frac{(\text{energy stored})\ (\text{angular frequency})}{\text{power radiated}} \tag{8.14}$$

The energy stored W in the plasma oscillations is

$$W = \frac{m A_o^2 \omega^2}{4} \frac{\text{joules}}{\text{electron}} n\ (\text{Vol})\ \text{electrons} \tag{8.15}$$

$$= \frac{m\varepsilon^2 E_p^2 \omega^2\ (\text{Vol})}{4 e^2 n}\ \text{joules} \tag{8.16}$$

The volume of the plasma is 0.82 cubic centimeters, the electron density 1.05×10^{12} electrons per cubic centimeter, and the radian frequency 5.625×10^{10} radians per second.

The Q is then

$$Q = \frac{W\omega}{P_r} = \frac{9.67 \times 10^{-8}}{\text{ohms}} \frac{E_p^2}{P_r} \tag{8.17}$$

$$= \frac{K_2 E_p^2}{P_r} \tag{8.18}$$

Let us calculate the power given to the plasma waves by the emission electrons. The working emission electrons bunch around the maximum retarding electric field of the plasma wave which is traveling in the same direction as the emission beam. Half of the electric field strength E_p for the 33.5 millimeter oscillation belongs to each of the two oppositely directed traveling plasma waves.

The emission current was 11.68 milliamperes. The non-working half of the emission electrons takes energy from the plasma waves during one loop into the plasma region while the working half of the emission electrons gives energy to the plasma waves as long as they stay in the decelerating phase of the plasma wave.

The radius R of the circular path of the 600 volt, 800 gauss, emission electrons is 0.1032 centimeters and the distance traveled per loop inside the plasma region is about πR since the cathode sheath thickness is also about a millimeter for mode $M = 4$. The instantaneous path direction is not always in the electric field direction. The work done by each working emission electron is

$$W = e \int \vec{E} \cdot \vec{ds} = eE\pi R \, \overline{\cos \theta} \tag{8.19}$$

where θ is the angle between the path direction and the electric field direction. The average of cos θ over the half of the loop which is inside the plasma region is

$$\frac{2}{\pi}\int_{-\frac{\pi}{4}}^{\frac{\pi}{4}} \cos\theta \, d\theta = \frac{2\sqrt{2}}{\pi} \tag{8.20}$$

All the working electrons are not bunched up in the maximum retarding phase. If they are spread uniformly over the decelerating phases, the average electric field seen by the working emission electrons is $\frac{2}{\pi}$ of the maximum value.

A 600 volt electron makes on the average about 30.8 loops through air at 10 microns pressure before it suffers an ionizing collision. However, the ionization probability increases with decreasing energy and has a maximum at about 100 electron volts of more than double that at 600 electron volts. The emission electrons thus execute less than 30.8 loops.

Finkelnburg (41, p. 95) shows the ionization probability for electrons as a function of the electron energy eV_A. An empirical relation which is a good approximation for the distance an electron will travel on the average before making an ionizing collision is

$$L = \frac{2.275\ V_A^{0.7}\ \text{microns centimeters}}{P\ (\text{volts})^{0.7}} = \frac{k\ V_A^{0.7}}{P} \tag{8.21}$$

where V_A is the anode voltage of the tube. This is a good approximation in the range from about 200 to 2000 volts. The emission electron loses energy to the plasma wave, on the average, at the rate

$\frac{eE_p}{\pi^2}\sqrt{2} = K'$ but at high pressures the electron has not had its energy reduced too much below the anode voltage before it mades an ionizing collision and equation (8.20) holds. At lower pressures the emission electrons have their energies reduced sufficiently during their free paths that a suitable average of equation (8.20) must be taken to find the effective path length between ionizing collisions $\bar{L}$. An expression for this average is

$$\bar{L} = \frac{1}{K'\bar{L}} \int_{V_A - K'\bar{L}}^{V_A} L\,dV = \frac{1}{K'\bar{L}} \int_{V_A - K'\bar{L}}^{V_A} \frac{KV^{0.7}}{P}\,dV$$

$$= \frac{K}{1.7\,K'\bar{L}\,P}\left[V_A^{1.7} - (V_A - K'\bar{L})^{1.7}\right] \qquad (8.22)$$

For still lower pressures the emission electrons give up all their energy, on the average, before traversing their mean free path between ionizations and an expression for $\bar{L}$ is

$$\bar{L} = \frac{V_A}{K'} \qquad (8.23)$$

For an intermediate pressure P' for which the distance traveled to give up all the emission electron's energy to the plasma wave equals the distance between ionizing collisions the $\bar{L}$ value is

$$\bar{L} = \frac{1}{V_A} \int_0^{V_A} L\,dV = \frac{K}{V_A P} \int_0^{V_A} V^{0.7}\,dV = \frac{K\,V_A^{0.7}}{1.7\,P} \qquad (8.24)$$

The high pressure limit indicated that about half of the collisions of the emission electrons were ionizing collisions and the rest were exciting and elastic collisions. Thus a working electron makes, on the average, about $\frac{30.8}{1.7 \times 2} = 9.05$ loops through air at 10 microns pressure.

Putting all this together, the power input to the plasma wave is

$$P_o = \frac{2}{\pi}\left[\frac{E_p}{2}\right]\left[i_e\right]\left[\frac{9.05 \text{ loops} - 1 \text{ loop}}{2}\right]$$

$$\left[\frac{2\sqrt{2}}{\pi}\right]\left[\pi\, 1.032 \times 10^{-3}\,\frac{m}{\text{loop}}\right]$$

$$= 4.37 \times 10^{-5}\, E_p\, \frac{\text{watts meters}}{\text{volt}} \qquad (8.25)$$

Except for the small amount of power lost to collision damping the power input to the plasma waves is equal to the power radiated by the plasma waves.

$$P_r = K_3\, E_p \qquad (8.26)$$

There are now three equations (8.13), (8.18), and (8.26) and three unknowns P_r, E_p, and Q. The solution of this set of equations is

$$P_r = K_1^{1/3} K_2^{-2/3} K_3^{4/3} = 1.0 \text{ watt} \tag{8.27}$$

$$E_p = K_1^{1/3} K_2^{-2/3} K_3^{1/3} = 230 \text{ volts per centimeter} \tag{8.28}$$

$$Q = K_1^{1/3} K_2^{1/3} K_3^{-2/3} = 51 \tag{8.29}$$

The plate current during a pulse was 56.7 milliamperes so the plate power input to the tube is

$$P_{in} = 56.7 \times 10^{-3} \text{ amperes } 600 \text{ volts} = 34 \text{ watts} \tag{8.30}$$

and the plate efficiency is

$$\text{efficiency} = \frac{P_r}{P_{in}} = 3.0 \text{ percent} \tag{8.31}$$

If all the working emission electrons gave all their energy to the plasma waves, the tube would be operating at maximum efficiency. The maximum efficiency for the 33.5 millimeter oscillation is

$$\text{max. eff.} = \frac{i_e}{2i_p} = 10.3 \text{ percent} \tag{8.32}$$

The filament power is

$$P_f = 2.5 \text{ volts } 6 \text{ amperes} = 15 \text{ watts} \tag{8.33}$$

The total efficiency is then 2.05 percent. The excitation mechanism of the plasma-magnetron oscillator is similar to that of the high-vacuum magnetron oscillator whose efficiencies are of the order of 50 to 80 percent.

The results of some other power measurements are shown in Figure (8.2) with the measured and assumed values used in the calculations. It is seen that the radiated power is about one to five watts, the Q's about 20 to 90, the plasma electric field about 200 to 400 volts per centimeter and efficiencies about three to six percent. The trend seems to be an increase in radiated power and a decrease in Q with increasing frequency. Because of the indirect nature of the measurements they should be regarded as only order of magnitude.

One of the uncertain quantities involved in the calculation of the performance of the dipole antenna is the dipole antenna self impedance, obtained by extrapolating the calculated values for thinner antennas to the thick antenna used. Another uncertain quantity is the effect that the size of the gap between the two halves of the antenna has on the antenna self impedance.

Another uncertain quantity is the magnitude of the barrier layer capacitance of the crystal detector. The neglect of the

Figure (8.2)

V = 600 volts

B = 800 gauss

P = 10 microns

P (filament) = 2.5 volts 6 amperes = 15 watts

Antenna half-length h = 8.75 mm

Crystal resistance
R (forward) = 305 ohms
R (backward) = 59,000 ohms

Distance from tube to receiving antenna = 3 in.

Duty cycle = $30 \frac{\text{pulse}}{\text{sec}} \; 200 \frac{\mu \text{ sec}}{\text{pulse}} = \frac{1}{167}$

Receiver input capacitance = 192.7 $\mu\mu$f

Receiver bandwidth = $\frac{1}{2\pi(305\Omega)192.7 \; \mu\mu\text{f}}$ = 2.715 mc

M	λ mm	f kmc	V_{in}(ave) mv	i_p(ave) ma	i_e(ave) ma	G	h_e mm	Z_a ohms
2	67	4.48	7.5	.22	.04	1.95	4.62	39.1
4	33.5	8.95	6.0	.34	.07	2.75	5.72	82.5
6	22.35	13.43	7.5	.78	.20	3.25	10.02	150
8	16.77	17.91	6.0	.92	.26	3.5	8.38	89.5

M	n electrons/m^3 x 10^{18}	E_{rms} v/m	Q	E_p v/m x 10^4	P_r watts	P_{in} watts	plate eff. %	Max. eff. %
2	0.23	15.7	86.6	3.9	0.98	22	4.5	9.1
4	1.05	5.51	51	2.3	1.00	34	3.0	10.3
6	2.7	2.55	20.5	2.0	2.50	78	3.2	12.8
8	6.0	3.53	25.8	3.1	5.02	92	5.5	14.14

shunting barrier layer capacitance of the crystal in the equivalent circuit of the receiving dipole antenna causes a pessimistic result for the radiated power and efficiency calculations. The barrier layer capacitance short circuits the output voltage of the crystal at very high frequencies. The 1N26 crystal is a standard silicon K-band type, 1.25 cm, so it probably loses much of its rectifying ability in the region around a centimeter.

Measured barrier capacitances range from 0.02 to 1.0 μμf, the smaller values being found in crystals prepared for use in the one-centimeter band. There is considerable variation in the magnitude of the barrier layer capacitance between individual crystals of the same type.

Since $E_p = \frac{en}{\epsilon} A_o$ the maximum displacement of the plasma electrons for the 33.5 millimeter oscillation is

$$A_o = 1.211 \times 10^{-6} \text{ meters} \tag{8.34}$$

The largest propagation constant k for this mode is about 8×10^3 radians per meter so

$$\left| kA_o \right| = 0.97 \times 10^{-2} = \left| \frac{n_1}{n} \right| \tag{8.35}$$

The plasma electron density changes during the oscillations by about one percent from its average value and the approximations, equations

(1.11) and (1.12), used in deriving the frequency of oscillation are justified.

The oscillating plasma voltage is

$$V_p = -\int E_p \cos(kr\phi) \cos \omega t \, d(r\phi)$$

$$= -\frac{E_p}{k} \sin(kr\phi) \cos \omega t \qquad (8.36)$$

For the plate radius of 3.75 millimeters $k = \frac{2M}{r} = 2135$ radians per meter and at the cathode sheath boundary of about one millimeter k equals 8000 radians per meter. The amplitude of the oscillating plasma voltage is then 2.88 volts near the cathode and 10.8 volts near the plate. The plasma oscillations thus change the gas discharge conditions by a negligible amount. The plate current is a smooth continuous function of the filament current as the tube passes through the oscillation modes.

The average energy given to the plasma wave by an emission electron is

$$W = e\left[\frac{2.3 \times 10^4 \text{ volts}}{2 \quad \text{m}}\right]\left[\frac{2}{\pi}\right]\left[\frac{2\sqrt{2}}{\pi}\right]$$

$$\left[\pi \, 1.032 \times 10^{-3} \frac{\text{m}}{\text{loop}}\right] \qquad (8.37)$$

$$= 21.4 \text{ electron volts per loop} \qquad (8.37)$$

The average working emission electron thus gives up 21.4 $\frac{\text{volts}}{\text{loop}}$ x 9.05 loops = 194 volts before suffering a collision and the average non-working emission electron takes 21.4 electron volts of energy from the wave before striking the filament.

The radius of the loop of a 600 volt, 800 gauss, emission electron is 1.032 millimeters and the loop radius of a (600 minus 21.4) volt, 800 gauss, electron is 1.012 millimeters. On the first loop the electron returns with its orbit decreased by 0.02 millimeters or 2 percent. This is small compared with the filament diameter of 0.254 millimeters so the emission electrons do not have their loop radii decreased so much that they miss the filament. The non-working electrons are certain to strike the filament and the working electrons run quite directly up the potential energy hill at the filament, get within 21.4 volts of the filament potential, and then run back down hill again.

The emission efficiency is rather low because tungsten is the emitter. Several hundreds of volts potential difference across the cathode space charge sheath is necessary to make the emission electron orbit radii large enough so that the emission electrons can enter the plasma region.

The bombardment of positive ions on the cathode often destroys the coating of thorium or barium on composite cathodes and causes rapid loss of their emitting properties (86, pp. 83-219). However, a threshold value of ion energy, and hence of plasma to cathode potential difference, is found below which the cathode does not lose

its activity. The disintegration voltages are 22 volts for mercury, 25 volts for argon, and 27 volts for neon; the positive ions have no injurious effect on the cathode, whether it be oxide-coated or thoriated tungsten, when the plasma to cathode potential difference is kept below these values.

An outstanding advantage of tungsten over other types of emitters is that it is much less subject to loss of emitting properties as a result of the bombardment by positive ions. While mechanically fragile because of recrystallization, tungsten is electrically rugged. Tungsten is the only pure metal which is suitable as a practical emitter and the only cathode material available for the plasma-magnetron oscillator.

Let us see how broadband the thick dipole antenna is. Figure (2.4) shows the shape of the dipole antenna. The length is 1.75 centimeters and the diameter 0.55 centimeters. The impedance is a minimum at about $h = \frac{\lambda}{4}$ and equal to about 73 ohms. The detector gain for $\lambda = 35$ millimeters is

$$V_{in} = 0.0618\ V_e \tag{8.38}$$

and the effective half-length

$$h_e = 0.637\ h = 557\ mm \tag{8.39}$$

The antenna and detector gain is then

$$V_{in} = (0.0618)\ (0.637)\ 2hE \tag{8.40}$$

The impedance is a maximum at about $h = \frac{\lambda}{2}$. Extrapolating the maximum input impedance Z_a for the thinner cylindrical antennas, with higher average characteristic impedances Z_o, to the value of 102 ohms gives a maximum input impedance of about 150 ohms at λ equal to about 23 millimeters. The detector gain is

$$V_{in} = 0.104\ V_e \tag{8.41}$$

and the effective half-length

$$h_e = 1.062\ h = 9.3\ mm \tag{8.42}$$

The antenna and detector gain is

$$V_{in} = (0.104)\ (1.062)\ 2hE \tag{8.43}$$

For the same electric field strength the ratio of the input voltages into the amplifier for maximum and minimum antenna input impedances is only 2.8 which means that the antenna is a broad band antenna.

The Q with respect to the collision damping is 855 for a gas pressure of 10 microns so the radiation damping is much larger than the collision damping.

The height of the pulse displayed on the oscilloscope represents the intensity of the electromagnetic standing wave pattern seen by the antenna. During an oscillation, when the interferometer plate moves, the pulse height on the oscilloscope goes through maxima and minima of almost zero height indicating that the electromagnetic radiation has a definite wavelength. The pulse displayed on the oscilloscope is not a clean pulse that would be obtained from a monochromatic radiation. The pulse has a noise-like structure indicating a band of frequencies in the radiation instead of a single frequency. The band still must be narrow enough to give essentially a single wavelength.

The quality factor is

$$Q = \frac{f}{\Delta f} = \frac{\lambda}{\Delta \lambda} \tag{8.44}$$

With a Q for the plasma of 51 for the 33.5 millimeter, 8.95×10^9 cycle per second oscillation, the frequency difference between the upper and lower half power points of the resonance curve is

$$\Delta f = \frac{8.95 \times 10^9}{51} = 1.755 \times 10^8 \text{ cycles/sec} \tag{8.45}$$

This bandwidth of the plasma oscillation is large compared with the 2.715×10^6 cycle per second bandwidth of the receiver so the narrow band, 1.96 percent, plasma oscillation looks like a very wide band signal to the receiver.

The wavelength difference between the upper and lower half power points of the resonance curve is

$$\Delta\lambda = \frac{33.5 \text{ mm}}{51} = 0.656 \text{ millimeters} \tag{8.46}$$

The interferometer thus gives a definite wavelength value.

A screen of about 50 percent transparency was inserted radially in a constant ϕ plane into the discharge region to define a node of the standing plasma waves. As a result the oscillation intensities were reduced but the usual noise-like trace on the oscilloscope cleared up until it more nearly resembled a trace from a continuous monochromatic oscillation. The pulse height still varied from a maximum to a minimum of almost zero as the interferometer plate was moved.

These effects were more pronounced at the start of the experiment. Examination of the screen after the experiment showed that the part closest to the filament had been melted away. The introduction of the radial screen may have anchored a node thus preventing the plasma standing wave pattern from rotating and modulating the 10^{10} cycle per second radiation.

Since the Q decreases with increasing frequency the bandwidth of the radiated signal increases with increasing frequency. It is expected that at high mode numbers the bandwidth of the radiated signal is larger than the frequency separation between modes so the plasma is unstable at all higher frequencies.

As the magnetic flux density approaches zero, the cyclotron frequency $\omega_c = \frac{eB}{m}$ approaches zero, the mode number for a given frequency $M = \frac{\omega}{\omega_c}$ approaches infinity, the Q approaches zero, the bandwidth of each mode Δf approaches infinity, and the instability regions increase in frequency width until above a certain mode number all frequencies are unstable. The analysis in section seven of plasma oscillations not in a magnetic field shows that such plasmas are slightly unstable at all frequencies. Thus the analysis for plasma oscillations in a magnetic field goes over smoothly to the case of plasma oscillations not in a magnetic field.

In a magnetic field a plasma is quite unstable for frequencies near integer multiples of the cyclotron frequency for electrons and stable at the frequencies in between for low mode numbers. For frequencies which are large compared with the cyclotron frequency a plasma in a magnetic field is unstable at all frequencies.

A Q value of 232 is obtained from the Mathieu equation approximation which is valid for mode number $M = 2$ and is shown in equation (7.26). The Mathieu function derivation of Q expresses the finite bandwidth where the plasma is unstable and depends upon the

measurement of the plasma electron temperature and a choice of an average radius of the plasma region.

The measured finite bandwidth due to the radiation resistance for M = 2 is 51.7 megacycles and the Q is 87. The Mathieu function approximation is only valid for mode 2 so an expression for the bandwidth of the unstable regions for higher mode numbers has not been obtained but it is seen from Figure (7.2) that the widths of the unstable regions increase with increasing mode number.

The lower the Q of the combination of circuit elements which determines the frequency of oscillation in an oscillator circuit, the broader is the resonance curve of the frequency determining elements and the broader is the band of frequencies generated by the oscillator. The instantaneous frequency may be considered to be wandering around at random within the resonance curve producing a signal which is frequency and amplitude modulated at random and thus has a continuous sideband distribution around the midfrequency. In the plasma-magnetron oscillator the power output stage is not buffered from the frequency determining stage so the load resistance (radiation resistance) contributes toward lowering the Q of the oscillator.

Radiation models

Let us consider the radiation pattern from a circular loop antenna as an approximation to the radiation from the standing

plasma waves in the tube. The radiation field at a distance $\vec{r}$ from an oscillating electric dipole of strength $\vec{p}$ is

$$\vec{E} = -\frac{k^2}{4\pi r} \vec{R}_o \times (\vec{R}_o \times \vec{p})\, e^{ikr-i\omega t} \tag{8.48}$$

where $\vec{R}_o = \nabla r = \vec{\varepsilon}_r$ is a unit vector directed from the dipole toward the observer (122, p. 435). For a tangential dipole direction on the circular loop

$$\vec{P} = |p| \left[\vec{\varepsilon}_r \cos\left(\alpha - \phi + \frac{\pi}{2}\right) \sin\theta + \vec{\varepsilon}_\theta \cos\left(\alpha - \phi + \frac{\pi}{2}\right) \right.$$

$$\left. \cos\theta + \vec{\varepsilon}_\phi \cos(\alpha - \phi) \right] \tag{8.49}$$

where $\vec{\varepsilon}_r$, $\vec{\varepsilon}_\theta$, $\vec{\varepsilon}_\phi$ are the unit vectors of the observer position, $(a, \frac{\pi}{2}, \alpha)$ is the dipole position, and (R, θ, ϕ) is the observer position in spherical coordinates. Then

$$\vec{R}_o \times (\vec{R}_o \times \vec{p}) = |p| \left[\vec{\varepsilon}_\theta \cos\theta \sin(\alpha - \phi) \right.$$

$$\left. - \vec{\varepsilon}_\phi \cos(\alpha - \phi) \right] \tag{8.50}$$

For a sinusoidal dipole amplitude distribution in the azimuthal direction and uniform amplitude distributions in the radial and axial directions

$$d\,|p| = -\,ens\,d(Vol) = -\,en\,A_o\,ha\cos(N\alpha)\,d\alpha da \qquad (8.51)$$

The displacement amplitude $A_o(r,z)$ and the plasma electric field $E_p(r,z)$ are not required to be zero at the anode and end tab sheath boundaries since the space charge sheath thickness is usually much larger than the plasma electron displacements. For a plasma of 10^{12} electrons per cubic centimeter and 10 volts positive with respect to an electrode potential, the sheath thickness is about 4.8×10^{-3} centimeters, while from equation (8.34) the maximum electron displacement was 1.2×10^{-4} centimeters or $\frac{1}{40}$ the sheath thickness.

The electric field at the observer position is the integral of the contributions from all the dipoles.

$$\vec{E} = \left[-\frac{k^2}{4\pi\varepsilon}\right]\left[-\,enA_o h\right]\frac{e^{ikR-i\omega t}}{R}\int_0^{2\pi}\int_{r_1}^{r_2}\cos(N\alpha)$$

$$e^{-ika\cos(\alpha-\phi)\sin\theta}\left[\vec{\varepsilon}_\theta\cos\theta\sin(\alpha-\phi)\right.$$

$$\left.-\,\vec{\varepsilon}_\phi\cos(\alpha-\phi)\right]\,ada\,d\alpha \qquad (8.52)$$

For simplicity let us consider the plasma concentrated at the radius a. Equation (8.52), with a change of variable $\alpha - \phi = \xi$, $d\alpha = d\xi$, becomes

$$\vec{E} = \frac{k^2 enA_o h}{4\pi\epsilon R} \quad \frac{r_2^2 - r_1^2}{2} \quad e^{ikR - i\omega t} \int_{-\phi}^{2\pi-\phi} \cos N(\phi + \xi)$$

$$e^{-ika \cos\xi \sin\theta} \left[\vec{\epsilon}_\theta \cos\theta \sin\xi - \vec{\epsilon}_\phi \cos\xi\right] d\alpha \qquad (8.53)$$

By expanding the exponential function in an infinite series of Bessel functions

$$e^{-ika \cos\xi \sin\theta} = \sum_{m=-\infty}^{\infty} (i)^m J_m(-ka \sin\theta) \cos m\xi \qquad (8.54)$$

and integrating term by term, the result of the integration is

$$\frac{\pi}{2}\Big\{ \vec{\epsilon}_\theta \cos\theta \sin(N\phi)(-i)^{N+1} \left[J_{N+1}(ka \sin\theta) + J_{N-1}(ka \sin\theta)\right] + \vec{\epsilon}_\phi \cos(N\phi)(-i)^{N+1} \left[J_{N-1}(ka \sin\theta) - J_{N+1}(ka \sin\theta)\right]\Big\} \qquad (8.55)$$

because of the orthogonality property of trigonometric functions on the interval 2π.

For the antenna at $\theta = \frac{\pi}{2}$ only the $\vec{\epsilon}_\phi$ component is present and $J_{N+1}(ka)$ is negligible compared to $J_{N-1}(ka)$ for small arguments. The field strength is then

$$|E| \approx \frac{E_p \, \pi \, (Vol)}{\lambda^2 \, 4R \, (N-1)!} \cos(N\phi)\left(\frac{\pi a}{\lambda}\right)^{N-1} \tag{8.56}$$

For $\lambda = 33.5$ millimeters, $R = 3$ inches, $(Vol) = 0.82$ cubic centimeters, $a = 2$ millimeters, and $N = 8$,

$$\frac{E}{E_p} \approx 1.23 \times 10^{-11} \tag{8.57}$$

which is much too low compared with the measured ratio

$$\frac{E}{E_p} = \frac{0.0051 \text{ v/cm}}{230 \text{ v/cm}} = 2.4 \times 10^{-4} \tag{8.58}$$

Thus the model that the standing plasma waves radiate like a circular loop antenna seems to be not correct.

Let us consider the model that the electrons in each half wavelength region which are all oscillating together in phase radiate independently of the rest of the plasma standing wave.

The power radiated is then

$$P_r = \frac{\omega^4 \mu e^2 A_o^2}{24 \pi c} \left[\frac{n \, Vol}{4M}\right]^2 4M \tag{8.59}$$

$$= \frac{\omega^4 \varepsilon E_p^2 (Vol)^2}{96 \pi c^3 M} \tag{8.60}$$

The radiated powers calculated from this model and using the measured values of E_p are

M	Calculated P_r watts	Measured P_r watts
2	0.35	0.98
4	0.97	1.0
6	2.5	2.5
8	14.0	5.0

These values agree within the experimental accuracy. Let us call this model one.

Let us call radiation model two the case in which the radiated power is from a constant number of half wave sections of the plasma standing wave with the fields from the other half wave sections cancelling each other. The radiated power for these two cases is proportional to

$$P_{r_1} \sim \omega^4 A_o^2 \left(\frac{n\,Vol}{M}\right)^2 M \sim M^3 A_o^2 n^2 (Vol)^2 \qquad (8.61)$$

$$P_{r_2} \sim \omega^4 A_o^2 \left(\frac{n\,Vol}{M}\right)^2 \sim M^2 A_o^2 n^2 (Vol)^2 \qquad (8.62)$$

The power fed to the plasma oscillations for constant V, B, and pressure is proportional to

$$P_o \sim E_p I_e \sim n A_o I_e \tag{8.63}$$

These two powers are equal except for the small amount of plasma oscillation power lost to collisions

$$n A_o I_e \sim P_o \approx P_{r_1} \sim M^3 A_o^2 n^2 (Vol)^2 \tag{8.64}$$

$$\approx P_{r_2} \sim M^2 A_o^2 n^2 (Vol)^2 \tag{8.65}$$

so

$$n A_o \sim \frac{I_e}{M^3 (Vol)^2} \sim E_{p_1} \tag{8.66}$$

$$n A_o \sim \frac{I_e}{M^2 (Vol)^2} \sim E_{p_2} \tag{8.67}$$

The total input power is proportional to

$$P_{in} \sim I_p \sim I_e \sim n \sim \omega_p^2 \sim M^2 - 1 \tag{8.68}$$

so

$$I_e \sim M^2 \tag{8.69}$$

and the input power is proportional to the frequency squared.

$$P_{r_1} \sim \frac{M}{(Vol)^2} \tag{8.70}$$

$$P_{r_2} \sim \frac{M^2}{(Vol)^2} \tag{8.71}$$

so the radiated power is proportional to the first or second power of the frequency, depending on the choice of radiation model. Experimentally P_r seems to vary more nearly as M^2 corresponding to model two. The radiated power calculated from this model using the measured values of E_p seem to be about one order of magnitude too low, however.

The efficiency for constant V, B, and pressure is proportional to

$$\text{eff.}_1 = \frac{P_r}{P_{in}} \sim \frac{M}{M^2 (Vol)^2} \tag{8.72}$$

$$\text{eff.}_2 \sim \frac{M^2}{M^2 (Vol)^2} \tag{8.73}$$

The part of the input power which does not go to the plasma oscillations goes to ionize the gas and later heats the electrodes as the electrons and positive ions recombine at the electrode surfaces.

The Q is proportional to

$$Q_1 = \frac{W\omega}{P_r} \sim \frac{A_o^2\, \omega^3\, n\, (Vol)}{M^3\, A_o^2\, n^2\, (Vol)^2} \sim \frac{1}{M^2\, (Vol)} \tag{8.74}$$

$$Q_2 \sim \frac{1}{M\, (Vol)} \tag{8.75}$$

Dependence of radiated power, efficiency, and Q on the operating parameters

Let us consider the effect of magnetic flux density B, plate voltage V_A, gas pressure P, emission current i_e, electron temperature T_-, and tube dimensions on the radiated power P_r, the input power P_{in}, the quality factor Q, and the efficiency of the tube, so that better tube designs may be made. The assumption is used that each half wave of the standing wave pattern in the plasma radiates independently. The corresponding expressions for radiation model two differ by a factor M as shown in the previous section.

From equations (7.42), (8.16), (8.17), and (8.59)

$$Q = \frac{m_e\, 2\pi\, c}{\omega_c\, \mu\, e^2\, n\, (Vol)} = \frac{2\pi\, c^3}{\omega_c\, (Vol)\, \omega_p^2}$$

$$= \frac{2\pi\, c^3 \exp\left\{-\frac{k^2\overline{A^2}}{4}\right\}}{(Vol)\, (M^2 - 1)\, \omega_c^3} \tag{8.76}$$

where m_e is the electron mass, c the velocity of light, $\omega_c = \frac{eB}{m_e}$ the cyclotron angular frequency for electrons, μ the permeability of free space, e the electronic charge, n the electron density, (Vol) the volume of the plasma region, $\omega_p = \frac{e^2 n}{\epsilon m_e}$ the angular plasma frequency, $M = \frac{\omega}{\omega_c}$ the mode number, $\left(\overline{A^2}\right)^{1/2} = \frac{\left(\overline{v_{\perp}^2}\right)^{1/2}}{\omega_c}$ the average radius of the helical path of the plasma electrons due to their thermal motions, $k = \frac{2\pi}{\lambda_p}$ the propagation constant of the plasma wave, and λ_p the wavelength of the plasma wave.

From equation (8.59) the radiated power is

$$P_r = \frac{\mu e^2}{96\pi c} M^3 \overline{A_o}^2 n^2 (Vol)^2 \omega_c^4$$

$$= \frac{\epsilon E_p^2}{96\pi c^3} M^3 (Vol)^2 \omega_c^4 \qquad (8.77)$$

where $\overline{A_o}$ is the average amplitude of the plasma oscillation electron displacements, ω the angular oscillation frequency, and the other symbols are given with equation (8.76).

The power fed to the plasma waves P_o is proportional to the product of the electric field strength in the plasma E_p, the emission current I_e, and the distance L that the working emission

electrons travel in phase with the plasma wave before suffering a collision and being knocked out of the working phase of the wave.

$$P_o = E_p I_e L \tag{8.78}$$

From equations (7.36) and (8.21)

$$P_o = \frac{en\overline{A_o}}{\epsilon} I_e \frac{K_1 V_A^{0.7}}{P} \tag{8.79}$$

where ϵ is the permittivity of free space and K_1 the constant in equation (8.21). Except for the small amount of plasma oscillation power lost to collisions, the power fed to the plasma waves equals the radiated power.

$$\frac{en\overline{A_o} I_e K_1 V_A^{0.7}}{\epsilon P} = \frac{\mu e^2}{96\pi c} M^3 \overline{A_o}^2 n^2 (Vol)^2 \omega_c^4 \tag{8.80}$$

$$n\overline{A_o} = \frac{96 \pi c^3 I_e K_1 V_A^{0.7}}{e P M^3 (Vol)^2 \omega_c^4} = \frac{\epsilon E_p}{e} \tag{8.81}$$

From Figure (5.8) the plate current I_p is approximately proportional to the square root of the plate voltage. The plate current is proportional to the emission current. The plate current is approximately not a function of the gas pressure as shown by

Figure (5.2). The small decrease in emission current with increasing pressure and constant filament current is due to the increased cooling of the filament by the gas.

It has not been determined experimentally what function the plate current is of the size of the tube. From the reasoning that the increase in plate current with increasing magnetic flux density is caused by the increased number of ionizing collisions necessary to scatter an emission electron to the anode, an increase in the plate diameter would have the same effect. In two tubes whose ratio of plate diameters is $\frac{d_1}{d_2} = \gamma$ and whose ratio of magnetic flux densities is $\frac{B_1}{B_2} = \frac{1}{\gamma}$ with the other parameters equal, emission electrons would make an equal number of ionizing collisions, on the average, before being scattered to the plate and therefore both tubes should have the same plate current. Thus the plate current is a function of the product of B and d. From Figure (5.16) the plate current I_p is approximately proportional to $\sqrt{B}$ so I_p should also be proportional to $\sqrt{d}$. Combining all this we obtain

$$I_p = K_2 I_e \sqrt{V_a B d} \qquad (8.82)$$

where K_2 is approximately $\frac{0.0069}{(\text{volts gauss centimeters})^{1/2}}$.

Equation (8.82) was obtained from a consideration of the ionization process. Another expression can be obtained for the

plate current by a consideration of the charge collection processes. An approximate expression for the current to the electrodes, from equation (5.13) and (5.16) is

$$I_p = K_3 S n \sqrt{\frac{T_-}{hP}} \tag{8.83}$$

where K_3 is approximately $\frac{6.4 \times 10^{-16} \text{ amperes cm } \sqrt{\text{microns of Hg cm}}}{\text{electrons } \sqrt{{}^oK}}$, h a suitable average of the length and diameter of the tube, and S the total area of the electrodes.

Let l be a linear scaling factor for the size of the tube so that $d \approx l$, length $\approx 3l$, $S \approx 3\pi l^2$, $(\text{Vol}) \approx \frac{3\pi l^3}{4}$.

From equations (8.82) and (8.83),

$$I_e = \frac{3\pi K_3 n l \sqrt{T_-}}{K_2 \sqrt{V_a BP}} = \frac{3\pi K_3 l \sqrt{T_-}}{K_2 \sqrt{V_a BP}} (M^2-1) \omega_c{}^2 \exp\left\{\frac{k^2 \overline{A^2}}{4}\right\} \tag{8.84}$$

The power input to the tube is

$$P_{in} = I_p V_a = K_2 I_e B^{0.5} l^{0.5} V_a{}^{1.5} = 3\pi K_3 l^{1.5} n V_a \frac{T_-{}^{0.5}}{p^{0.5}}$$

$$= 3\pi K_3 l^{1.5} V_a \frac{T_-{}^{0.5}}{p^{0.5}} \frac{\varepsilon m_e}{e^2} (M^2-1) \omega_c{}^2 \exp\left\{\frac{M^2 2KT_-}{r^2 m_e \omega_c{}^2}\right\}$$

$$= K_4 l^{1.5} V_a \frac{T_-^{0.5}}{p^{0.5}} (\omega^2 - \omega_c^2) \exp\left\{\frac{\omega^2 KT_-}{\omega_c^2 4eV_a}\right\} \qquad (8.85)$$

where K is Boltzmann's constant, and r is an average radius in the plasma. The r value chosen is the diameter of the orbits of the emission electrons since this is the position of maximum interaction between the emission electrons and the plasma waves.

The power radiated by the tube, from equation (8.77), is

$$P_r = \frac{864 \pi^3 c^3 K_1^2 K_3^2 V_a^{0.4} n^2 l^2 T_-}{\varepsilon K_2^2 p^3 M^3 (Vol)^2 \omega_c^4 B}$$

$$= \frac{K_5 V_a^{0.4} T_- n^2}{p^3 l^4 \omega^3 \omega_c^2}$$

$$= \frac{K_5 V_a^{0.4} T_- (\omega^2 - \omega_c^2)^2}{p^3 l^4 \omega^3 \omega_c^2} \exp\left\{2 \frac{\omega^2 KT_-}{\omega_c^2 4eV_a}\right\} \qquad (8.86)$$

The electric field strength of the plasma oscillation E_p, from equation (8.81), is

$$E_p = \frac{288\,\pi^2\,c^3\,K_1\,K_3\,T_-^{0.5}\,V_a^{0.2}\,l\,n}{\epsilon K_2\,M^3\,P^{1.5}\,(Vol)^2\,\omega_c^4\,B^{0.5}}$$

$$= \frac{K_6\,T_-^{0.5}\,V_a^{0.2}\,n}{P^{1.5}\,l^5\,\omega^3\,\omega_c^{1.5}}$$

$$= \frac{K_6\,T_-^{0.5}\,V_a^{0.2}\,(\omega^2 - \omega_c^2)}{P^{1.5}\,l^5\,\omega^3\,\omega_c^{1.5}} \exp\left\{\frac{\omega^2\,KT_-}{\omega_c^2\,4eV_a}\right\} \qquad (8.87)$$

and

$$\frac{}{A_o} = \frac{e\,K_6\,T_-^{0.5}\,V_a^{0.2}}{m\,P^{1.5}\,l^5\,\omega^3\,\omega_c^{1.5}} \qquad (8.88)$$

The efficiency of the tube is

$$\text{Eff.} = \frac{P_r}{P_{in}} = \frac{K_5\,T_-^{0.5}\,(\omega^2 - \omega_c^2)\exp\left\{\frac{\omega^2\,KT_-}{\omega_c^2\,4eV_a}\right\}}{K_4\,V_a^{0.6}\,l^{5.5}\,p^{2.5}\,\omega^3\,\omega_c^2} \qquad (8.89)$$

$$Q = \frac{K_6}{l^3\,(\omega^2 - \omega_c^2)\,\omega_c \exp\left\{\frac{\omega^2\,KT_-}{\omega_c^2\,4eV_a}\right\}} \qquad (8.90)$$

The exponent of the exponential term equals 1 for M equal to about 12.8 and the exponential term starts to exert an influence on the relation for M above about 5.

The efficiency and the Q decrease, and the radiated power increases with increasing frequency. The radiated power and efficiency decrease with increasing pressure as expected. The radiated power and efficiency are low powered functions of the anode voltage and electron temperature. For a certain oscillation frequency, the radiated power and efficiency decrease with increasing magnetic flux density. For a certain oscillation frequency, the Q is infinite for mode M = 1. This is of no consequence since the radiated power is zero for mode one. Then the Q goes through a minimum at M = $\sqrt{3}$ of

$$Q_{min} \approx \frac{24\,\pi\,c^3}{(Vol)\,\omega^3}\,(2.56) \tag{8.91}$$

The Q has a maximum at $M \approx \left[\frac{2\,e\,V_a}{K\,T_-}\right]^{1/2} \approx 9.07$ of

$$Q_{max} \approx \frac{24\,\pi\,c^3}{(Vol)\,\omega^3}\,(5.58) \tag{8.92}$$

The Q then approaches zero as the mode number increases further and the magnetic flux density decreases.

The most unexpected result is that the radiated power, efficiency, and the Q decrease as the volume increases, contrary to the usual situation. This is because the oscillating electric field strength E_p in the plasma is stronger in a smaller volume and the power taken from the emission electron beam is proportional to E_p. The thickness of the space charge sheath at the filament decreases as the electron density increases so the plasma volume increases with increasing frequency. The cathode sheath thicknesses are about 2.1 millimeters for 6 centimeter radiation, 1.1 mm for $\lambda = 3$ cm, and 0.6 mm for $\lambda = 1.5$ cm.

A range of a factor of four in the design values of the magnetic flux density and the linear dimension of the tube give a range in available Q values, radiated power, and efficiency, at a certain frequency, of several hundred times.

The vapor pressure of mercury is about one micron at 20°C, 6 microns at 40°C, 26 microns at 60°C, etc. A tube could be filled and sealed with a density of mercury vapor corresponding, for example, to 6 microns pressure. The cold tube would have 1/6 of the mercury in the vapor state and 5/6 as a liquid but for gas temperatures above 40°C, where the tube operates during a discharge, all the mercury will be in the vapor state and the gas density is constant. The concentration of the gas in sealed tubes does change slowly during the life of the tubes because of a clean-up action that occurs. The gas disappears by being trapped in the walls and electrodes of the tube as a result of the action of the discharge.

CONCLUSIONS

The plasma-magnetron oscillator and the associated plasma oscillation phenomena seem to be fairly well understood. Plasma oscillations with a finite wavelength, in a magnetic field, and with a Maxwellian velocity distribution of the plasma electrons, were considered as a consistent field problem.

One result is the prediction of unstable frequencies at integer multiples M of the cyclotron frequency for electrons. The magnetron exciting mechanism, where the standing wave pattern of the plasma oscillations acts like the anode structure of a high vacuum multi-segment anode magnetron, is available for exciting oscillations with frequencies equal to integer multiples N of half the cyclotron frequency for electrons. The plasma oscillates and radiates at those frequencies at which (1) the plasma is unstable and (2) an excitation mechanism exists.

Another result is the new dispersion relation. Oscillations are obtained for those combinations of magnetic flux density, gas pressure, filament current, and anode voltage which produce a plasma electron density which satisfies the dispersion relation at an unstable frequency. The new dispersion relation puts a lower wavelength limit for oscillations, at about 0.5 centimeters, for practically attainable plasma electron densities.

The oscillator has Q's of the order of a hundred at the lower microwave frequencies. The Q's decrease with increasing frequency.

The frequency of the oscillator is continuously variable over the whole microwave frequency range and into the millimeter wavelength range by changing the magnetic flux density and one other variable such as the filament current. The very wide tuning range is the result of the frequency being determined by the plasma electron density and not the dimensions of a cavity.

The measured power at 3.4 centimeters was about one watt with an efficiency of about three percent. The radiated power increases with increasing frequency.

For two centimeter radiation, a ten mil tungsten filament lasts of the order of five hours in 15 microns pressure of air for pulsed plate voltages with a duty cycle of $\frac{1}{167}$. Continuous, rather than pulsed, operation decreases the filament life by only a factor of the order of two. The filament life decreases with increasing frequency. Gas purity may be found to affect filament life.

The plasma-magnetron oscillator might find application as a very wide tuning range, medium power, microwave signal and noise generator with expendable sealed tubes with about five to ten microns gas pressure of mercury vapor or a noble gas. Mechanical tolerances of the tube are not critical.

BIBLIOGRAPHY

1. Adler, F. P. and H. Margenau. Electron conductivity and mean free paths. Physical review 79:970-971. 1950.

2. Adler, Fred P. Measurement of the complex conductivity of an ionized gas at microwave frequencies. Journal of applied physics 20:1125-1129. 1949.

3. Alfvén, H. Cosmical electrodynamics. Oxford, Clarendon press, 1950. 237 p.

4. Armstrong, E. B. Plasma-electron oscillations. Nature 160:713. 1947.

5. Åström, E. Magneto-hydrodynamic waves in a plasma. Nature 165:1019-1020. 1950.

6. Bailey, V. A. and K. Landecker. Electro-magneto-ionic waves. Nature 166:259-261. 1950.

7. Bailey, V. A. Electro-magneto-ionic optics. Journal and proceedings of the royal society of New South Wales 82:107-113. 1948.

8. Bailey, V. A. Space-charge wave amplification effects. Physical review 75:1104-1105. 1949.

9. Bailey, V. A. The growth of circularly polarized waves in the sun's atmosphere and their escape into space. Physical review 78:428-443. 1950.

10. Bailey, V. A. The relativistic theory of electro-magneto-ionic waves. Physical review 83:439-454. 1951.

11. Barnes, B. T. The dynamic characteristics of a low pressure discharge. Physical review 86:351-358. 1952.

12. Bayet, Michel M. Electromagnetic properties of plasmas. Journal de physique et le radium 13:579-586. 1952.

13. Bierens de Haan, David. New tables of definite integrals. New York, G. E. Stechert and Co., 1939. 716 p.

14. Biondi, Manfred A. Measurement of the electron density in ionized gases by microwave techniques. Review of scientific instruments 22:500-502. 1951.

15. Biondi, M. A. Microwave gas discharges. Electrical engineering 69:806-809. 1950.

16. Bohm, D. and E. P. Gross. Effects of plasma boundaries in plasma oscillations. Physical review 79:992-1001. 1950.

17. Bohm, D. and E. P. Gross. Plasma oscillations as a cause of acceleration of cosmic-ray particles. Physical review 74:624. 1948.

18. Bohm, D. and E. P. Gross. Theory of plasma oscillations A. Origin of medium-like behavior. Physical review 75:1851-1864. 1949.

19. Bohm, D. and E. P. Gross. Theory of plasma oscillations B. Excitation and damping of oscillations. Physical review 75:1864-1876. 1949.

20. Bohm, D. Excitation of plasma oscillations. Physical review 70:448. 1946.

21. Borgnis, F. On the theory of electron plasma oscillations. Helvetica physica acta 20:207-221. 1947.

22. Boyd, R. L. F. The collection of positive ions by a probe in an electrical discharge. Proceedings of the royal society of London, series A 201:329-347. 1950.

23. Brillouin, Léon. Wave propagation in periodic structures. New York, McGraw-Hill, 1946. 247 p.

24. Brode, Robert B. The quantitative study of the collisions of electrons with atoms. Reviews of modern physics 5:257-279. 1933.

25. Brown, A. E. The effect of a magnetic force on high frequency discharges in pure gases. Philosophical magazine and journal of science 29:302-309. 1940.

26. Brown, Sanborn C. and A. D. MacDonald. Limits for the diffusion theory of high frequency gas discharge breakdown. Physical review 76:1629-1633. 1949.

27. Brown, Sanborn C. High-frequency gas-discharge breakdown. Proceedings of the institute of radio engineers 39:1493-1501. 1951.

28. Brown, Sanborn C. Physics of some loss mechanisms in gas discharges. Electrical engineering 71:501-503. 1952.

29. Champion, K. S. W. The theory of gaseous arcs I. The fundamental relations for the positive columns. Proceedings of the physical society of London, series B 65:329-344. 1952.

30. Champion, K. S. W. The theory of gaseous arcs II. The energy balance equation for the positive columns. Proceedings of the physical society of London, series B 65:345-356. 1952.

31. Chapman, Sydney and T. G. Cowling. The mathematical theory of non-uniform gases. Cambridge, University press, 1939. 404 p.

32. Cleeton, Claud E. Grating theory and study of the magnetostatic oscillator frequency. Physics 6:207-209. 1935.

33. Cobine, J. D. and C. J. Gallagher. Effects of magnetic field on oscillations and noise in hot cathode arcs. Journal of applied physics 18:110-116. 1947.

34. Cobine, J. D. and C. J. Gallagher. Noise and oscillations in hot cathode arcs. Journal of the franklin institute 243:41-54. 1947.

35. Dickey Jr., F. R. The production of millimeter waves by spark discharges. Cambridge, Harvard university, 1951. 74 p. (Harvard university. Cruft laboratory. Technical report no. 123)

36. Donahue, T. and G. H. Dieke. Oscillatory phenomena in direct current glow discharges. Physical review 81:248-261. 1951.

37. Druyvesteyn, M. J. and F. M. Penning. The mechanism of electrical discharges in gases of low pressure. Reviews of modern physics 12:87-174. 1940.

38. Dwight, Herbert Bristol. Tables of integrals and other mathematical data. New York, MacMillan, 1947. 250 p.

39. Everhart, Edgar. An experiment for the direct measurement of magnetostatic fields. American journal of physics 19:474-475. 1951.

40. Feinstein, J. and H. K. Sen. Radio wave generation by multi-stream charge interaction. Physical review 83:405-412. 1951.

41. Finkelnburg, Wolfgang. Atomic physics. New York, McGraw-Hill, 1950. 498 p.

42. Gabor, D. Plasma oscillations. British journal of applied physics 2:209-218. 1951.

43. Gabor, D. Wave theory of plasmas. Proceedings of the royal society of London, series A 213:73-86. 1952.

44. Glagoleva-Arkadieva, A. A. and N. A. Sokolov. On the method of resonance thermocouples used for the investigation of complete radiation in the ultra-Hertz band. Comptes rendus (doklady) de l'académie des sciences de l'U.R.S.S. 32:543-545. 1941.

45. Glagoleva-Arkadieva A. A new radiation source of short electromagnetic waves of ultra-Hertz frequency. Zeitschrift für physik 24:153-165. 1924.

46. Glagoleva-Arkadieva, A. A. Short electromagnetic waves of wave length up to 82 microns. Nature 113:640. 1924.

47. Golden, Vernon Edgar. The effect of pressure on the wave length of plasma oscillations in argon and nitrogen. Master's thesis. Corvallis, Oregon state college, 1952. 35 numb. leaves.

48. Goldman, Stanford. Frequency analysis, modulation and noise. New York, McGraw-Hill, 1948. 434 p.

49. Gross, E. P. Plasma oscillations in a static magnetic field. Physical review 82:232-242. 1951.

50. Guthrie, A. and R. K. Wakerling (eds.) The characteristics of electrical discharges in magnetic fields. New York, McGraw-Hill, 1949. 376 p.

51. Haeff, Andrew V. On the origin of solar radio noise. Physical review 75:1546-1551. 1949.

52. Haeff, Andrew V. Space-charge wave amplification effects. Physical review 74:1532-1533. 1948.

53. Haeff, Andrew V. The electron-wave tube -- a novel method of generation and amplification of microwave energy. Proceedings of the institute of radio engineers 37:4-10. 1949.

54. Hartman, L. M. Theory of high frequency gas discharges III. High frequency breakdown. Physical review 73:316-325. 1948.

55. Herlofson, N. Magneto-hydrodynamic waves in a compressible fluid conductor. Nature 165:1020-1021. 1950.

56. Hollenberg, A. V. Experimental observation of amplification by interaction between two electron streams. Bell system technical journal 28:52-58. 1949.

57. Hollmann, H. E. The behavior of electron oscillators in a magnetic field. Elektrische nachrichten-technik 6:377-386. 1929.

58. Hopfield, John J. Glass variable microleaks for gases. Review of scientific instruments 21:671-672. 1950.

59. Howe, R. M. Probe studies of energy distributions and radial potential variations in a low pressure mercury arc. Journal of applied physics 24:881-894. 1953.

60. Jahnke, Eugene and Fritz Emde. Tables of functions. 4th ed., New York, Dover, 1945. 382 p.

61. Johnson, E. O. and L. Malter. A floating double probe method for measurements in gas discharges. Physical review 80:58-68. 1950.

62. Johnson, E. O. and L. Malter. Double-probe method for determination of electron-temperatures in steady and time-varying gas discharges. Physical review 76:1411-1412. 1949.

63. Johnson, E. O. and W. M. Webster. The plasmatron, a continuously controllable gas-discharge developmental tube. Proceedings of the institute of radio engineers 40:645-659. 1952.

64. Kennard, Earle H. Kinetic theory of gases. New York, McGraw-Hill, 1938. 483 p.

65. Kihara, T. The mathematical theory of electrical discharges in gases. Reviews of modern physics 24:45-61. 1952.

66. King, Roland and Charles W. Harrison Jr. The receiving antenna. Proceedings of the institute of radio engineers 32:18-34. 1944.

67. Knudsen, H. L. Radiation resistance and gain of homogeneous ring quasi-array. Proceedings of the institute of radio engineers 42:686-695. 1954.

68. Knudsen, H. L. The field radiated by a ring quasi-array of an infinite number of tangential or radial dipoles. Proceedings of the institute of radio engineers 41:781-789. 1953.

69. Kwal, Bernard. Loss of energie of charged particles in a very strongly ionized medium (ionic plasma). Le journal de physique et le radium 12:805-810. 1951.

70. Labrum, N. R. and E. K. Bigg. Observations on radio-frequency oscillations in low-pressure electrical discharges. Proceedings of the physical society of London, series B 65:356-368. 1952.

71. Laffineur, M. and C. Pecker. Radioelectric emission due to the gyromagnetic effect in a discharge. Comptes rendus de l'académie des sciences 231:1446-1447. 1950.

72. Landau, L. On the vibrations of the electronic plasma. Journal of physics 10:25-34. 1946.

73. Lax, Benjamin, W. P. Allis, and Sanborn C. Brown. The effect of magnetic field on the breakdown of gases at microwave frequencies. Journal of applied physics 21:1297-1304. 1950.

74. Loeb, Leonard B. Fundamental processes of electrical discharge in gases. New York, Wiley, 1939. 717 p.

75. Lüdi, F. Observations on the effect of plasma oscillations in transit time tubes. Zeitschrift fur angewandte mathematik und physik 3:390-393. 1952.

76. MacDonald, A. D. and Sanborn C. Brown. High frequency gas discharge breakdown in helium. Physical review 75:411-418. 1949.

77. MacDonald, A. D. and Sanborn C. Brown. High frequency gas discharge breakdown in hydrogen. Physical review 76: 1634-1639. 1949.

78. Malmfors, K. G. Unstable oscillations in an electron gas. Arkiv för Fysik 1:569-578. 1950.

79. Malter, L. and W. M. Webster. Rapid determination of gas discharge constants from probe data. RCA review 12:191-210. 1951.

80. Margenau, H. and L. M. Hartman. Theory of high frequency gas discharges II. Harmonic components of the distribution function. Physical review 73:309-315. 1948.

81. Margenau, H. Conduction and dispersion of ionized gases at high frequencies. Physical review 69:508-513. 1946.

82. Margenau, H. Theory of high frequency gas discharges I. Methods for calculating electron distribution functions. Physical review 73:297-308. 1948.

83. Margenau, H. Theory of high frequency gas discharges IV. Note on the similarity principle. Physical review 73:326-328. 1948.

84. Martin, John R. and Carl F. Schunemann. Measuring wavelength in millimeters. Electronics 26:184-187. 1953.

85. Martyn, D. F. Polarization of solar radio-frequency emissions. Nature 158:308. 1946.

86. Massachusetts institute of technology. Department of electrical engineering. Applied electronics. New York, Wiley, 1943. 772 p.

87. Massey, H. S. W. Negative ions. Cambridge, University press, 1950. 133 p.

88. McLachlan, N. W. Theory and application of Mathieu functions. Oxford, Clarendon press, 1947. 401 p.

89. Merrill, Harrison J. and Harold W. Webb. Electron scattering and plasma oscillations. Physical review 55:1191-1198. 1939.

90. Meyeren, W. von. A movable probe for gas discharge experiments. Zeitschrift für physik 125:539-540. 1949.

91. Miller, Jr., P. H. and B. Goodman. Optical microwave detector. Physical review 70:110. 1946.

92. Mimno, H. R. The physics of the ionosphere. Reviews of modern physics 9:1-43. 1937.

93. Montgomery, Carol G. Technique of microwave measurements. New York, McGraw-Hill, 1947. 939 p.

94. Morse, P. M., W. P. Allis, and E. S. Lamar. Velocity distributions for elastically colliding electrons. Physical review 48:412-419. 1935.

95. Mulholland, H. P. and S. Goldstein. The characteristic numbers of the Mathieu equation with purely imaginary parameter. Philosophical magazine and journal of science 8:834-840. 1929.

96. Müller-Lübeck, K. On ambipolar space charge flow between plane electrodes. Zeitschrift für angewandte physik 3:409-415. 1951.

97. Neill, T. R. Plasma-electron oscillations. Nature 163:59-60. 1949.

98. Nergaard, Leon S. Analysis of a simple model of a two-beam growing wave tube. RCA review 9:585-601. 1948.

99. Nichols, E. F. and J. D. Tear. Short electric waves. Physical review 21:587-610. 1923.

100. Olsen, H. N. and W. S. Huxford. Dynamic characteristics of the plasma in discharges through rare gases. Physical review 87:922-930. 1952.

101. Parzen, Philip. Space-charge wave propagation in a cylindrical electron beam of finite lateral extension. Journal of applied physics 23:215-219. 1952.

102. Pierce, J. R. and W. B. Hebenstreit. A new type of high-frequency amplifier. Bell system technical journal 28:33-51. 1949.

103. Pierce, J. R. A note on plasma oscillations. Physical review 76:565. 1949.

104. Pierce, J. R. Increasing space-charge waves. Journal of applied physics 20:1060-1066. 1949.

105. Pierce, J. R. Limiting stable current in electron beams in the presence of ions. Journal of applied physics 15:721-726. 1944.

106. Pierce, J. R. Possible fluctuations in electron streams due to ions. Journal of applied physics 19:231-236. 1948.

107. Ramo, Simon and John R. Whinnery. Fields and waves in modern radio. New York, Wiley, 1944. 502 p.

108. Ramo, Simon. Space charge and field waves in an electron beam. Physical review 56:276-283. 1939.

109. Ramo, Simon. The electronic-wave theory of velocity-modulation tubes. Proceedings of the institute of radio engineers 27:757-763. 1939.

110. Roberts, J. A. Wave amplification by interaction with a stream of electrons. Physical review 76:340-344. 1949.

111. Rohrbaugh, J. H. A study of the generation and detection of electromagnetic waves in the millimeter wave region. 6 progress reports. New York, New York university and U. S. Air Force, 1952-53. (U. S. Air Force. Progress reports No. 15-20, Contract AF19(122)-4, March 1, 1952-Sept. 30, 1953)

112. Rossi, B. B. and H. H. Staub. Ionization chambers and counters. New York, McGraw-Hill, 1949. 243 p.

113. Schlüter, Arnulf. Dynamics of plasmas I. Fundamental equations of a plasma in crossed fields. Zeitschrift für naturforschung, series A 5:72-78. 1950.

114. Schumann, W. O. On longitudinal and transverse electric waves in uniformly moving plasma. Zeitschrift für angewandte physik 3:178-181. 1951.

115. Schumann, W. O. Plasma phenomena set up by sudden pulses. Annalen der physik 43:369-382. 1943.

116. Schumann, W. O. Selfexcited oscillations and density and current fluctuations for the case of the free fall of electrons through a region with constant positive density. Naturwissenschaften 31:140-143. 1943.

117. Seeliger, R. The diffusion theory of discharge plasmas. Naturwissenschaften 39:78-81. 1952.

118. Seeliger, R. Theory of electron-plasma oscillations. Zeitschrift für physik 118:618-623. 1942.

119. Slutzkin, A. A. and D. S. Steinberg. The production of shortwave undamped oscillations by application of the magnetic field. Annalen der physik 1:658-670. 1929.

120. Spangenberg, Karl R. Vacuum tubes. New York, McGraw-Hill, 1948. 860 p.

121. Steele Jr., Howard L. Note on gaseous discharge super-high-frequency noise sources. Proceedings of the institute of radio engineers 40:1603-1604. 1952.

122. Stratton, Julius Adams. Electromagnetic theory. New York, McGraw-Hill, 1941. 615 p.

123. Thonemann, P. C. and R. B. King. Production of high frequency energy by an ionized gas. Nature 158:414. 1946.

124. Thonemann, P. C., W. T. Cowhig, and P. A. Davenport. Interaction of travelling magnetic fields with ionized gases. Nature 169:34-35. 1952.

125. Tonks, Lewi and Irving Langmuir. Oscillations in ionized gases. Physical review 33:195-210. 1929.

126. Torrey, Henry C. and Charles A. Whitmer. Crystal rectifiers. New York, McGraw-Hill, 1948. 443 p.

127. Townsend, J. S. and E. W. B. Gill. Generalization of the theory of electrical discharges. Philosophical magazine and journal of science 26:290-311. 1938.

128. Twiss, R. Q. On Bailey's theory of amplified circularly polarized waves in an ionized medium. Physical review 84:448-457. 1951.

129. Twiss, R. Q. On Bailey's theory of growing circularly polarized waves in a sunspot. Physical review 80:767-768. 1950.

130. U. S. national bureau of standards. National applied mathematics laboratories. Computation laboratory. Tables relating to Mathieu functions. New York, Columbia university press, 1951. 278 p.

131. Walker, L. R. Note on wave amplification by interaction with a stream of electrons. Physical review 11:1721-1722. 1949.

132. Wenzel, F. Wall currents, ionic mobilities, and ion temperatures in plasmas. Zeitschrift für angewandte physik 3:332-343. 1951.

133. Wolff, I., E. G. Linder, and R. A. Braden. Transmission and reception of centimeter waves. Proceedings of the institute of radio engineers 23:11-23. 1935.

134. Yunker, E. A. Generation of millimeter electromagnetic waves. 10 progress reports. Corvallis, Oregon, Oregon state college and U. S. Air Force, 1948-53. (U. S. Air Force. Progress reports, Contract W19-122-ac-34, June 30, 1948-March 31, 1953).